Computers and Mathematics with Applications 202 (2026) 59–87

Contents lists available at ScienceDirect

Computers and Mathematics with Applications

journal homepage: www.elsevier.com/locate/camwa

A second order accurate, and structure-preserving numerical scheme for the thermodynamical consistent Keller–Segel–Navier–Stokes model

Rui Wang [a], Cheng Wang [b], Yuzhe Qin [c,], Zhengru Zhang [a,*]

[a] School of Mathematical Sciences, Beijing Normal University, No. 19, Xinjiekouwai Street, Haidian District, Beijing, 100875, Beijing, China
[b] Mathematics Department, University of Massachusetts Dartmouth, 285 Old Westport Road, North Dartmouth, MA, 02747, USA
[c] School of Mathematics and Statistics, Shanxi University, No. 92 Wucheng Road, Taiyuan, 030006, Shanxi, China

ARTICLE INFO

MSC:
35K35
35K55
65M06
65M12

Keywords:
Keller–Segel–Navier–Stokes system
Positivity-preserving property
Energy stability
Optimal rate convergence analysis
Higher-order asymptotic expansion
Rough and refined error estimates

ABSTRACT

In this work, we propose a Keller–Segel–Navier–Stokes (KSNS) model for describing chemotactic phenomena, formulated within the framework of the Energetic Variational Approach (EnVarA). A second-order accurate numerical scheme is developed that rigorously preserves three fundamental properties in discrete sense: the positivity of cell density, mass conservation of cell density, and total energy dissipation. The Keller–Segel subsystem is reformulated as a coupling between an H^{-1} gradient flow with non-constant mobility and an L^2 gradient flow, enabling the effective treatment of the nonlinear and singular logarithmic energy potential via a modified Crank-Nicolson scheme. Artificial regularization terms are introduced to enforce positivity preservation. For the fluid dynamics component, we adopt a second-order semi-implicit time discretization. The marker-and-cell (MAC) finite difference approximation is used as the spatial discretization, which ensures a discretely divergence-free velocity field. The proposed numerical method guarantees unique solvability, mass conservation, and total energy stability. Furthermore, through detailed asymptotic expansions and rigorous error analysis, we establish optimal convergence rates. A series of numerical experiments are presented to validate the effectiveness and robustness of both the physical model and the numerical scheme.

1. Introduction

Chemotaxis is a fundamental biological process in which cells move directionally in response to chemoattractant gradients. It plays a crucial role in physiological and pathological processes such as immune responses, embryonic development, and cancer metastasis [1]. Mathematical models have been developed to describe and predict chemotactic behavior, providing insights into cellular dynamics and potential therapeutic strategies [2,21,22]. Among these models, the Keller–Segel–Navier–Stokes (KSNS) system is particularly representative, as it combines the Keller–Segel (KS) equations with the Navier–Stokes (NS) equations to describe the interaction between cell movement, chemoattractant diffusion, and fluid dynamics. This coupling offers a more comprehensive framework for modeling chemotactic behavior, taking into account the effects of fluid motion on the chemoattractant diffusion and the cell movement [23,24,26].

* Corresponding author.
E-mail addresses: rwang0913@mail.bnu.edu.cn (R. Wang), cwang1@umassd.edu (C. Wang), yzqin@sxu.edu.cn (Y. Qin), zrzhang@bnu.edu.cn (Z. Zhang).

https://doi.org/10.1016/j.camwa.2025.11.005
Received 20 May 2025; Received in revised form 2 October 2025; Accepted 15 November 2025

The KS equations describe the interaction between cells and chemoattractants, focusing on cell migration in response to chemoattractant concentration gradients, as well as the changes in chemoattractant distribution due to cellular secretion and diffusion [21,25,39]. These parabolic-parabolic partial differential equations model the dynamics of cell density and chemoattractant concentration, both of which are key to understand chemotaxis. In contrast, the Navier-Stokes equations describe the flow of viscous, incompressible fluids [36]. The fluid velocity field is influenced by both the cell movement and the chemoattractant diffusion, while the cells themselves are affected by fluid motion, creating a feedback loop between these two processes. This feedback is essential for accurately modeling the dynamics of chemotaxis in fluid environments. Therefore, the KSNS model captures the interplay between the transport of cells and chemoattractants by the surrounding fluid and the feedback effects of moving cells on fluid motion [26]. Detailed modeling of this system is presented in Section 2, where we explore various mathematical techniques employed to simulate this complex interaction.

In recent years, significant theoretical efforts have focused on understanding the long-term behavior of the KSNS model, exploring the existence, uniqueness, and regularity of its solutions [15,26]. These studies aim to reveal the fundamental properties of the model under various initial and boundary conditions. For instance, Kozono proved the existence of global mild solutions with small initial data in scaling-invariant spaces [26]. However, despite these analytical advances, there have been relatively few numerical studies addressing the KSNS system. The challenges posed by the KS equations and the strong coupling between chemotaxis and fluid motion make the associated numerical simulations especially complicated.

The properties of the KS equation, including positivity preservation, mass conservation, and energy dissipation, as well as the strong coupling between KS evolution and fluid motion, present two main challenges in numerical studies [10,12,20,37]. Many existing methods focus on maintaining positivity through specific spatial discretizations, which may lead to a strict CFL constraint on the time step [3,23]. For example, Chertock et al. used a high-order positivity-preserving mixed finite volume-finite difference method to ensure the energy dissipation [9]. Shen and Xu employed the Galerkin method to address these properties while ensuring energy dissipation [34]. Filbet, using a finite volume method, solved and analyzed the existence, uniqueness, and convergence of numerical solutions [16]. Other numerical approaches, such as the scalar auxiliary variable (SAV) method developed by Huang and Shen, unconditionally preserve the properties of the KS equations [24]. Furthermore, Zeng and Zhou proposed a linearly decoupled numerical scheme using the finite element approximation to the fluid equation and the upwind finite volume method for the chemotaxis equation, which ensures positivity preservation and provides an optimal error estimate [41].

Despite the progress in addressing individual aspects of the KSNS system, a unified approach that satisfies all the necessary properties (positivity preservation, energy dissipation, and convergence) has remained elusive. This work proposes a second-order numerical scheme for the KSNS system that theoretically guarantees three essential properties: (i) positivity of cell density and unique solvability, (ii) total energy stability, and (iii) optimal rate convergence estimate. The KS component is reformulated as the coupling of a non-constant mobility H^{-1} gradient flow and an L^2 gradient flow. A key challenge in this approach is to handle the nonlinear and singular logarithmic energy potential while preserving the variational structure [7,11,13,27,29,33].

To address these challenges, we apply a second-order extrapolation to the mobility function to ensure unique solvability, and use a modified Crank-Nicolson approximation to the logarithmic nonlinear term to ensure a stability based on the Flory-Huggins energy [8,11,29]. Nonlinear artificial regularization terms further enhance the positivity-preserving property of cell density. For convection terms in the fluid velocity, cell density, and chemoattractant transport, a second-order semi-implicit discretization is employed, which strikes a balance between accuracy and computational efficiency. The marker-and-cell (MAC) mesh is used as finite difference spatial discretization, ensuring a discrete divergence-free velocity field, which simplifies the numerical analysis and helps preserve mass conservation [3,18,24,31].

A combination of singular logarithmic terms and system monotonicity enables a theoretical proof of unique solvability and positivity preservation. Consequently, total energy stability follows from a detailed energy estimate, and an optimal rate convergence is justified through higher-order asymptotic expansion and refined error analysis. To our knowledge, this is the first effort to design a second-order accurate scheme for the KSNS system that preserves all three theoretical properties, providing a solid foundation for future numerical modeling of chemotaxis-fluid interactions. This work lays the groundwork for more robust simulations of chemotaxis in complex fluid environments, facilitating the development of more accurate models for biological and biomedical applications.

The rest of the paper is organized as follows. In Section 2, we go over the mathematical model based on the Energetic Variational Approach (EnVarA). In Section 3, the numerical scheme is proposed. In Section 4, we prove the unique solvability, positivity-preserving property. The total energy stability is established in Section 5. In Section 6, an optimal rate convergence estimate is provided. Some numerical experiments are presented in Section 7. Finally, conclusions are drawn in Section 8.

2. Model derivation

2.1. Assumptions and notations

In this section, we focus on deriving the mathematical model that describes the dynamics of chemotaxis based on the EnVarA, which has been used in [30,35]. The beginning point is the following kinematic assumptions on the laws of conservation:

$$\begin{cases} \dfrac{\mathrm{D}n}{\mathrm{D}t} + \nabla \cdot \boldsymbol{j}_n = 0, & \text{(a)} \\ \dfrac{\mathrm{D}c}{\mathrm{D}t} = j_c, & \text{(b)} \\ \rho \dfrac{\mathrm{D}\boldsymbol{u}}{\mathrm{D}t} = \nabla \cdot \boldsymbol{\sigma}_\eta + \boldsymbol{F}, & \text{(c)} \\ \nabla \cdot \boldsymbol{u} = 0, & \text{(d)} \end{cases} \tag{2.1}$$

where equation (2.1a) is the conservation law of cell density, denoted by $n(x,t)$, and $\boldsymbol{j}_n$ represents the flux of cell density, equation (2.1b) stands for the L^2 type gradient flow dynamics of the chemo-attractant $c(x,t)$ and a phenomenological term j_c eventually takes the form of generalized diffusion. In the momentum equation (2.1c), $\boldsymbol{u}$ is the fluid velocity, ρ is the constant fluid density and $\boldsymbol{F}$ is the source term determined by the interaction among fluid, cell density and chemotaxis, and incompressible condition is stated as equation (2.1d). Notice that $\frac{\mathrm{D}f}{\mathrm{D}t} = \frac{\partial f}{\partial t} + (\boldsymbol{u} \cdot \nabla) f$ is the material derivative in system (2.1). To make the system closed, we choose the following boundary conditions

$$\boldsymbol{j}_n \cdot \boldsymbol{n}|_{\partial\Omega} = 0, \quad \boldsymbol{j}_c \cdot \boldsymbol{n}|_{\partial\Omega} = 0, \quad (\boldsymbol{u} \cdot \boldsymbol{n})|_{\partial\Omega} = \frac{(\boldsymbol{u} \cdot \tau)}{\partial \boldsymbol{n}}|_{\partial\Omega} = 0, \quad \boldsymbol{F} \cdot \boldsymbol{n}|_{\partial\Omega} = 0, \tag{2.2}$$

where $\boldsymbol{n}$ is the outward normal vector on the domain boundary $\partial\Omega$.

Next, we determine all the unknown variables $\boldsymbol{j}_n$, j_c, $\boldsymbol{\sigma}_\eta$ and $\boldsymbol{F}$ with the help of EnVarA. The total energy, which consists of kinetic, entropy, and phase-mixing energy, is given by

$$E_{total} = \int_\Omega \frac{\rho}{2}|\boldsymbol{u}|^2 \mathrm{d}\boldsymbol{x} + \int_\Omega n(\ln n - 1)\mathrm{d}\boldsymbol{x} - \int_\Omega nc\mathrm{d}\boldsymbol{x} + \frac{1}{2}\int_\Omega (|\nabla c|^2 + \alpha c^2)\mathrm{d}\boldsymbol{x}. \tag{2.3}$$

Moreover, the following total energy dissipation law is satisfied:

$$\frac{\mathrm{d}}{\mathrm{d}t} E_{total} = -Q, \tag{2.4}$$

where the dissipative functional Q consists of fluid friction and gradient of the chemical potential of the substance, defined as

$$Q = \int_\Omega 2\eta |\boldsymbol{D}_\eta|^2 \mathrm{d}\boldsymbol{x} + \int_\Omega n|\nabla \mu_n|^2 \mathrm{d}\boldsymbol{x} + \int_\Omega |\mu_c|^2 \mathrm{d}\boldsymbol{x}. \tag{2.5}$$

In more details, η is the fluid viscosity, $\boldsymbol{D}_\eta = \frac{\nabla \boldsymbol{u} + (\nabla \boldsymbol{u})^T}{2}$ is the rate of strain, μ_n and μ_c are the chemical potential for n and c, respectively.

In terms of the free energy, we are able to derive the chemical potentials

$$\mu_n = \frac{\delta E}{\delta n} = \ln n - c, \tag{2.6a}$$

$$\mu_c = \frac{\delta E}{\delta c} = -\Delta c + \alpha c - n. \tag{2.6b}$$

2.2. Governing equations

The detailed derivation is affiliated in Appendix A, by normalizing all relevant coefficients. A simplified system is available:

$$\begin{cases} n_t + \boldsymbol{u} \cdot \nabla n = \nabla \cdot (n \nabla \mu_n), & \text{(a)} \\ c_t + \boldsymbol{u} \cdot \nabla c = -\mu_c, & \text{(b)} \\ \boldsymbol{u}_t + \boldsymbol{u} \cdot \nabla \boldsymbol{u} + \nabla p = \Delta \boldsymbol{u} - (n \nabla \mu_n + c \nabla \mu_c), & \text{(c)} \\ \nabla \cdot \boldsymbol{u} = 0, & \text{(d)} \\ \mu_n = \delta_n E = \ln n - c, & \text{(e)} \\ \mu_c = \delta_c E = -\Delta c + \alpha c - n, & \text{(f)} \end{cases} \tag{2.7}$$

with the following boundary condition

$$\nabla n \cdot \boldsymbol{n}|_{\partial\Omega} = 0, \quad \nabla c \cdot \boldsymbol{n}|_{\partial\Omega} = 0, \quad \boldsymbol{u}|_{\partial\Omega} = 0, \quad \boldsymbol{F} \cdot \boldsymbol{n}|_{\partial\Omega} = 0.$$

The total energy dissipation law is satisfied:

$$\frac{\mathrm{d}}{\mathrm{d}t} E(\boldsymbol{u}, n, c) = \frac{\mathrm{d}}{\mathrm{d}t} \int_\Omega \left\{ n(\ln n - 1) - nc + \frac{1}{2}(|\nabla c|^2 + \alpha c^2) + \frac{1}{2}|\boldsymbol{u}|^2 \right\} \mathrm{d}\boldsymbol{x} = -\int_\Omega |\nabla \boldsymbol{u}|^2 \mathrm{d}\boldsymbol{x} - \int_\Omega n|\nabla \mu_n|^2 \mathrm{d}\boldsymbol{x} - \int_\Omega |\mu_c|^2 \mathrm{d}\boldsymbol{x} \le 0. \tag{2.8}$$

Remark 2.1. The periodic boundary condition could also be adopted in the above derivation, and similar equations could be obtained.

Remark 2.2. For a closed system composed by (2.1) and boundary condition (2.2), the local cell mass density is conservative, i.e.

$$\frac{\mathrm{d}}{\mathrm{d}t}\int_{\Omega} n\mathrm{d}\boldsymbol{x} = 0.$$

Remark 2.3. We have omitted the dimensionalization process, because the key point in our paper is the model derivation and the numerical analysis in the following sections, other than the effect of the parameters. Henceforth, for the convenience of mathematical analysis, we take all the unit physical parameters. The details of dimensionalization process are left to the interested readers.

3. The second order accurate numerical scheme

System (2.7) satisfies the energy dissipation in (2.8) and preserves the positivity of the cell density (for n). In this section, we develop a second order accurate numerical scheme, both in time and space, for the KSNS model. This scheme ensures unconditional total energy stability, meaning the total energy dissipation is independent of the time step, and it preserves the positivity of the cell density. This is achieved by employing the convex splitting approach, which has been widely used in the literature (see [32], [28], etc.).

3.1. The convex-concave decomposition of the free energy

The convex-concave decomposition of the free energy part is stated in the following lemma.

Lemma 3.1. *Suppose that $\Omega \in \mathbb{R}^d, d = 2, 3$ is a bounded domain, and $n, c : \Omega \to \mathbb{R}$ are sufficiently regular functions. Define the following energy functionals*

$$E_c[n,c] = \int_{\Omega} n(\ln n - 1) + \frac{1}{2}|\nabla c|^2 + \frac{\alpha}{2}c^2 + \frac{1}{2}(n-c)^2 \mathrm{d}\boldsymbol{x}, \quad E_e[n,c] = \int_{\Omega} \frac{1}{2}n^2 + \frac{1}{2}c^2 \mathrm{d}\boldsymbol{x}.$$

Then $E_c[n,c]$ and $E_e[n,c]$ are both convex with respect to n and c, with $E[n,c] = E_c[n,c] - E_e[n,c]$.

3.2. The finite difference spatial discretization

The numerical scheme is based on the equivalently reformulated system (2.7). For simplicity of presentation, a 2-D rectangular domain $\Omega = (0, L_x) \times (0, L_y)$ is considered, with $L_x = L_y = L > 0$. Let N be a positive integer such that $h = \frac{L}{N}$, which stands for the spatial mesh size. All the scalar variables, such as the cell density n, the chemo-attracted c, chemical potential μ_q (where q is taken as n or c for different equation), and pressure p, are evaluated at the cell-centered mesh points: $((i+\frac{1}{2})h, (j+\frac{1}{2})h)$, at the component-wise level. In this section, we use f to represent the scalar variable, and $\boldsymbol{w}$ as the vector variable. In turn, the discrete gradient of f is evaluated at the mesh points $(ih, (j+\frac{1}{2})h), ((i+\frac{1}{2})h, jh)$, respectively:

$$(D_x f)_{i,j+\frac{1}{2}} = \frac{f_{i+\frac{1}{2},j+\frac{1}{2}} - f_{i-\frac{1}{2},j+\frac{1}{2}}}{h}, \quad (D_y f)_{i+\frac{1}{2},j} = \frac{f_{i+\frac{1}{2},j+\frac{1}{2}} - f_{i+\frac{1}{2},j-\frac{1}{2}}}{h}.$$

Similarly, the wide-stencil differences for cell-centered functions could be introduced as

$$(\tilde{D}_x f)_{i+\frac{1}{2},j+\frac{1}{2}} = \frac{f_{i+\frac{3}{2},j+\frac{1}{2}} - f_{i-\frac{1}{2},j+\frac{1}{2}}}{2h}, \quad (\tilde{D}_y f)_{i+\frac{1}{2},j+\frac{1}{2}} = \frac{f_{i+\frac{1}{2},j+\frac{3}{2}} - f_{i+\frac{1}{2},j-\frac{1}{2}}}{2h}.$$

The Laplacian operator Δ is discretized using the standard five-point approximation. Meanwhile, a staggered grid is used for the velocity field, in which the individual components of a given velocity, say, $\boldsymbol{w} = (w^x, w^y)$, are defined at the east-west cell edge points $(ih, (j+\frac{1}{2})h)$, and the north-south cell edge points $((i+\frac{1}{2})h, jh)$, respectively. This staggered mesh is also known as the marker and cell (MAC) grid; it was first proposed in [19] to deal with the incompressible Navier-Stokes equations, and a detailed analysis has been provided in [14,38], etc.

The discrete divergence of $\boldsymbol{w} = (w^x, w^y)^T$ is defined at the cell center points $((i+\frac{1}{2})h, (j+\frac{1}{2})h)$ as follows:

$$(\nabla_h \cdot \boldsymbol{w})_{i+\frac{1}{2},j+\frac{1}{2}} := (D_x w^x)_{i+\frac{1}{2},j+\frac{1}{2}} + (D_y w^y)_{i+\frac{1}{2},j+\frac{1}{2}}.$$

One key advantage of the MAC grid approach is that the discrete divergence of the velocity vector will always be identically zero at every cell center point. Such a divergence-free property comes from the special structure of the MAC grid and assures that the velocity field is ℓ^2-orthogonal to the corresponding pressure gradient at the discrete level; also see the related reference work [14].

For $\boldsymbol{u} = (u^x, u^y)^T$, $\boldsymbol{w} = (w^x, w^y)$, evaluated at the staggered mesh points $(x_i, y_{j+\frac{1}{2}})$, $(x_{i+\frac{1}{2}}, y_j)$, respectively, and the cell-centered variable f, the following terms are computed as

$$\boldsymbol{u}\cdot\nabla_h\boldsymbol{w}=\begin{pmatrix} u^x_{i,j+\frac12}\tilde{D}_x w^x_{i,j+\frac12}+\mathcal{A}_{xy}u^y_{i,j+\frac12}\tilde{D}_y w^x_{i,j+\frac12} \\ \mathcal{A}_{xy}u^x_{i+\frac12,j}\tilde{D}_x w^y_{i+\frac12,j}+u^y_{i+\frac12,j}\tilde{D}y w^y_{i+\frac12,j}\end{pmatrix},\quad \nabla\cdot(\boldsymbol{w}\boldsymbol{u}^T)=\begin{pmatrix}\tilde{D}_x(u^x w^x)_{i,j+\frac12}+\tilde{D}_y(\mathcal{A}_{xy}u^y w^x)_{i,j+\frac12}\\ \tilde{D}_x(\mathcal{A}_{xy}u^x w^y)_{i+\frac12,j}+\tilde{D}_y(u^y w^y)_{i+\frac12,j}\end{pmatrix},$$

$$\mathcal{A}_h f\nabla_h\mu=\begin{pmatrix}\left((D_x\mu\cdot\mathcal{A}_x f)_{i,j+\frac12}\right)_{i,j+\frac12}\\ \left((D_y\mu\cdot\mathcal{A}_y f)_{i+\frac12,j}\right)_{i+\frac12,j}\end{pmatrix},\quad \nabla_h\cdot(\mathcal{A}_h f\boldsymbol{u})=D_x(u^x\mathcal{A}_x f)_{i+\frac12,j+\frac12}+D_y(u^y\mathcal{A}_y f)_{i+\frac12,j+\frac12},$$

in which the averaging operators have been employed:

$$\mathcal{A}_{xy}u^x_{i+\frac12,j}=\frac14\left(u^x_{i,j-\frac12}+u^x_{i,j+\frac12}+u^x_{i+1,j-\frac12}+u^x_{i+1,j+\frac12}\right),\quad \mathcal{A}_x f_{i,j+\frac12}=\frac12\left(f_{i-\frac12,j+\frac12}+f_{i+\frac12,j+\frac12}\right).$$

A few other average terms, such as $\mathcal{A}_{xy}u^y_{i,j+\frac12}$, $\mathcal{A}_y f_{i+\frac12,j}$, could be defined in the same manner.

Definition 3.1. For any pair of variables u^a, u^b which are evaluated at the mesh points $(i,j+\frac12)$, the discrete ℓ^2-inner product is defined by

$$\langle u^a,u^b\rangle_A=h^2\sum_{j=1}^{N}\sum_{i=1}^{N}u^a_{i,j+\frac12}u^b_{i,j+\frac12}.$$

For any pair of variables v^a, v^b which are evaluated at the mesh points $(i+\frac12,j)$, the discrete ℓ^2-inner product is defined by

$$\langle v^a,v^b\rangle_B=h^2\sum_{j=1}^{N}\sum_{i=1}^{N}v^a_{i+\frac12,j}v^b_{i+\frac12,j}.$$

For any pair of variables f^a, f^b which are evaluated at the mesh points $(i+\frac12,j+\frac12)$, the discrete ℓ^2-inner product is defined by

$$\langle f^a,f^b\rangle_C=h^2\sum_{j=1}^{N}\sum_{i=1}^{N}f^a_{i+\frac12,j+\frac12}f^b_{i+\frac12,j+\frac12}.$$

In addition, for two velocity vector $\boldsymbol{u}=(u^x,u^y)^T$ and $\boldsymbol{w}=(w^x,w^y)^T$, we denote their vector inner product as

$$\langle\boldsymbol{u},\boldsymbol{w}\rangle_1=\langle u^x,w^x\rangle_A+\langle u^y,w^y\rangle_B.$$

The associated ℓ^2 norms, namely $\|\cdot\|_2$ norm, can be accordingly defined. It is clear that all the discrete ℓ^2 inner products defined above are second order accurate. In addition to the standard ℓ^2 norm, we also introduce the $\ell^p, 1\le p\le\infty$, and ℓ^∞ norms for a grid function f evaluated at mesh points $(i+\frac12,j+\frac12)$:

$$\|f\|_\infty:=\max_{i,j}|f_{i+\frac12,j+\frac12}|,\quad \|f\|_p:=\left(h^2\sum_{i,j=1}^{N}|f_{i+\frac12,j+\frac12}|^p\right)^{\frac1p},\quad 1\le p<+\infty.$$

Meanwhile, the discrete average is denoted as $\overline{f}:=\frac{1}{|\Omega|}\langle f,\mathbf{1}\rangle_C$, for any cell centered function f. For the convenience of the later analysis, an $\langle\cdot,\cdot\rangle_{-1,h}$ inner product and $\|\cdot\|_{-1,h}$, norm need to be introduced, for any $\varphi\in\mathring{C}_\Omega:=\left\{f\,|\langle f,\mathbf{1}\rangle_C\right\}=0$:

$$\langle\varphi_1,\varphi_2\rangle_{-1,h}=\langle\varphi_1,(-\Delta_h)^{-1}\varphi_2\rangle_C,\quad \|\varphi\|_{-1,h}=(\langle\varphi,(-\Delta_h)^{-1}(\varphi)\rangle_C)^{\frac12},$$

where the operator Δ_h is equipped with either periodic or discrete homogeneous Neumann boundary condition.

Lemma 3.2. *[4,5] For two discrete grid vector functions $\boldsymbol{u}=(u^x,u^y)$, $\boldsymbol{w}=(w^x,w^y)$, where u^x,u^y and w^x,w^y are defined on east-west and north-south respectively, and two cell centered functions f,g, the following identities are valid, if $\boldsymbol{u},\boldsymbol{w}$ are implemented with free slip boundary condition and homogeneous Neumann boundary condition is imposed for f and g:*

$$\langle\boldsymbol{w},\boldsymbol{u}\cdot\nabla_h\boldsymbol{w}\rangle_1+\langle\boldsymbol{w},\nabla_h\cdot(\boldsymbol{w}\boldsymbol{u}^T)\rangle_1=0, \tag{3.1a}$$

$$\langle\boldsymbol{u},\nabla_h f\rangle_1=0,\quad \textit{if}\quad \nabla_h\cdot\boldsymbol{u}=0, \tag{3.1b}$$

$$-\langle\boldsymbol{w},\Delta_h\boldsymbol{w}\rangle_C=\|\nabla_h\boldsymbol{w}\|_2^2, \tag{3.1c}$$

$$-\langle f,\Delta_h f\rangle_C=\|\nabla_h f\|_2^2, \tag{3.1d}$$

$$-\langle g,\nabla_h\cdot(\mathcal{A}_h f\boldsymbol{u})\rangle_C=\langle\boldsymbol{u},\mathcal{A}_h f\nabla_h g\rangle_1. \tag{3.1e}$$

The same conclusion is true if all the variables are equipped with periodic boundary conditions.

The following Poincaré-type inequality will be useful in the later analysis.

Proposition 3.1. *1. There are constants $C_0, \breve{C}_0 > 0$, independent of $h > 0$, such that $\|f\|_2 \le C_0\|\nabla_h f\|_2$, $\|f\|_{-1,h} \le C_0\|f\|_2$, $\|f\|_2 \le \breve{C}_0 h^{-1}\|f\|_{-1,h}$, for all $f \in \mathring{\mathcal{C}}_\Omega := \{f | \langle f, 1\rangle_C = 0\}$.*

2. For a velocity vector $\boldsymbol{w}$, with a discrete no-penetration boundary condition $\boldsymbol{w}\cdot\boldsymbol{n} = 0$ on $\partial\Omega$, a similar Poincaré inequality is also valid: $\|\boldsymbol{w}\|_2 \le C_0\|\nabla_h \boldsymbol{w}\|_2$, which C_0 only dependent on Ω.

3.3. The fully discrete numerical scheme

Suppose $(\boldsymbol{u}^m, p^m, n^m, c^m)$ are given, we solve $\left(\boldsymbol{u}^{m+1}, p^{m+1}, n^{m+1}, c^{m+1}\right)$ by the following modified Crank-Nicolson scheme [31,17]:

$$\frac{\hat{\boldsymbol{u}}^{m+1} - \boldsymbol{u}^m}{\tau} + \frac{1}{2}(\tilde{\boldsymbol{u}}^{m+\frac12}\cdot\nabla_h\hat{\boldsymbol{u}}^{m+\frac12} + \nabla_h\cdot(\hat{\boldsymbol{u}}^{m+\frac12}(\tilde{\boldsymbol{u}}^{m+\frac12})^T)) - \Delta_h\hat{\boldsymbol{u}}^{m+\frac12} + \nabla_h p^m = -(\mathcal{A}_h\tilde{n}^{m+\frac12}\nabla_h\mu_n^{m+\frac12} + \mathcal{A}_h\tilde{c}^{m+\frac12}\nabla_h\mu_c^{m+\frac12}), \tag{3.2a}$$

$$\frac{n^{m+1} - n^m}{\tau} + \nabla_h\cdot(\mathcal{A}_h\tilde{n}^{m+\frac12}\hat{\boldsymbol{u}}^{m+\frac12}) = \nabla_h\cdot(\breve{n}^{m+\frac12}\nabla_h\mu_n^{m+\frac12}), \tag{3.2b}$$

$$\frac{c^{m+1} - c^m}{\tau} + \nabla_h\cdot(\mathcal{A}_h\tilde{c}^{m+\frac12}\hat{\boldsymbol{u}}^{m+\frac12}) = -\mu_c^{m+\frac12}, \tag{3.2c}$$

$$\mu_n^{m+\frac12} = \frac{n^{m+1}\ln n^{m+1} - n^m\ln n^m}{n^{m+1} - n^m} - 1 + \tau\ln\frac{n^{m+1}}{n^m} + n^{m+\frac12} - c^{m+\frac12} - \tilde{n}^{m+\frac12}, \tag{3.2d}$$

$$\mu_c^{m+\frac12} = -\Delta_h c^{m+\frac12,*} + \alpha c^{m+\frac12} - n^{m+\frac12} + c^{m+\frac12} - \tilde{c}^{m+\frac12}, \tag{3.2e}$$

$$\frac{\boldsymbol{u}^{m+1} - \hat{\boldsymbol{u}}^{m+1}}{\tau} + \frac12\nabla_h(p^{m+1} - p^m) = 0, \tag{3.2f}$$

$$\nabla_h\cdot\boldsymbol{u}^{m+1} = 0, \tag{3.2g}$$

where

$$\tilde{\boldsymbol{u}}^{m+\frac12} := \frac32\boldsymbol{u}^m - \frac12\boldsymbol{u}^{m-1},\quad \hat{\boldsymbol{u}}^{m+\frac12} := \frac12\hat{\boldsymbol{u}}^{m+1} + \frac12\boldsymbol{u}^m,\quad \tilde{n}^{m+\frac12} := \frac32 n^m - \frac12 n^{m-1},\quad n^{m+\frac12} := \frac12(n^{m+1} + n^m),$$

$$\tilde{c}^{m+\frac12} := \frac32 c^m - \frac12 c^{m-1},\quad c^{m+\frac12} := \frac12(c^{m+1} + c^m),\quad c^{m+\frac12,*} := \frac34 c^{m+1} + \frac14 c^{m-1},$$

$$\breve{n}^{m+\frac12}_{i+\frac12,j} := \begin{cases} \mathcal{A}_x\tilde{n}^{m+\frac12}_{i+\frac12,j}, & \text{if } \mathcal{A}_x\tilde{n}^{m+\frac12}_{i+\frac12,j} > 0,\\ ((\mathcal{A}_x\tilde{n}^{m+\frac12}_{i+\frac12,j})^2 + \tau^8)^{\frac12}, & \text{if } \mathcal{A}_x\tilde{n}^{m+\frac12}_{i+\frac12,j} \le 0,\end{cases} \quad \breve{n}^{m+\frac12}_{i,j+\frac12} := \begin{cases} \mathcal{A}_y\tilde{n}^{m+\frac12}_{i,j+\frac12}, & \text{if } \mathcal{A}_y\tilde{n}^{m+\frac12}_{i,j+\frac12} > 0,\\ ((\mathcal{A}_y\tilde{n}^{m+\frac12}_{i,j+\frac12})^2 + \tau^8)^{\frac12}, & \text{if } \mathcal{A}_y\tilde{n}^{m+\frac12}_{i,j+\frac12} \le 0,\end{cases}$$

with either periodic boundary condition, or the discrete physical boundary condition:

$$(\hat{\boldsymbol{u}}^{m+1}\cdot\boldsymbol{n})|_\Gamma = 0,\quad (\nabla_h(\hat{\boldsymbol{u}}^{m+1}\cdot\boldsymbol{\tau})\cdot\boldsymbol{n})|_\Gamma = 0,\quad \boldsymbol{u}^{m+1}\cdot\boldsymbol{n}|_\Gamma = 0,\quad (\nabla p^{m+1}\cdot\boldsymbol{n})|_\Gamma = 0,$$

$$\partial_{\boldsymbol{n}} n^{m+1}|_\Gamma = \partial_{\boldsymbol{n}} c^{m+1}|_\Gamma = 0,\quad \partial_{\boldsymbol{n}}\mu_n^{m+\frac12}|_\Gamma = \partial_{\boldsymbol{n}}\mu_c^{m+\frac12}|_\Gamma = 0.$$

Remark 3.1. At the initial time step, we can inversely evaluate the system of partial differential equations to obtain locally second-order accurate approximations to n^{-1}, c^{-1} and $\boldsymbol{u}^{-1}$. In turn, the numerical implementation of the proposed algorithm (3.2) results in a second-order local truncation error at $m = 0$.

Remark 3.2. It is clear that the mass conservation identity is valid for the cell density variable:

$$\overline{n^{m+1}} = \overline{n^m} = \cdots = \overline{n^0}.$$

To simplify the notation in the later analysis, the following smooth function is introduced:

$$F_a(x) := \frac{G(x) - G(a)}{x - a},\ G(x) = x\ln x,\ \text{for any fixed } a > 0.$$

This notation leads to a rewritten form of (3.2d):

$$\mu_n^{m+\frac12} = F_{n^m}(n^{m+1}) - 1 + \tau(\ln n^{m+1} - \ln n^m) + n^{m+\frac12} - c^{m+\frac12} - \tilde{n}^{m+\frac12}.$$

Lemma 3.3. *[4,6,28] Let $a > 0$ be fixed, then*

1. $F_a'(x) = \frac{G'(x)(x-a)-(G(x)-G(a))}{(x-a)^2} \geq 0$, *for any* $x > 0$.
2. $F_a(x)$ *is an increasing function of* x, *and* $F_a(x) \leq F_a(a) = \ln a + 1$ *for any* $0 < x < a$.

Remark 3.3. The modified Crank-Nicolson approximation of the nonlinear logarithmic term, denoted as $G^1_{n^m}(n^{m+1})$, ensures that its inner product with $n^{m+1} - n^m$ exactly corresponds to the difference in logarithmic energy between consecutive time steps. This property greatly simplifies the energy stability analysis, as will be derived in later sections. However, a key challenge arises in proving the positivity-preserving property, as the proposed nonlinear approximation lacks singularity when $n^{m+1} \to 0$. To address this difficulty, we introduce a nonlinear regularization term, $\tau(\ln n^{m+1} - \ln n^m)$. While this term is of order $O(\tau^2)$, it brings a singularity as $n^{m+1} \to 0$, which is essential to establish a theoretical proof of positivity preservation for the proposed numerical scheme (3.2a)-(3.2g).

4. The positivity-preserving property and unique solvability

Since the implicit part of the numerical scheme (3.2) corresponds to a monotone, singular, non-symmetric nonlinear system, a three-step procedure is required to establish its unique solvability and positivity-preserving analysis.

Step 1: A connection between $(n^{m+1}, c^{m+1}, \hat{\boldsymbol{u}}^{m+1})$ and $(\mu_n^{m+\frac{1}{2}}, \mu_c^{m+\frac{1}{2}})$ is needed.
First, the following equivalent form of (3.2a) is observed:

$$\begin{aligned}&\frac{2\hat{\boldsymbol{u}}^{m+\frac{1}{2}} - 2\boldsymbol{u}^m}{\tau} + \frac{1}{2}\left(\tilde{\boldsymbol{u}}^{m+\frac{1}{2}} \cdot \nabla_h \hat{\boldsymbol{u}}^{m+\frac{1}{2}} + \nabla_h \cdot \left(\hat{\boldsymbol{u}}^{m+\frac{1}{2}} (\tilde{\boldsymbol{u}}^{m+\frac{1}{2}})^T\right)\right) + \nabla_h p^m - \Delta_h \hat{\boldsymbol{u}}^{m+\frac{1}{2}} \\ &\qquad = -\mathcal{A}_h \tilde{n}^{m+\frac{1}{2}} \nabla_h \mu_n^{m+\frac{1}{2}} - \mathcal{A}_h \tilde{c}^{m+\frac{1}{2}} \nabla_h \mu_c^{m+\frac{1}{2}}, \end{aligned} \tag{4.1a}$$

$$\hat{\boldsymbol{u}}^{m+1} = 2\hat{\boldsymbol{u}}^{m+\frac{1}{2}} - \boldsymbol{u}^m. \tag{4.1b}$$

For any specified field (μ_n, μ_c), the velocity vector $\boldsymbol{w} = \mathcal{L}_h^{NC}(\mu_n, \mu_c)$ is uniquely determined as the solution to the following discrete convection-diffusion equation:

$$\frac{2\boldsymbol{w} - 2\boldsymbol{u}^m}{\tau} + \frac{1}{2}\left(\tilde{\boldsymbol{u}}^{m+\frac{1}{2}} \cdot \nabla_h \boldsymbol{w} + \nabla_h \cdot (\boldsymbol{w}(\tilde{\boldsymbol{u}}^{m+\frac{1}{2}})^T)\right) + \nabla_h p^m - \Delta_h \boldsymbol{w} = -\mathcal{A}_h \tilde{n}^{m+\frac{1}{2}} \nabla_h \mu_n^{m+\frac{1}{2}} - \mathcal{A}_h \tilde{c}^{m+\frac{1}{2}} \nabla_h \mu_c^{m+\frac{1}{2}}. \tag{4.2}$$

Next, the intermediate velocity is computed as $\hat{\boldsymbol{u}}^{m+\frac{1}{2}} = \mathcal{L}_h^{NC}(\mu_n^{m+\frac{1}{2}}, \mu_c^{m+\frac{1}{2}})$ and is then used together with formula (4.1b) to obtain $\hat{\boldsymbol{u}}^{m+1}$. Moreover, $\boldsymbol{u}^{m+1}$ is derived by applying the discrete Helmholtz projection to $\hat{\boldsymbol{u}}^{m+1}$ so that it belongs to the divergence-free space, as indicated by (3.2f) and (3.2g).

Second, a substitution of $\hat{\boldsymbol{u}}^{m+\frac{1}{2}} = \mathcal{L}_h^{NC}(\mu_n^{m+\frac{1}{2}}, \mu_c^{m+\frac{1}{2}})$ into (3.2b) and (3.2c) yields

$$\frac{n^{m+1} - n^m}{\tau} + \nabla_h \cdot (\mathcal{A}_h \tilde{n}^{m+\frac{1}{2}} \mathcal{L}_h^{NC}(\mu_n^{m+\frac{1}{2}}, \mu_c^{m+\frac{1}{2}})) = \nabla_h \cdot (\check{n}^{m+\frac{1}{2}} \nabla_h \mu_n^{m+\frac{1}{2}}), \tag{4.3a}$$

$$\frac{c^{m+1} - c^m}{\tau} + \nabla_h \cdot (\mathcal{A}_h \tilde{c}^{m+\frac{1}{2}} \mathcal{L}_h^{NC}(\mu_n^{m+\frac{1}{2}}, \mu_c^{m+\frac{1}{2}})) = -\mu_c^{m+\frac{1}{2}}. \tag{4.3b}$$

In turn, we define $\boldsymbol{\mu} = (\mu_n, \mu_c)$, $\boldsymbol{\psi} = (n, c)$ and $\mathcal{L}_h^{NC} : 2\mathbb{R}^{N^2} \to 2\mathbb{R}^{N^2}$ as

$$\mathcal{L}_h^N(\mu_n) = \nabla_h \cdot \left(\mathcal{A}_h \tilde{n}^{m+\frac{1}{2}} \mathcal{L}_h^{NC}(\boldsymbol{\mu})\right) - \nabla_h \cdot (\check{n}^{m+\frac{1}{2}} \nabla_h \mu_n), \quad \mathcal{L}_h^C(\mu_c) = \nabla_h \cdot \left(\mathcal{A}_h \tilde{c}^{m+\frac{1}{2}} \mathcal{L}_h^{NC}(\boldsymbol{\mu})\right) + \mu_c.$$

For brevity, the above system is reformulated as

$$\mathcal{L}_h^{NC}(\boldsymbol{\mu}) = \nabla_h \cdot \left(\mathcal{A}_h \tilde{\boldsymbol{\psi}}^{m+\frac{1}{2}} \mathcal{L}_h^{NC}(\boldsymbol{\mu})\right) + M\boldsymbol{\mu}, \quad M = \begin{pmatrix} -\nabla_h \cdot (\check{n}^{m+\frac{1}{2}}) \nabla_h \\ \boldsymbol{I} \end{pmatrix}. \tag{4.4}$$

Since $\mathcal{L}_h^{NC}$ is a linear operator satisfying either periodic or homogeneous Neumann boundary conditions, an alternative form of (4.3) can be expressed as:

$$\frac{\boldsymbol{\psi}^{m+1} - \boldsymbol{\psi}^m}{\tau} = -\mathcal{L}_h^{NC}(\boldsymbol{\mu}^{m+\frac{1}{2}}). \tag{4.5}$$

Step 2: Prove that the operator $\mathcal{L}_h^{NC}$ is invertible, ensuring that $(\mathcal{L}_h^{NC})^{-1}$ is well defined. Using an approach similar to that in [5], we subsequently establish the following two properties of $\mathcal{L}_h^{NC}$.

Lemma 4.1. *The linear operator* $\mathcal{L}_h^{NC}$ *preserves the monotonicity estimate:*

$$\langle \mathcal{L}_h^{NC}(\boldsymbol{\mu}_1) - \mathcal{L}_h^{NC}(\boldsymbol{\mu}_2), \boldsymbol{\mu}_1 - \boldsymbol{\mu}_2 \rangle_C \geq \| \sqrt{\tilde{n}^{m+\frac{1}{2}}} \nabla_h (\mu_{n,1} - \mu_{n,2}) \|_2^2 + \| \mu_{c,1} - \mu_{c,2} \|_2^2 \geq 0, \tag{4.6}$$

for any $\boldsymbol{\mu}_1, \boldsymbol{\mu}_2$. *As a result, the operator* $\mathcal{L}_h^{NC}$ *is invertible.*

Proof. For any given $\boldsymbol{\mu}_1$, $\boldsymbol{\mu}_2$, define their difference as $\boldsymbol{\mu}_D := \boldsymbol{\mu}_1 - \boldsymbol{\mu}_2$. Owing to the linearity of $\mathcal{L}_h^{NC}$, it follows that:

$$\mathcal{L}_h^{NC}(\boldsymbol{\mu}_1) - \mathcal{L}_h^{NC}(\boldsymbol{\mu}_2) = \mathcal{L}_h^{NC}(\boldsymbol{\mu}_D) = \nabla_h \cdot \left(\mathcal{A}_h \tilde{\boldsymbol{\psi}}^{m+\frac{1}{2}} \mathcal{L}_h^{NC}(\boldsymbol{\mu}_D)\right) + M\boldsymbol{\mu}_D. \tag{4.7}$$

Taking the discrete inner product with (4.7) by $\boldsymbol{\mu}_D$ yields

$$\langle \mathcal{L}_h^{NC}(\boldsymbol{\mu}_D), \boldsymbol{\mu}_D\rangle_C = -\langle \mathcal{A}_h \tilde{\boldsymbol{\psi}}^{m+\frac{1}{2}} \mathcal{L}_h^{NC}(\boldsymbol{\mu}_D), \nabla_h \boldsymbol{\mu}_D\rangle_1 + \langle M\boldsymbol{\mu}_D, \boldsymbol{\mu}_D\rangle_1 = -\langle \mathcal{A}_h \tilde{\boldsymbol{\psi}}^{m+\frac{1}{2}} \nabla_h \boldsymbol{\mu}_D, \mathcal{L}_h^{NC}(\boldsymbol{\mu}_D)\rangle_1 + \langle M\boldsymbol{\mu}_D, \boldsymbol{\mu}_D\rangle_1. \tag{4.8}$$

Moreover, define $\boldsymbol{w}_j := \mathcal{L}_h^{NC}(\boldsymbol{\mu}_j), j = 1, 2$, and set $\boldsymbol{w}_D := \boldsymbol{w}_1 - \boldsymbol{w}_2 = \mathcal{L}_h^{NC}(\boldsymbol{\mu}_D)$ by the linearity of $\mathcal{L}_h^{NC}$. In addition, the definition of $\mathcal{L}_h^{NC}$ in (4.2) shows that

$$\frac{2\boldsymbol{w}_D}{\tau} + \frac{1}{2}\left(\tilde{\boldsymbol{u}}^{m+\frac{1}{2}} \cdot \nabla_h \boldsymbol{w}_D + \nabla_h \cdot (\boldsymbol{w}_D(\tilde{\boldsymbol{u}}^{m+\frac{1}{2}})^T)\right) - \Delta_h \boldsymbol{w}_D + \mathcal{A}_h \tilde{n}^{m+\frac{1}{2}} \nabla_h \mu_{n,D}^{m+\frac{1}{2}} + \mathcal{A}_h \tilde{c}^{m+\frac{1}{2}} \nabla_h \mu_{c,D}^{m+\frac{1}{2}} = 0. \tag{4.9}$$

Since the non-homogeneous source terms $\frac{\boldsymbol{u}^m}{\tau}$ and $\nabla_h p^m$ cancel out in this difference equation, taking the discrete inner product with (4.9) by $\boldsymbol{w}_D = \mathcal{L}_h^{NC}(\boldsymbol{\mu}_D)$ results in

$$\frac{2}{\tau}\|\boldsymbol{w}_D\|_2^2 + \|\nabla_h \boldsymbol{w}_D\|_2^2 + \langle \mathcal{A}_h \tilde{\boldsymbol{\psi}}^{m+\frac{1}{2}} \nabla_h \boldsymbol{\mu}_D, \mathcal{L}_h^{NC}(\boldsymbol{\mu}_D)\rangle_1 = 0, \tag{4.10}$$

in which the following identities have been used:

$$\langle \tilde{\boldsymbol{\mu}}^{m+\frac{1}{2}} \cdot \nabla_h \boldsymbol{w}_D + \nabla_h \cdot \left(\boldsymbol{w}_D(\tilde{\boldsymbol{u}}^{m+\frac{1}{2}})\right)^T, \boldsymbol{w}_D\rangle_1 = 0, \quad -(\boldsymbol{w}_D, \Delta_h \boldsymbol{w}_D) = \|\nabla_h \boldsymbol{w}_D\|_2^2.$$

A combination of (4.10) and (4.8) results in

$$\langle \mathcal{L}_h^{NC}(\boldsymbol{\mu}_D), \boldsymbol{\mu}_D\rangle_C = \frac{2}{\tau}\|\tilde{\boldsymbol{w}}\|_2^2 + \|\nabla_h \tilde{\boldsymbol{w}}\|_2^2 + \langle M\boldsymbol{\mu}_D, \boldsymbol{\mu}_D\rangle_1, \tag{4.11a}$$

$$\langle M\boldsymbol{\mu}_D, \boldsymbol{\mu}_D\rangle_1 = \left\langle \begin{pmatrix} -\nabla_h \cdot (\check{n}^{m+\frac{1}{2}}) \nabla_h \mu_{n,D} \\ \mu_{c,D} \end{pmatrix}, (\mu_{n,D}, \mu_{c,D}) \right\rangle = \|\sqrt{\check{n}^{m+\frac{1}{2}}} \nabla_h \mu_{n,D}\|_2^2 + \|\mu_{c,D}\|_2^2, \tag{4.11b}$$

or equivalently,

$$\langle \mathcal{L}_h^{NC}(\boldsymbol{\mu}_1) - \mathcal{L}_h^{NC}(\boldsymbol{\mu}_2), \boldsymbol{\mu}_1 - \boldsymbol{\mu}_2\rangle_C = \langle \mathcal{L}_h^{NC}(\boldsymbol{\mu}_D), \boldsymbol{\mu}_D\rangle_C \geq \|\sqrt{\check{n}^{m+\frac{1}{2}}} \nabla_h(\mu_{n,1} - \mu_{n,2})\|_2^2 + \|\mu_{c,1} - \mu_{c,2}\|_2^2 \geq 0,$$

so that (4.6) has been proved. The proof of Lemma 4.1 is completed. □

Because $\mathcal{L}_h^{NC}$ maps $2\mathbb{R}^{N^2}$ into itself, its inverse $(\mathcal{L}_h^{NC})^{-1}$ does as well. Consequently, by Lemma 4.1, the following monotonicity analysis holds.

Proposition 4.1. *The linear operator $(\mathcal{L}_h^{NC})^{-1}$ also preserves the monotonicity estimate:*

$$\langle (\mathcal{L}_h^{NC})^{-1}(\boldsymbol{\psi}_1) - (\mathcal{L}_h^{NC})^{-1}(\boldsymbol{\psi}_2), \boldsymbol{\psi}_1 - \boldsymbol{\psi}_2\rangle_C \geq C_1^2 \|(\mathcal{L}_h^{NC})^{-1}(\boldsymbol{\psi}_1 - \boldsymbol{\psi}_2)\|_2^2 \geq 0,$$

for any $\boldsymbol{\psi}_1, \boldsymbol{\psi}_2$. In fact, the constant C is related to the minimum of $\check{n}^{m+\frac{1}{2}}$, and the discrete Poincaré regularity condition: $\|\nabla_h f\|_2 \geq C_0^{-1}\|f\|_2$, which holds for every function f satisfying $\overline{f} = 0$, as stated in Proposition 3.1.

Proof. We denote $\boldsymbol{\mu} = (\mathcal{L}_h^{NC})^{-1}(\boldsymbol{\psi})$, an equivalent statement of $\boldsymbol{\psi} = \mathcal{L}_h^{NC}(\boldsymbol{\mu})$. Therefore, an application of (4.6) implies that

$$\begin{aligned}
\langle (\mathcal{L}_h^{NC})^{-1}(\boldsymbol{\psi}_1) - (\mathcal{L}_h^{NC})^{-1}(\boldsymbol{\psi}_2), \boldsymbol{\psi}_1 - \boldsymbol{\psi}_2\rangle_C &= \langle \mathcal{L}_h^{NC}(\boldsymbol{\mu}_1) - \mathcal{L}_h^{NC}(\boldsymbol{\mu}_2), \boldsymbol{\mu}_1 - \boldsymbol{\mu}_2\rangle_C \\
&\geq \|\sqrt{\check{n}^{m+\frac{1}{2}}} \nabla_h(\mu_{n,1} - \mu_{n,2})\|_2^2 + \|\mu_{c,1} - \mu_{c,2}\|_2^2 \geq C_1^2 \|\mu_{n,1} - \mu_{n,2}\|_2^2 + \|\mu_{c,1} - \mu_{c,2}\|_2^2 \\
&\geq C_1^2 \|\boldsymbol{\mu}_1 - \boldsymbol{\mu}_2\|_2^2 = C_1^2 \|(\mathcal{L}_h^{NC})^{-1}(\boldsymbol{\psi}_1 - \boldsymbol{\psi}_2)\|_2^2 \geq 0,
\end{aligned}$$

with $C_1 = \min\{\min\{\sqrt{\check{n}^{m+\frac{1}{2}}} C_0^{-1}\}, 1\} C_0^{-1}$. The proof of Proposition 4.1 is finished. □

Based on the construction (4.2) and the definition (4.4) for $\mathcal{L}_h^{NC}$, the following homogenization formula will be helpful in the later analysis:

$$\mathcal{L}_h^{NC}(\boldsymbol{\mu}) = \mathcal{L}_{h,1}^{NC}(\boldsymbol{\mu}) + \mathcal{L}_{h,2}^{NC}, \quad \mathcal{L}_{h,2}^{NC} = \nabla_h \cdot \left(\mathcal{A}_h \tilde{\boldsymbol{\psi}}^{m+\frac{1}{2}} (\boldsymbol{u}^m - \frac{\tau}{2} \nabla_h p^m)\right), \tag{4.12}$$

for any $\overline{\mu}_n = 0$, and $\mathcal{L}_{h,1}^{NC}$ denotes a homogeneous linear operator. In particular, it satisfies the linearity property, unlike the operator $\mathcal{L}_h^{NC}$ defined in (4.2). In addition, the following $\|\cdot\|_2$ bound could always be assumed for the non-homogeneous source term, dependent on the numerical solution at the previous time steps:

$$\|\mathcal{L}_{h,2}^{NC}\|_2 \le A^*. \tag{4.13}$$

Proposition 4.2. *For any n with $\overline{n} = 0$, the following $\|\cdot\|_2$ bound is valid:*

$$\|(\mathcal{L}_h^{NC})^{-1}(\boldsymbol{\psi})\|_2 \le C_1^{-2}\left(\|\boldsymbol{\psi}\|_2 + A^*\right). \tag{4.14}$$

Proof. We denote $\boldsymbol{\mu} = (\mathcal{L}_h^{NC})^{-1}(\boldsymbol{\psi})$, for any $\boldsymbol{\psi}$ with $\overline{n} = 0$. The homogenization decomposition (4.12) implies that $\mathcal{L}_h^{NC}(\boldsymbol{\mu}) = \boldsymbol{\psi}_D := \boldsymbol{\psi} - \mathcal{L}_{h,2}^{NC}$. On the other hand, the monotonicity estimate (4.6) indicates that

$$\langle \mathcal{L}_{h,1}^{NC}(\boldsymbol{\mu}), \boldsymbol{\mu}\rangle_C \ge C_1^2\|\boldsymbol{\mu}\|_2^2, \quad \text{so that} \quad \|\boldsymbol{\mu}\|_2^2 \le C_1^{-2}\langle \mathcal{L}_{h,1}^{NC}(\boldsymbol{\mu}), \boldsymbol{\mu}\rangle_C \le C_1^{-2}\|\mathcal{L}_{h,1}^{NC}(\boldsymbol{\mu})\|_2 \cdot \|\boldsymbol{\mu}\|_2, \quad \|\boldsymbol{\mu}\|_2 \le C_1^{-2}\|\mathcal{L}_{h,1}^{NC}(\boldsymbol{\mu})\|_2,$$

with an application of Cauchy inequality. Therefore, the following inequality is available:

$$\|(\mathcal{L}_h^{NC})^{-1}(\boldsymbol{\psi})\|_2 = \|\boldsymbol{\mu}\|_2 \le C_1^{-2}\|\mathcal{L}_{h,1}^{NC}(\boldsymbol{\mu})\|_2 = C_1^{-2}\|\boldsymbol{\psi} - \mathcal{L}_{h,2}^{NC}\|_2 \le C_1^{-2}\left(\|\boldsymbol{\psi}\|_2 + \|\mathcal{L}_{h,2}^{NC}\|_2\right).$$

The proof of Proposition 4.2 is completed. □

Based on (4.3) and (4.4), (4.5), we conclude that the numerical solution (3.2b)-(3.2f) could be equivalently represented as the following nonlinear system, in terms of $\boldsymbol{\psi}^{m+1}$:

$$\begin{aligned}
&\boldsymbol{\mu}^{m+\frac{1}{2}} + \frac{1}{\tau}(\mathcal{L}_h^{NC})^{-1}(\boldsymbol{\psi}^{m+1} - \boldsymbol{\psi}^m) = \begin{pmatrix} \frac{n^{m+1}\ln n^{m+1} - n^m \ln n^m}{n^{m+1} - n^m} - 1 + \tau \ln \frac{n^{m+1}}{n^m} + n^{m+\frac{1}{2}} - c^{m+\frac{1}{2}} - \tilde{n}^{m+\frac{1}{2}} \\ -\Delta_h c^{m+\frac{1}{2},*} + \alpha c^{m+\frac{1}{2}} - n^{m+\frac{1}{2}} + c^{m+\frac{1}{2}} - \tilde{c}^{m+\frac{1}{2}} \end{pmatrix} + \frac{1}{\tau}(\mathcal{L}_h^{NC})^{-1}(\boldsymbol{\psi}^{m+1} - \boldsymbol{\psi}^m) \\
&= A_1\left(\frac{\boldsymbol{\psi}^{m+1}\ln\boldsymbol{\psi}^{m+1} - \boldsymbol{\psi}^m \ln \boldsymbol{\psi}^m}{\boldsymbol{\psi}^{m+1} - \boldsymbol{\psi}^m} - 1 + \tau \ln \frac{\boldsymbol{\psi}^{m+1}}{\boldsymbol{\psi}^m}\right) + A_2\left(-\Delta_h \boldsymbol{\psi}^{m+\frac{1}{2},*} + \alpha \boldsymbol{\psi}^{m+\frac{1}{2}}\right) \\
&\quad + \boldsymbol{\psi}^{m+\frac{1}{2}} - A_3\boldsymbol{\psi}^{m+\frac{1}{2}} - \tilde{\boldsymbol{\psi}}^{m+\frac{1}{2}} + \frac{1}{\tau}(\mathcal{L}_h^{NC})^{-1}(\boldsymbol{\psi}^{m+1} - \boldsymbol{\psi}^m) = 0,
\end{aligned} \tag{4.15}$$

with

$$A_1 = \begin{pmatrix} 1 & 0 \\ 0 & 0 \end{pmatrix}, A_2 = \begin{pmatrix} 0 & 0 \\ 0 & 1 \end{pmatrix}, A_3 = \begin{pmatrix} 0 & 1 \\ 1 & 0 \end{pmatrix}.$$

Step 3: Prove the existence of $\boldsymbol{\psi}^{m+1}$ in (4.15). Since the operator $(\mathcal{L}_h^{NC})^{-1}$ is non-symmetric, the discrete energy minimization technique cannot be applied directly. Additionally, the Browder-Minty lemma is not directly applicable, due to the singularity of $\ln n$ as $n \to 0$. To address these challenges, we construct a fixed-point sequence to facilitate the analysis. Similar approaches have been used in [5,4] to handle the Flory-Huggins-Cahn-Hilliard-Navier-Stokes system.

Define the nonlinear iteration, at the $(k+1)$-th stage:

$$\begin{aligned}
\mathcal{G}_h(n^{(k+1)}) :&= F_{n^m}(n^{(k+1)}) - 1 + \tau(\ln n^{(k+1)} - \ln n^m) + \frac{1}{2}(n^{(k+1)} + n^m) - \frac{1}{2}(c^{(k+1)} + c^m) - \tilde{n}^{m+\frac{1}{2}} + An^{(k+1)} \\
&= -\frac{1}{\tau}(\mathcal{L}_h^{NC})^{-1}(n^{(k)} - n^m) + An^{(k)}, \quad \text{with } n^{(0)} = n^{(m)},
\end{aligned} \tag{4.16a}$$

$$\begin{aligned}
\mathcal{G}_h(c^{(k+1)}) :&= -\frac{3}{4}\Delta_h c^{(k+1)} - \frac{1}{4}\Delta_h c^{m-1} + \frac{1}{2}\alpha c^{(k+1)} + \frac{1}{2}\alpha c^m - \frac{1}{2}n^{(k+1)} - \frac{1}{2}n^m + \frac{1}{2}c^{(k+1)} + \frac{1}{2}c^m - \tilde{c}^{m+\frac{1}{2}} + Ac^{(k+1)} \\
&= -\frac{1}{\tau}(\mathcal{L}_h^{NC})^{-1}(c^{(k)} - c^m) + Ac^{(k)}, \quad \text{with } c^{(0)} = c^{(m)}.
\end{aligned} \tag{4.16b}$$

The unique solvability and positivity-preserving property of the numerical system (4.16) at each iteration stage are stated in the following proposition. The proof follows similar ideas as in [8], with technical details omitted for brevity.

Proposition 4.3. *Given cell-centered functions $n^m, n^{m-1}, n^{(k)}, c^m, c^{m-1}, c^{(k)}$, with a positivity condition $n^m, n^{m-1} > 0$, and $\overline{n^m} = \overline{n^{m-1}} = \overline{n^{(k)}} = \beta_0 < 1$, then there exists a unique solution $(n^{(k+1)}, c^{k+1})$ to (4.16), with $n^{k+1} > 0$, at a point-wise level, and $\overline{n^{k+1}} = \beta_0$. Meanwhile, because $n^m, n^{m-1}, c^m, c^{m-1}$ are discrete variables, there is $0 < \delta_{m-1}, \delta_m, \delta_{(k)} < \frac{1}{2}$, such that $n^m \ge \delta_m$, $n^{m-1} \ge \delta_{m-1}$, $n^{(k)} \ge \delta_{(k)}$. In addition, $n^{(k+1)}$ preserves the estimate $n^{(k+1)} \ge \delta_{(k+1)}$, where $\delta_{(k+1)} = \min(\frac{1}{2}, \hat{\delta})$ and $\hat{\delta}$ satisfies the following equality:*

$$\tau(\ln\hat{\delta} - \ln\beta_0) + 2\tau|\ln\delta_m| + 1 - \frac{2(G(\beta_0) - G(\delta_m))}{\beta_0 - \delta_m} + B^* = 0, \tag{4.17}$$

with $B^* = \tau^{-1}C_1^{-2}h^{-\frac{d}{2}}(\|n^{(k)} - n^m\|_2 + A^*) + A\beta_0|\Omega|h^{-2} + \tilde{C}$, *and* $\tilde{C}$ *is a positive constant.*

The main result of this section is stated below.

Theorem 4.2. *Given cell-centered functions* $n^m, n^{m-1} > 0$ *pointwise, with* $\overline{n^m} = \overline{n^{m-1}} = \beta_0$, *there exists a unique cell-centered solution* n^{m+1} *and* c^{m+1} *to* (3.2), *satisfying* $n^{m+1} > 0$ *pointwise and* $\overline{n^{m+1}} = \beta_0$.

Proof. With $n^{(0)} = n^m$, $c^{(0)} = c^m$, the iteration solution generated by (4.16) satisfies $n^{(1)} \geq \delta_{(1)} = \min(\frac{1}{2}, \hat{\delta}_{(1)})$, where $\hat{\delta}_{(1)}$ satisfies equality (4.17). In more details, the following inequality is observed

$$B^* = \tau^{-1}C_1^{-2}h^{-\frac{d}{2}}(\|n^{(k)} - n^m\|_2 + A^*) + A\beta_0|\Omega|h^{-2} + \tilde{C} \leq \tau^{-1}C_1^{-2}h^{-\frac{d}{2}}(2M_h|\Omega|^{\frac{1}{2}} + A^*) + A\beta_0|\Omega|h^{-2} + \tilde{C} =: \hat{C}^*,\ M_h = h^{-2}\beta_0.$$

Notice that as long as the numerical solutions remain positive, we have $\|n^m\|_\infty, \|n^{(k)}\|_\infty \leq M_h$, for any $k \geq 0$. Consequently, we can replace B^* with $\hat{C}^*$ and obtain a modified version of (4.17), ensuring that $\hat{\delta}$ remains independent of the iteration stage k. Therefore, if the sequence generated by (4.16) has a limit, denoted as (n^{m+1}, c^{m+1}), its lower bound has to satisfy (4.17), with B^* replaced by $\hat{C}^*$, since the later one is independent of iteration stage k.

Next, we have to prove that $\mathcal{G}_h$ is a contraction mapping, so that the existence analysis could be derived by taking $k \to \infty$ on both sides of (4.16a) and (4.16b). To perform such an analysis, the difference function between two consecutive iteration stages is defined as

$$\zeta_n^{(k)} := n^{(k)} - n^{(k-1)}, \quad \zeta_c^{(k)} := c^{(k)} - c^{(k-1)}, \quad \text{for } k \geq 1. \tag{4.18}$$

By the fact that $\overline{n^{(k)}} = \overline{n^{(k-1)}} = \beta_0$, we immediately get $\overline{\zeta_n^{(k)}} = 0$. Taking a difference of (4.16a) and (4.16b), between the k^{th} and $(k+1)^{\text{th}}$ solutions, yields

$$\mathcal{G}_h(n^{(k+1)}) - \mathcal{G}_h(n^{(k)}) := F_{n^m}(n^{(k+1)}) - F_{n^m}(n^{(k)}) + \tau(\ln n^{(k+1)} - \ln n^{(k)}) + \frac{1}{2}\zeta_n^{(k+1)} + A\zeta_n^{(k+1)} = -\frac{1}{\tau}(\mathcal{L}_h^{NC})^{-1}(\zeta_n^{(k)}) + A\zeta_n^{(k)}, \tag{4.19a}$$

$$\mathcal{G}_h(c^{(k+1)}) - \mathcal{G}_h(c^{(k)}) := -\frac{3}{4}\Delta_h\zeta_c^{(k+1)} + \frac{1}{2}\alpha\zeta_c^{(k+1)} + \frac{1}{2}\zeta_c^{(k+1)} + A\zeta_c^{(k+1)} = -\frac{1}{\tau}(\mathcal{L}_h^{NC})^{-1}(\zeta_c^{(k)}) + A\zeta_c^{(k)}. \tag{4.19b}$$

Taking a discrete inner product with (4.19a) and (4.19b), by $\zeta_n^{(k+1)}$ and $\zeta_c^{(k+1)}$ separately, gives

$$\begin{aligned}&\langle F_{n^m}(n^{(k+1)}) - F_{n^m}(n^{(k)}), \zeta_n^{(k+1)}\rangle_C + \tau\langle \ln n^{(k+1)} - \ln n^{(k)}, \zeta_n^{(k+1)}\rangle_C + \frac{1}{2}\|\zeta_n^{(k+1)}\|_2^2 + A\|\zeta_n^{(k+1)}\|_2^2 \\ &\qquad = -\frac{1}{\tau}\langle(\mathcal{L}_h^{NC})^{-1}(\zeta_n^{(k)}), \zeta_n^{(k+1)}\rangle_C + A\langle\zeta_n^{(k)}, \zeta_n^{(k+1)}\rangle_C,\end{aligned} \tag{4.20a}$$

$$\frac{3}{4}\|\nabla_h\zeta_c^{(k+1)}\|_2^2 + \frac{\alpha+1}{2}\|\zeta_c^{(k+1)}\|_2^2 + A\|\zeta_c^{(k+1)}\|_2^2 = -\frac{1}{\tau}\langle(\mathcal{L}_h^{NC})^{-1}(\zeta_c^{(k)}), \zeta_n^{(k+1)}\rangle_C + A\langle\zeta_c^{(k)}, \zeta_n^{(k+1)}\rangle_C. \tag{4.20b}$$

As an application of Lemma 3.3, combined with the monotonicity of the logarithmic function, it is clear that the first two terms of (4.20a) have to be non-negative:

$$\langle F_{n^m}(n^{(k+1)}) - F_{n^m}(n^{(k)}), \zeta_n^{(k+1)}\rangle_C \geq 0, \quad \langle \ln n^{(k+1)} - \ln n^{(k)}, \zeta_n^{(k+1)}\rangle_C \geq 0. \tag{4.21}$$

In terms of the iteration relaxation, an application of triangular equality reveals that

$$\langle\zeta_n^{(k+1)}, \zeta_n^{(k+1)} - \zeta_n^{(k)}\rangle_C = \frac{1}{2}\left(\|\zeta_n^{(k+1)}\|_2^2 - \|\zeta_n^{(k)}\|_2^2 + \|\zeta_n^{(k+1)} - \zeta_n^{(k)}\|_2^2\right), \tag{4.22a}$$

$$\langle\zeta_c^{(k+1)}, \zeta_c^{(k+1)} - \zeta_c^{(k)}\rangle_C = \frac{1}{2}\left(\|\zeta_c^{(k+1)}\|_2^2 - \|\zeta_c^{(k)}\|_2^2 + \|\zeta_c^{(k+1)} - \zeta_c^{(k)}\|_2^2\right). \tag{4.22b}$$

The right hand side terms of (4.20) is related to the asymmetric operator $(\mathcal{L}_h^{NC})^{-1}$. The following bounds could be derived:

$$\begin{aligned}\langle(\mathcal{L}_h^{NC})^{-1}(\zeta_n^{(k)}), \zeta_n^{(k+1)}\rangle_C &= \langle(\mathcal{L}_h^{NC})^{-1}(\zeta_n^{(k)}), \zeta_n^{(k)}\rangle_C + \langle(\mathcal{L}_h^{NC})^{-1}(\zeta_n^{(k)}), \zeta_n^{(k+1)} - \zeta_n^{(k)}\rangle_C \\ &\geq \langle(\mathcal{L}_h^{NC})^{-1}(\zeta_n^{(k)}), \zeta_n^{(k+1)} - \zeta_n^{(k)}\rangle_C \geq -\|(\mathcal{L}_h^{NC})^{-1}(\zeta_n^{(k)})\|_2 \cdot \|\zeta_n^{(k+1)} - \zeta_n^{(k)}\|_2 \\ &\geq -C_1^{-2}\|\zeta_n^{(k)}\|_2 \cdot \|\zeta_n^{(k+1)} - \zeta_n^{(k)}\|_2 \geq -\frac{\tau}{4}\|\zeta_n^{(k)}\|_2^2 - \frac{1}{C_1^4\tau}\|\zeta_n^{(k+1)} - \zeta_n^{(k)}\|_2^2,\end{aligned} \tag{4.23a}$$

$$\langle(\mathcal{L}_h^{NC})^{-1}(\zeta_c^{(k)}), \zeta_c^{(k+1)}\rangle_C \geq -\frac{\tau}{2}\|\zeta_c^{(k)}\|_2^2 - \frac{1}{2C_1^4\tau}\|\zeta_c^{(k+1)} - \zeta_c^{(k)}\|_2^2. \tag{4.23b}$$

Notice that the inequality used in the fourth step, $\|(\mathcal{L}_h^{NC})^{-1}(\zeta_n^{(k)})\|_2 \leq C_1^{-2}\|\zeta_n^{(k)}\|_2$, comes from estimate (4.14) in Proposition 4.2, combined with the fact that all the non-homogeneous parts have been canceled. Therefore, a substitution of (4.21)-(4.23) into (4.20) results in

$$\frac{A+1}{2}\|\zeta_n^{(k+1)}\|_2^2+\frac{A}{2}\|\zeta_n^{(k+1)}-\zeta_n^{(k)}\|_2^2\le(\frac{A}{2}+\frac{1}{4})\|\zeta_n^{(k)}\|_2^2+\frac{1}{C_1^4\tau^2}\|\zeta_n^{(k+1)}-\zeta_n^{(k)}\|_2^2,$$

$$\frac{A+\alpha+1}{2}\|\zeta_c^{(k+1)}\|_2^2+\frac{A}{2}\|\zeta_c^{(k+1)}-\zeta_c^{(k)}\|_2^2\le\frac{A+1}{2}\|\zeta_c^{(k)}\|_2^2+\frac{1}{2C_1^4\tau^2}\|\zeta_c^{(k+1)}-\zeta_c^{(k)}\|_2^2.$$

As a result, by taking $A\ge A_0:=2C_1^{-4}\tau^{-2}$, a constant that may depend on τ and Ω, and setting $B_0=\frac{A+\alpha+1}{2}$, $B_1=\frac{A+1}{2}$, we arrive at the following inequality:

$$2\|\zeta_n^{(k+1)}\|_2^2\le\|\zeta_n^{(k)}\|_2^2,\quad B_0\|\zeta_c^{(k+1)}\|_2^2\le B_1\|\zeta_c^{(k)}\|_2^2.$$

Consequently, the nonlinear iteration (4.19) is a contraction mapping since $B_0>B_1$. As a result, the fixed-point iteration must converge to a unique solution, which is precisely the solution of (4.15), or equivalently, the numerical system (3.2), thereby establishing the existence of the proposed numerical scheme. In addition, since the operator $\mathcal{G}_h$ corresponds to a strictly convex energy, and the linear operator $\mathcal{L}_h^{-1}(\boldsymbol{\mu})$ is monotone, the uniqueness analysis for the numerical solution of (4.15) follows a standard monotonicity analysis. After obtaining the unique intermediate velocity vector $\hat{\boldsymbol{u}}^{m+1}$, the numerical vector $\boldsymbol{u}^{m+1}$ is determined as the discrete Helmholtz projection of $\hat{\boldsymbol{u}}^{m+1}$ onto the divergence-free vector space, which is equivalent to a discrete Poisson solver. This finishes the proof of Theorem 4.2. □

5. Unconditional total energy stability

In the finite difference setting, the discrete energy is defined as

$$E_h(n,c):=\langle n(\ln n-1),\mathbf{1}\rangle_C+\frac{1}{2}\|\nabla c\|_2^2-\langle n,c\rangle_C+\left\langle\frac{1}{2}\alpha c^2,\mathbf{1}\right\rangle_C,\quad E_{h,total}(n,c,\boldsymbol{u}):=E_h(n,c)+\frac{1}{2}\|\boldsymbol{u}\|_2^2.$$

We are not able to guarantee that the energy $E_{h,total}(n,c,\boldsymbol{u})$ is non-increasing in time, while we could ensure the dissipation of another modified energy, defined as

$$\begin{aligned}\tilde{E}_h(n^{m+1},c^{m+1},\boldsymbol{u}^{m+1},p^{m+1}):=&E_{h,total}(n^{m+1},c^{m+1},\boldsymbol{u}^{m+1})+\frac{\tau^2}{8}\|\nabla_h p^{m+1}\|^2+\frac{1}{4}\|n^{m+1}-n^m\|_2^2\\&+\frac{1}{8}\|\nabla_h(c^{m+1}-c^m)\|_2^2+\frac{1}{4}\|c^{m+1}-c^m\|_2^2.\end{aligned}\tag{5.1}$$

The total energy dissipation law is stated in the following theorem.

Theorem 5.1 *(Total energy stability). For the numerical solution (3.2), with starting values n^0, c^0, $\boldsymbol{u}^0$ and p^0, is unconditionally energy stable with respect to (5.1), i.e., for any $\tau>0$ and $h>0$,*

$$\tilde{E}_h(n^{m+1},c^{m+1},\boldsymbol{u}^{m+1},p^{m+1})\le\tilde{E}_h(n^m,c^m,\boldsymbol{u}^m,p^m).$$

Proof. By taking the discrete inner product of (3.2a) with $\hat{\boldsymbol{u}}^{m+\frac{1}{2}}=\frac{1}{2}(\hat{\boldsymbol{u}}^{m+1}+\boldsymbol{u}^m)$ leads to

$$\frac{\|\hat{\boldsymbol{u}}^{m+1}\|_2^2-\|\boldsymbol{u}^m\|_2^2}{2\tau}+\langle\nabla_h p^m,\hat{\boldsymbol{u}}^{m+\frac{1}{2}}\rangle_1+\|\nabla_h\hat{\boldsymbol{u}}^{m+\frac{1}{2}}\|_2^2+\langle\mathcal{A}_h\tilde{n}^{m+\frac{1}{2}}\nabla_h\mu_n^{m+\frac{1}{2}},\hat{\boldsymbol{u}}^{m+\frac{1}{2}}\rangle_1+\langle\mathcal{A}_h\tilde{c}^{m+\frac{1}{2}}\nabla_h\mu_c^{m+\frac{1}{2}},\hat{\boldsymbol{u}}^{m+\frac{1}{2}}\rangle_1=0,\tag{5.2}$$

with an application of the summation-by-parts formula (3.1a):

$$\left\langle\hat{\boldsymbol{u}}^{m+\frac{1}{2}},\tilde{\boldsymbol{u}}^{m+\frac{1}{2}}\cdot\nabla_h\hat{\boldsymbol{u}}^{m+\frac{1}{2}}+\nabla_h\cdot\left(\hat{\boldsymbol{u}}^{m+\frac{1}{2}}(\tilde{\boldsymbol{u}}^{m+\frac{1}{2}})^T\right)\right\rangle_1=0.$$

Furthermore, taking the discrete inner product with (3.2g) by $\boldsymbol{u}^{m+1}$, via the summation-by-parts formula (3.1b), gives

$$\|\boldsymbol{u}^{m+1}\|_2^2-\|\hat{\boldsymbol{u}}^{m+1}\|_2^2+\|\boldsymbol{u}^{m+1}-\hat{\boldsymbol{u}}^{m+1}\|_2^2=\|\boldsymbol{u}^{m+1}\|_2^2-\|\hat{\boldsymbol{u}}^{m+\frac{1}{2}}\|_2^2+\frac{1}{4}\tau^2\|\nabla_h(p^{m+1}-p^m)\|_2^2=0.\tag{5.3}$$

Subsequently, a combination of (5.2) and (5.3) yields

$$\begin{aligned}&\frac{\|\boldsymbol{u}^{m+1}\|_2^2-\|\boldsymbol{u}^m\|_2^2}{2\tau}+\langle\nabla_h p^m,\hat{\boldsymbol{u}}^{m+\frac{1}{2}}\rangle_1+\frac{1}{8}\tau\|\nabla_h(p^{m+1}-p^m)\|_2^2+\|\nabla_h\hat{\boldsymbol{u}}^{m+\frac{1}{2}}\|_2^2\\&+\langle\mathcal{A}_h\tilde{n}^{m+\frac{1}{2}}\nabla_h\mu_n^{m+\frac{1}{2}},\hat{\boldsymbol{u}}^{m+\frac{1}{2}}\rangle_1+\langle\mathcal{A}_h\tilde{c}^{m+\frac{1}{2}}\nabla_h\mu_c^{m+\frac{1}{2}},\hat{\boldsymbol{u}}^{m+\frac{1}{2}}\rangle_1=0.\end{aligned}\tag{5.4}$$

The pressure gradient term $\langle\nabla_h p^m,\hat{\boldsymbol{u}}^{m+\frac{1}{2}}\rangle_1$ can be analyzed using the discrete divergence relation $\nabla_h\cdot\hat{\boldsymbol{u}}^{m+1}=\frac{\tau}{2}\Delta_h(p^{m+1}-p^m)$ derived from (3.2f) and (3.2g), leading to

$$\begin{aligned}\langle\nabla_h p^m,\hat{\boldsymbol{u}}^{m+\frac{1}{2}}\rangle_1=&-\langle p^m,\nabla_h\cdot\hat{\boldsymbol{u}}^{m+\frac{1}{2}}\rangle_C=-\frac{1}{2}\langle p^m,\nabla_h\cdot\hat{\boldsymbol{u}}^{m+1}\rangle_C=-\frac{1}{4}\tau\langle p^m,\Delta_h(p^{m+1}-p^m)\rangle_C\\=&\frac{1}{4}\tau\langle\nabla_h p^m,\nabla_h(p^{m+1}-p^m)\rangle_1=\frac{\tau}{8}\left(\|\nabla_h p^{m+1}\|_2^2-\|\nabla_h p^m\|_2^2-\|\nabla_h(p^{m+1}-p^m)\|_2^2\right).\end{aligned}\tag{5.5}$$

A combination of (5.5) with (5.4) gives

$$\begin{aligned}&\frac{\|\boldsymbol{u}^{m+1}\|_2^2-\|\boldsymbol{u}^m\|_2^2}{2\tau}+\frac{1}{8}\tau\left(\|\nabla_h p^{m+1}\|_2^2-\|\nabla_h p^m\|_2^2\right)+\|\nabla_h\hat{\boldsymbol{u}}^{m+\frac{1}{2}}\|_2^2\\&\quad+\langle\mathcal{A}_h\tilde{n}^{m+\frac{1}{2}}\nabla_h\mu_n^{m+\frac{1}{2}},\hat{\boldsymbol{u}}^{m+\frac{1}{2}}\rangle_1+\langle\mathcal{A}_h\tilde{c}^{m+\frac{1}{2}}\nabla_h\mu_c^{m+\frac{1}{2}},\hat{\boldsymbol{u}}^{m+\frac{1}{2}}\rangle_1=0.\end{aligned}\tag{5.6}$$

Meanwhile, taking inner product with (3.2b) and (3.2c) by $\tau\mu_n^{m+\frac{1}{2}}$ and $\tau\mu_c^{m+\frac{1}{2}}$, respectively, reveals that

$$\begin{aligned}&\langle n^{m+1}-n^m,\mu_n^{m+\frac{1}{2}}\rangle_C+\langle c^{m+1}-c^m,\mu_c^{m+\frac{1}{2}}\rangle_C-\tau\langle\mathcal{A}_h\tilde{n}^{m+\frac{1}{2}}\nabla_h\mu_n^{m+\frac{1}{2}},\hat{\boldsymbol{u}}^{m+\frac{1}{2}}\rangle_C-\tau\langle\mathcal{A}_h\tilde{c}^{m+\frac{1}{2}}\nabla_h\mu_c^{m+\frac{1}{2}},\hat{\boldsymbol{u}}^{m+\frac{1}{2}}\rangle_C\\&\qquad+\tau\left([\tilde{n}^{m+\frac{1}{2}}\nabla_h\mu_n^{m+\frac{1}{2}},\nabla_h\mu_n^{m+\frac{1}{2}}]+[\mu_c^{m+\frac{1}{2}},\mu_c^{m+\frac{1}{2}}]\right)=0.\end{aligned}\tag{5.7}$$

Additionally, we can establish the following set of identities and estimates:

$$\langle n^{m+1}-n^m,F_{n^m}(n^{m+1})\rangle_C=\langle n^{m+1}\ln n^{m+1},\mathbf{1}\rangle-\langle n^m\ln n^m,\mathbf{1}\rangle,\tag{5.8}$$

$$\langle n^{m+1}-n^m,\ln n^{m+1}-\ln n^m\rangle_C\geq 0,\tag{5.9}$$

$$\langle n^{m+1}-n^m,n^{m+\frac{1}{2}}\rangle_C+\langle c^{m+1}-c^m,(1+\alpha)c^{m+\frac{1}{2}}\rangle_C=\frac{1}{2}\|n^{m+1}\|_2^2-\frac{1}{2}\|n^m\|_2^2+\frac{1+\alpha}{2}\|c^{m+1}\|_2^2-\frac{1+\alpha}{2}\|c^m\|_2^2,\tag{5.10}$$

$$\langle n^{m+1}-n^m,-c^{m+\frac{1}{2}}\rangle_C+\langle c^{m+1}-c^m,-u^{m+\frac{1}{2}}\rangle_C=\langle -n^{m+1}c^{m+1},1\rangle_C+\langle n^mc^m,1\rangle_C,\tag{5.11}$$

$$\begin{aligned}-\langle n^{m+1}-n^m,\tilde{n}^{m+\frac{1}{2}}\rangle_C&=-\langle n^{m+1}-n^m,m^m\rangle_C-\frac{1}{2}\langle n^{m+1}-n^m,n^m-m^{m-1}\rangle_C\\&\geq-\frac{1}{2}\|n^{m+1}\|_2^2+\frac{1}{2}\|n^m\|_2^2+\frac{1}{4}\|n^{m+1}-n^m\|_2^2-\frac{1}{4}\|n^m-n^{m-1}\|_2^2,\end{aligned}\tag{5.12}$$

$$-\langle c^{m+1}-c^m,\tilde{c}^{m+\frac{1}{2}}\rangle_C\geq-\frac{1}{2}\|c^{m+1}\|_2^2+\frac{1}{2}\|c^m\|_2^2+\frac{1}{4}\|c^{m+1}-c^m\|_2^2-\frac{1}{4}\|c^m-c^{m-1}\|_2^2,\tag{5.13}$$

$$\begin{aligned}\langle c^{m+1}-c^m,-\Delta_h c^{m+\frac{1}{2},*}\rangle_C&=\langle\nabla_h(c^{m+1}-c^m),\nabla_h(\frac{3}{4}c^{m+1}+\frac{1}{4}c^{m-1})\rangle_C\\&=\frac{1}{2}\langle(c^{m+1}-c^m),\nabla_h(c^{m+1}-c^m)\rangle_C+\frac{1}{4}\langle\nabla_h(c^{m+1}-c^m),\nabla_h(c^{m+1}-2c^m+c^{m-1})\rangle\\&\geq\frac{1}{2}(\|\nabla_h c^{m+1}\|_2^2-\|\nabla_h c^m\|_2^2)+\frac{1}{8}\left(\|\nabla_h(c^{m+1}-c^m)\|_2^2-\|\nabla_h(c^m-c^{m-1})\|_2^2\right).\end{aligned}\tag{5.14}$$

Therefore, substituting (5.8) - (5.14) into (5.7) and combining with (5.6), we have

$$\begin{aligned}&E_h(n^{m+1},c^{m+1},\boldsymbol{u}^{m+1})-E_h(n^m,c^m,\boldsymbol{u}^m)+\frac{1}{4}(\|n^{m+1}-n^m\|_2^2-\|n^m-n^{m-1}\|_2^2)+\frac{1}{4}(\|c^{m+1}-c^m\|_2^2-\|c^m-c^{m-1}\|_2^2)\\&+\frac{1}{8}(\|\nabla_h(c^{m+1}-c^m)\|_2^2-\|\nabla_h(c^m-c^{m-1})\|_2^2)+\frac{\tau^2}{8}\|\nabla_h p^{m+1}\|_2^2-\frac{\tau^2}{8}\|\nabla_h p^m\|_2^2\leq 0.\end{aligned}$$

The proof of Theorem 5.1 is finished. □

6. Optimal rate convergence analysis

This section focuses on the convergence analysis. Let (N,C,U,P) be the exact solution of the KSNS system (2.7). Assuming sufficiently smooth initial data, the exact solution is considered to be of the following regularity class:

$$N,C,U,P\in\mathcal{R}:=H^6\left(0,T;C_{per}(\Omega)\right)\cap H^5\left(0,T;C_{per}^2(\Omega)\right)\cap L^\infty\left(0,T;C_{per}^6(\Omega)\right).\tag{6.1}$$

A separation property is assumed for the exact cell density variable at a point-wise level for some $\delta>0$,

$$N\geq\delta.\tag{6.2}$$

To facilitate the $\|\cdot\|_{-1,h}$ error estimate, we introduce the Fourier projection of the exact solution into the space $\mathcal{B}^K$ of trigonometric polynomials of degree K (with $N=2K+1$): $N_N(\cdot,t):=\mathcal{P}_N N(\cdot,t)$, $C_N(\cdot,t):=\mathcal{P}_N C(\cdot,t)$. A standard projection estimate is available if $(N,C)\in L^\infty(0,T;H_{per}^l(\Omega))$ for some $l\in\mathbb{N}$, with $0\leq k\leq l$,

$$\left\|N_N-N\right\|_{L^\infty(0,T;H^k(\Omega))}\leq Bh^{l-k}\|N\|_{L^\infty(0,T;H^l(\Omega))},\quad\left\|C_N-C\right\|_{L^\infty(0,T;H^k(\Omega))}\leq Bh^{l-k}\|C\|_{L^\infty(0,T;H^l(\Omega))},\tag{6.3}$$

where $B>0$ is a constant. The Fourier projection estimate (6.3) does not automatically guarantee the positivity of the physical variables. Meanwhile, by choosing h sufficiently small, a similar separation property holds: $N_N\geq\frac{3}{4}\delta$. Let N_N^m and N^m denote $N_N(\cdot,t_m)$ and $N(\cdot,t_m)$, respectively, with $t_m=m\cdot\tau$. Since $N_N\in\mathcal{B}^m$, the mass conservation property holds at the discrete level.

$$\overline{N_N^m} = \frac{1}{|\Omega|}\int_\Omega N_N\left(\cdot, t_m\right)\mathrm{d}\boldsymbol{x} = \frac{1}{|\Omega|}\int_\Omega N_N\left(\cdot, t_{m+1}\right)\mathrm{d}\boldsymbol{x} = \overline{N_N^{m+1}}, \quad m\in\mathbb{N}. \tag{6.4}$$

On the other hand, the solution of (2.7) is also mass conservative at the discrete level:

$$\overline{n^m} = \overline{n^{m+1}}, \quad \forall m\in\mathbb{N}.$$

In turn, the error grid function is defined as

$$\mathring{n}^m := \mathcal{P}_h N_N^m - n^m, \quad \mathring{c}^m := C_N^m - c^m, \quad m\in\mathbb{N}. \tag{6.5}$$

Therefore, it follows that $\overline{\mathring{n}^m} = 0$, for any $m\in\mathbb{N}$, so that the discrete norm $\|\cdot\|_{-1,h}$ is well defined for the error grid function $\mathring{n}^m$.

In terms of the velocity and pressure variables, we consider the corresponding error functions directly

$$\mathring{\boldsymbol{u}}^m := \mathcal{P}_h\boldsymbol{U}^m - \boldsymbol{u}^m = (\mathring{u}^m, \mathring{v}^m)^T, \quad \mathring{p}^m = \mathcal{P}_h p^m - p^m, \quad \forall m\in\mathbb{N}.$$

The main result of this section is presented in the following theorem.

Theorem 6.1. *Assuming the initial data $N(\cdot,t=0), C(\cdot,t=0), \boldsymbol{U}(\cdot,t=0)\in C^6_{per}(\Omega)$, and that the exact solution to the KSNS system (2.7) is of the regularity class $\mathcal{R}$. Then under the condition that both τ and h are sufficiently small, and the linear refinement constraint $\lambda_1 h\le\tau\le\lambda_2 h$ holds, the following result is obtained*

$$\|\mathring{\boldsymbol{u}}^m\|_2 + \|\mathring{n}^m\|_2 + \|\mathring{c}^m\|_2 + \|\nabla_h\mathring{p}^m\|_2 \le B(\tau^2+h^2), \tag{6.6}$$

for all positive integers m, such that $t_m = m\tau\le T$, where λ_1, λ_2, and B are positive constants independent of τ and h.

6.1. Higher order consistency analysis of the numerical solution

By directly substituting the projected solution $(\boldsymbol{U}_N, P_N, N_N, C_N)$ into the numerical scheme (3.2), second-order accuracy in both time and space is ensured. However, this leading local truncation error alone is insufficient to derive an a-priori ℓ^∞ bound for the numerical solution, which is crucial to the theoretical proof of the separation property. To overcome this challenge, we conduct a higher-order consistency analysis, utilizing a linearization technique to establish the necessary bound. Specifically, we introduce a set of supplementary functions, $\check{\boldsymbol{U}}$, $\check{P}$, $\check{N}$, $\check{C}$ with the following expansion:

$$\check{N} = N_N + \mathcal{P}_N\left(\tau^2 N_{\tau,1} + \tau t^3 N_{\tau,2} + h^2 N_{h,1}\right), \tag{6.7a}$$

$$\check{C} = C_N + \mathcal{P}_N\left(\tau^2 C_{\tau,1} + \tau^3 C_{\tau,2} + h^2 C_{h,1}\right), \tag{6.7b}$$

$$\check{P} = \mathcal{I}_h\left(p + \tau^2 P_{\tau,1} + \tau^3 P_{\tau,2} + h^2 P_{h,1}\right), \tag{6.7c}$$

$$\check{\boldsymbol{U}} = \mathcal{P}_H\left(\boldsymbol{U} + \tau^2\boldsymbol{U}_{\tau,1} + \tau^3\boldsymbol{U}_{\tau,2} + h^2\boldsymbol{U}_{h,1}\right). \tag{6.7d}$$

Here $\mathcal{P}_H$ represents a discrete Helmholtz interpolation into the divergence-free space, while $\mathcal{I}_h$ denotes the standard point-wise interpolation. Substituting these constructed functions into the numerical scheme (3.2) yields a higher-order consistency of $O(\tau^4+h^4)$. The constructed functions, $\boldsymbol{U}_{\tau,i}$, $P_{\tau,i}$, $N_{\tau,i}$, $C_{\tau,i}$ $(i=1,2)$, $\boldsymbol{U}_{h,1}$, $P_{h,1}$, $N_{h,1}$, $C_{h,1}$, are derived using an asymptotic expansion technique and depend solely on the exact solution $(\boldsymbol{U}, P, N, C)$. Instead of directly analyzing the error between the numerical and projection solutions, we estimate the numerical error function relative to the constructed expansion profile.

To facilitate the nonlinear analysis, we introduce the following bilinear form:

$$b(\boldsymbol{u},\boldsymbol{w}) = \boldsymbol{u}\cdot\nabla\boldsymbol{w}, \quad b_h(\boldsymbol{u},\boldsymbol{w}) = \frac{1}{2}\left(\boldsymbol{u}\cdot\nabla\boldsymbol{w} + \nabla\cdot(\boldsymbol{u}\boldsymbol{w}^T)\right).$$

In addition, in the leading order consistency analysis, the following intermediate velocity vectors are required:

$$\hat{\boldsymbol{U}}^{m+1} = \boldsymbol{U}^{m+1} + \frac{1}{2}\tau\nabla(P^{m+1} - P^m).$$

A detailed Taylor expansion in time for $N_N, C_N, \boldsymbol{U}$, and $\hat{\boldsymbol{U}}$ further reveals that:

$$\frac{\hat{\boldsymbol{U}}^{m+1} - \boldsymbol{U}^m}{\tau} + b_h(\tilde{\boldsymbol{U}}^{m+\frac12}, \hat{\boldsymbol{U}}^{m+\frac12}) + \nabla P^m - \Delta\hat{\boldsymbol{U}}^{m+\frac12} = -\tilde{N}_N^{m+\frac12}\nabla M_n^{m+\frac12} - \tilde{C}_N^{m+\frac12}\nabla M_c^{m+\frac12} + \tau^2\boldsymbol{G}_0^{m+\frac12} + O(\tau^3+h^{m_0}), \tag{6.8a}$$

$$\frac{N_N^{m+1} - N_N^m}{\tau} + \nabla\cdot(\tilde{N}_N^{m+\frac12}\hat{\boldsymbol{U}}^{m+\frac12}) = \nabla\cdot(\tilde{N}_N^{m+\frac12}\nabla M_n^{m+\frac12}) + \tau^2 H_{n,0}^{m+\frac12} + O(\tau^3+h^{m_0}), \tag{6.8b}$$

$$M_n^{m+\frac12} = F_{N_N^m}(N_N^{m+1}) - 1 + \tau(\ln N_N^{m+1} - \ln N_N^m) + N_N^{m+\frac12} - C_N^{m+\frac12} - \tilde{N}_N^{m+\frac12}, \tag{6.8c}$$

$$\frac{C_N^{m+1} - C_N^m}{\tau} + \nabla\cdot(\tilde{C}_N^{m+\frac12}\hat{\boldsymbol{U}}^{m+\frac12}) = -M_c^{m+\frac12} + \tau^2 H_{c,0}^{m+\frac12} + O(\tau^3+h^{m_0}), \tag{6.8d}$$

$$M_c^{m+\frac{1}{2}} = -\Delta C_N^{m+\frac{1}{2},*} + \alpha C_N^{m+\frac{1}{2}} - N_N^{m+\frac{1}{2}} + C_N^{m+\frac{1}{2}} - \tilde{C}_N^{m+\frac{1}{2}}, \tag{6.8e}$$

$$\frac{\boldsymbol{U}^{m+1} - \hat{\boldsymbol{U}}^{m+1}}{\tau} + \frac{1}{2}\nabla(P^{m+1} - P^m) = 0, \tag{6.8f}$$

$$\nabla \cdot \boldsymbol{U}^{m+1} = 0, \tag{6.8g}$$

in which $\|\boldsymbol{G}_0^{m+\frac{1}{2}}\|, \|\boldsymbol{H}_0^{m+\frac{1}{2}}\| \le B$, and B depends only on the regularity of the exact solutions.

The correction functions $\boldsymbol{U}_{\tau,1}, P_{\tau,1}, N_{\tau,1}, C_{\tau,1}, M_{n,\tau,1}$ and $M_{c,\tau,1}$, are obtained by solving the following system of PDE system

$$\begin{aligned}
&\partial_t \boldsymbol{U}_{\tau,1} + (\boldsymbol{U}_{\tau,1}\cdot\nabla)\boldsymbol{U} + (\boldsymbol{U}\cdot\nabla)\boldsymbol{U}_{\tau,1} + \nabla P_{\tau,1} - \Delta \boldsymbol{U}_{\tau,1} = -N_{\tau,1}\nabla M_n - N_N \nabla M_{n,\tau,1} - C_{\tau,1}\nabla M_c - C_N \nabla M_{c,\tau,1} - \boldsymbol{G}_0,\\
&\partial N_{\tau,1} + \nabla\cdot(N_{\tau,1}\boldsymbol{U} + N_N \boldsymbol{U}_{\tau,1}) = \nabla\cdot(N_{\tau,1}\nabla M_n + N_N \nabla M_{n,\tau,1}) - H_{n,0},\\
&M_n = \ln N_N - C_N,\\
&M_{n,\tau,1} = \frac{1}{N_N} N_{\tau,1} - C_{\tau,1},\\
&\partial_t C_{\tau,1} + \nabla\cdot(C_{\tau,1}\boldsymbol{U} + C_N \boldsymbol{U}_{\tau,1}) = -M_{c,\tau,1},\\
&M_{c,\tau,1} = -\Delta C_{\tau,1} + \alpha C_{\tau,1} - N_{\tau,1},\\
&\nabla\cdot\boldsymbol{U}_{\tau,1} = 0.
\end{aligned}$$

Homogeneous Neumann boundary conditions are imposed on $N_{\tau,1}$ and $C_{\tau,1}$, while $\boldsymbol{U}_{\tau,1}$ satisfies a no-penetration and free-slip condition. The well-posedness of this linear parabolic system–both existence and uniqueness of solution–is straightforward to establish. Similarly, an intermediate velocity field is defined as

$$\hat{\boldsymbol{U}}_{\tau,1}^{m+1} = \boldsymbol{U}_{\tau,1}^{m+1} + \frac{1}{2}\tau\nabla(P_{\tau,1}^{m+1} - P_{\tau,1}^m).$$

Applying the temporal discretization to the above linear PDE system gives

$$\begin{aligned}
&\frac{\hat{\boldsymbol{U}}_{\tau,1}^{m+1} - \boldsymbol{U}_{\tau,1}^m}{\tau} + b(\tilde{\boldsymbol{U}}_{\tau,1}^{m+\frac{1}{2}}, \hat{\boldsymbol{U}}^{m+\frac{1}{2}}) + b(\tilde{\boldsymbol{U}}^{m+\frac{1}{2}}, \hat{\boldsymbol{U}}_{\tau,1}^{m+\frac{1}{2}}) + \nabla P_{\tau,1}^m - \Delta \boldsymbol{U}_{\tau,1}^{m+\frac{1}{2}}\\
&\qquad = -\tilde{N}_{\tau,1}^{m+\frac{1}{2}}\nabla M_n^{m+\frac{1}{2}} - \tilde{N}_N^{m+\frac{1}{2}}\nabla M_{n,\tau,1}^{m+\frac{1}{2}} - \tilde{C}_{\tau,1}^{m+\frac{1}{2}}\nabla M_c^{m+\frac{1}{2}} - \tilde{C}_N^{m+\frac{1}{2}}\nabla M_{c,\tau,1}^{m+\frac{1}{2}} - \boldsymbol{G}_0^{m+\frac{1}{2}} + O(\tau^2),
\end{aligned} \tag{6.10}$$

$$\frac{N_{\tau,1}^{m+1} - N_{\tau,1}^m}{\tau} + \nabla\cdot(\tilde{N}_{\tau,1}^{m+\frac{1}{2}}\hat{\boldsymbol{U}}^{m+\frac{1}{2}} + \tilde{N}_N^{m+\frac{1}{2}}\hat{\boldsymbol{U}}_{\tau,1}^{m+\frac{1}{2}}) = \nabla\cdot(\tilde{N}_{\tau,1}^{m+\frac{1}{2}}\nabla M_n^{m+\frac{1}{2}} + \tilde{N}_N^{m+\frac{1}{2}}\nabla M_{n,\tau,1}^{m+\frac{1}{2}}) - H_{n,0}^{m+\frac{1}{2}} + O(\tau^2), \tag{6.11}$$

$$M_{n,\tau,1}^{m+\frac{1}{2}} = \frac{1}{N_N^{m+\frac{1}{2}}} N_{\tau,1}^{m+\frac{1}{2}} - C_{\tau,1}^{m+\frac{1}{2}}, \tag{6.12}$$

$$\frac{C_{\tau,1}^{m+1} - C_{\tau,1}^m}{\tau} + \nabla\cdot(\tilde{C}_{\tau,1}^{m+\frac{1}{2}}\hat{\boldsymbol{U}}^{m+\frac{1}{2}} + \tilde{C}_N^{m+\frac{1}{2}}\hat{\boldsymbol{U}}_{\tau,1}^{m+\frac{1}{2}}) = -M_{c,\tau,1}^{m+\frac{1}{2}} - H_{c,0}^{m+\frac{1}{2}} + O(\tau^2), \tag{6.13}$$

$$M_{c,\tau,1}^{m+\frac{1}{2}} = -\Delta C_{\tau,1}^{m+\frac{1}{2},*} + \alpha C_{\tau,1}^{m+\frac{1}{2}} - N_{\tau,1}^{m+\frac{1}{2}} + C_{\tau,1}^{m+\frac{1}{2}} - \tilde{C}_{\tau,1}^{m+\frac{1}{2}}, \tag{6.14}$$

$$\frac{\boldsymbol{U}_{\tau,1}^{m+1} - \hat{\boldsymbol{U}}_{\tau,1}^{m+1}}{\tau} + \frac{1}{2}\nabla(P_{\tau,1}^{m+1} - P_{\tau,1}^m) = 0, \tag{6.15}$$

$$\nabla\cdot\boldsymbol{U}_{\tau,1}^{m+1} = 0. \tag{6.16}$$

By combining (6.8) and (6.10), we arrive at the following third-order truncation error expression for $\boldsymbol{U}_1 := \boldsymbol{U} + \tau^2\boldsymbol{U}_{\tau,1}$, $N_1 := N + \tau^2 N_{\tau,1}$, $C_1 := C + \tau^2 C_{\tau,1}$, $P_1 := P + \tau^2 P_{\tau,1}$:

$$\frac{\hat{\boldsymbol{U}}_1^{m+1} - \boldsymbol{U}_1^m}{\tau} + b_h(\tilde{\boldsymbol{U}}_1^{m+\frac{1}{2}}, \hat{\boldsymbol{U}}_1^{m+\frac{1}{2}}) + \nabla P_1^m - \Delta\hat{\boldsymbol{U}}_1^{m+\frac{1}{2}} = -\tilde{N}_1^{m+\frac{1}{2}}\nabla M_{n,1}^{m+\frac{1}{2}} - \tilde{C}_1^{m+\frac{1}{2}}\nabla M_{c,1}^{m+\frac{1}{2}} + \tau^3\boldsymbol{G}_1^{m+\frac{1}{2}} + O(\tau^4 + h^{m_0}), \tag{6.17a}$$

$$\frac{N_1^{m+1} - N_1^m}{\tau} + \nabla\cdot(\tilde{N}_1^{m+\frac{1}{2}}\hat{\boldsymbol{U}}_1^{m+\frac{1}{2}}) = \nabla\cdot(\tilde{N}_1^{m+\frac{1}{2}}\nabla M_{n,1}^{m+\frac{1}{2}}) + \tau^3 H_{n,1}^{m+\frac{1}{2}} + O(\tau^4 + h^{m_0}), \tag{6.17b}$$

$$M_{n,1}^{m+\frac{1}{2}} = F_{N_1^m}(N_1^{m+1}) - 1 + \tau(\ln N_1^{m+1} - \ln N_1^m) + N_1^{m+\frac{1}{2}} - C_1^{m+\frac{1}{2}} - \tilde{N}_1^{m+\frac{1}{2}}, \tag{6.17c}$$

$$\frac{C_1^{m+1} - C_1^m}{\tau} + \nabla\cdot(\tilde{C}_1^{m+\frac{1}{2}}\hat{\boldsymbol{U}}_1^{m+\frac{1}{2}}) = -M_{c,1}^{m+\frac{1}{2}} + \tau^3 H_{c,1}^{m+\frac{1}{2}} + O(\tau^4 + h^{m_0}), \tag{6.17d}$$

$$M_{c,1}^{m+\frac{1}{2}} = -\Delta C_1^{m+\frac{1}{2},*} + \alpha C_1^{m+\frac{1}{2}} - N_1^{m+\frac{1}{2}} + C_1^{m+\frac{1}{2}} - \tilde{C}_1^{m+\frac{1}{2}}, \tag{6.17e}$$

$$\frac{\boldsymbol{U}_1^{m+1}-\hat{\boldsymbol{U}}_1^{m+1}}{\tau}+\frac{1}{2}\nabla(P_1^{m+1}-P_1^m)=0, \tag{6.17f}$$

$$\nabla\cdot\boldsymbol{U}_1^{m+1}=0. \tag{6.17g}$$

Here, $\|G_1\|,\|H_1\|\le B$ and B depends only on the regularity of the exact solution. In fact, the above derivation makes use of the following linearized expansions:

$$\frac{1}{N_N^{m+\frac{1}{2}}}N_{\tau,1}^{m+\frac{1}{2}}=\frac{1}{2}\Big(\frac{1}{N_N^m}N_{\tau,1}^m+\frac{1}{N_N^{m+1}}N_{\tau,1}^{m+1}\Big)+O(\tau^2).$$

Similarly, the next order temporal correction functions, namely $\boldsymbol{U}_{\tau,2}, P_{\tau,2}, N_{\tau,2}$ and $C_{\tau,2}$, are determined by the following system of linear equations:

$$\begin{aligned}
&\partial_t\boldsymbol{U}_{\tau,2}+(\boldsymbol{U}_{\tau,2}\cdot\nabla)\boldsymbol{U}_1+(\boldsymbol{U}_1\cdot\nabla)\boldsymbol{U}_{\tau,2}+\nabla P_{\tau,2}-\Delta\boldsymbol{U}_{\tau,2}=-N_{\tau,2}\nabla M_{n,1}-N_1\nabla M_{n,\tau,2}-C_{\tau,2}\nabla M_{c,1}-C_1\nabla M_{c,\tau,2}-\boldsymbol{G}_1,\\
&\partial N_{\tau,2}+\nabla\cdot(N_{\tau,2}\boldsymbol{U}_1+N_1\boldsymbol{U}_{\tau,2})=\nabla\cdot(N_{\tau,2}\nabla M_{n,1}+N_1\nabla M_{n,\tau,2})-H_{n,1},\\
&M_{n,1}=\ln N_1-C_1,\\
&M_{n,\tau,2}=\frac{1}{N_1}N_{\tau,2}-C_{\tau,2},\\
&\partial_t C_{\tau,2}+\nabla\cdot(C_{\tau,2}\boldsymbol{U}_1+C_1\boldsymbol{U}_{\tau,2})=-M_{c,\tau,2},\\
&M_{c,\tau,2}=-\Delta C_{\tau,2}+\alpha C_{\tau,2}-N_{\tau,2},\\
&\nabla\cdot\boldsymbol{U}_{\tau,2}=0.
\end{aligned}$$

Again, the homogeneous Neumann boundary conditions are applied to $N_{\tau,2}$ and $C_{\tau,2}$, along with the no-penetration and free-slip conditions for $\boldsymbol{U}_{\tau,2}$. An intermediate velocity vector is similarly introduced

$$\hat{\boldsymbol{U}}_{\tau,2}^{m+1}=\boldsymbol{U}_{\tau,2}^{m+1}+\frac{1}{2}\tau\nabla(P_{\tau,2}^{m+1}-P_{\tau,2}^m).$$

In turn, applying temporal discretization to the above linear PDE system leads to the following result

$$\begin{aligned}
&\frac{\hat{\boldsymbol{U}}_{\tau,2}^{m+1}-\boldsymbol{U}_{\tau,2}^m}{\tau}+b(\tilde{\boldsymbol{U}}_{\tau,2}^{m+\frac{1}{2}},\hat{\boldsymbol{U}}_1^{m+\frac{1}{2}})+b(\tilde{\boldsymbol{U}}_1^{m+\frac{1}{2}},\hat{\boldsymbol{U}}_{\tau,2}^{m+\frac{1}{2}})+\nabla P_{\tau,2}^m-\Delta\hat{\boldsymbol{U}}_{\tau,2}^{m+\frac{1}{2}}\\
&\qquad=-\tilde{N}_{\tau,2}^{m+\frac{1}{2}}\nabla M_{n,1}^{m+\frac{1}{2}}-\tilde{N}_1^{m+\frac{1}{2}}\nabla M_{n,\tau,2}^{m+\frac{1}{2}}-\tilde{C}_{\tau,2}^{m+\frac{1}{2}}\nabla M_{c,1}^{m+\frac{1}{2}}-\tilde{C}_1^{m+\frac{1}{2}}\nabla M_{c,\tau,1}^{m+\frac{1}{2}}-\boldsymbol{G}_1^{m+\frac{1}{2}}+O(\tau^2),
\end{aligned} \tag{6.19a}$$

$$\frac{N_{\tau,2}^{m+1}-N_{\tau,2}^m}{\tau}+\nabla\cdot(\tilde{N}_{\tau,2}^{m+\frac{1}{2}}\hat{\boldsymbol{U}}_1^{m+\frac{1}{2}}+\tilde{N}_1^{m+\frac{1}{2}}\hat{\boldsymbol{U}}_{\tau,2}^{m+\frac{1}{2}})=\nabla\cdot(\tilde{N}_{\tau,2}^{m+\frac{1}{2}}\nabla M_{n,1}^{m+\frac{1}{2}}+\tilde{N}_1^{m+\frac{1}{2}}\nabla M_{n,\tau,2}^{m+\frac{1}{2}})-H_{n,1}^{m+\frac{1}{2}}+O(\tau^2), \tag{6.19b}$$

$$M_{n,1}^{m+\frac{1}{2}}=F_{N_1^m}(N_1^{m+1})+\tau(\ln N_1^{m+1}-\ln N_1^m)+N_1^{m+\frac{1}{2}}-C_1^{m+\frac{1}{2}}-\tilde{N}_1^{m+\frac{1}{2}}, \tag{6.19c}$$

$$M_{n,\tau,2}^{m+\frac{1}{2}}=\frac{1}{N_1^{m+\frac{1}{2}}}N_{\tau,2}^{m+\frac{1}{2}}-C_{\tau,2}^{m+\frac{1}{2}}, \tag{6.19d}$$

$$\frac{C_{\tau,2}^{m+1}-C_{\tau,2}^m}{\tau}+\nabla\cdot(\tilde{C}_{\tau,2}^{m+\frac{1}{2}}\hat{\boldsymbol{U}}_1^{m+\frac{1}{2}}+\tilde{C}_1^{m+\frac{1}{2}}\hat{\boldsymbol{U}}_{\tau,2}^{m+\frac{1}{2}})=-M_{c,\tau,2}^{m+\frac{1}{2}}-H_{c,1}^{m+\frac{1}{2}}+O(\tau^2), \tag{6.19e}$$

$$M_{c,\tau,2}^{m+\frac{1}{2}}=-\Delta C_{\tau,2}^{m+\frac{1}{2},*}+\alpha C_{\tau,2}^{m+\frac{1}{2}}-N_{\tau,2}^{m+\frac{1}{2}}+C_{\tau,2}^{m+\frac{1}{2}}-\tilde{C}_{\tau,2}^{m+\frac{1}{2}}, \tag{6.19f}$$

$$\frac{\boldsymbol{U}_{\tau,2}^{m+1}-\hat{\boldsymbol{U}}_{\tau,2}^{m+1}}{\tau}+\frac{1}{2}\nabla(P_{\tau,2}^{m+1}-P_{\tau,2}^m)=0, \tag{6.19g}$$

$$\nabla\cdot\boldsymbol{U}_{\tau,2}^{m+1}=0. \tag{6.19h}$$

A combination of (6.17) with (6.19) gives the fourth-order truncation error for $\boldsymbol{U}_2:=\boldsymbol{U}_1+\tau^3\mathcal{P}_N\boldsymbol{U}_{\tau,2}$, $N_2:=N_1+\tau^3\mathcal{P}_hN_{\tau,2}$, $C_2:=C_1+\tau^3C_{\tau,1}$, $P_2:=P_1+\tau^3P_{\tau,2}$:

$$\begin{aligned}
&\frac{\hat{\boldsymbol{U}}_2^{m+1}-\boldsymbol{U}_2^m}{\tau}+b_h(\tilde{\boldsymbol{U}}_2^{m+\frac{1}{2}},\hat{\boldsymbol{U}}_2^{m+\frac{1}{2}})+\nabla P_2^m-\Delta\hat{\boldsymbol{U}}_2^{m+\frac{1}{2}}=-\tilde{N}_2^{m+\frac{1}{2}}\nabla M_{n,2}^{m+\frac{1}{2}}-\tilde{C}_2^{m+\frac{1}{2}}\nabla M_{c,2}^{m+\frac{1}{2}}+O(\tau^4+h^{m_0}),\\
&\frac{N_2^{m+1}-N_2^m}{\tau}+\nabla\cdot(\tilde{N}_2^{m+\frac{1}{2}}\hat{\boldsymbol{U}}_2^{m+\frac{1}{2}})=\nabla\cdot(\tilde{N}_2^{m+\frac{1}{2}}\nabla M_{n,2}^{m+\frac{1}{2}})+O(\tau^4+h^{m_0}),\\
&M_{n,2}^{m+\frac{1}{2}}=F_{N_2^m}(N_2^{m+1})-1+\tau(\ln N_2^{m+1}-\ln N_2^m)+N_2^{m+\frac{1}{2}}-C_2^{m+\frac{1}{2}}-\tilde{N}_2^{m+\frac{1}{2}},
\end{aligned}$$

$$\frac{C_2^{m+1}-C_2^m}{\tau}+\nabla\cdot(\tilde{C}_2^{m+\frac{1}{2}}\hat{\boldsymbol{U}}_2^{m+\frac{1}{2}})=-M_{c,2}^{m+\frac{1}{2}}+O(\tau^4+h^{m_0}),$$
$$M_{c,2}^{m+\frac{1}{2}}=-\Delta C_2^{m+\frac{1}{2},*}+\alpha C_2^{m+\frac{1}{2}}-N_2^{m+\frac{1}{2}}+C_2^{m+\frac{1}{2}}-\tilde{C}_2^{m+\frac{1}{2}},$$
$$\frac{\boldsymbol{U}_2^{m+1}-\hat{\boldsymbol{U}}_2^{m+1}}{\tau}+\frac{1}{2}\nabla(P_2^{m+1}-P_2^m)=0,$$
$$\nabla\cdot\boldsymbol{U}_2^{m+1}=0,$$

where $\|G_2\|$, $\|H_{n,2}\|$, and $\|H_{c,2}\|$ are bounded by a constant B, which depends only on the regularity of the exact solution.

Next, to enhance spatial accuracy, we proceed by constructing a spatial correction function. A key difficulty in the spatial discretization lies in the fact that the velocity field $\boldsymbol{U}_2$ is not discretely divergence-free, which may lead to a nonzero discrete inner product with the pressure gradient. To resolve this issue, we introduce a spatial interpolation operator $\mathcal{P}_H$. For any divergence-free vector field $\boldsymbol{u}\in H^1(\Omega)$, there exists an exact stream function ψ such that $\boldsymbol{u}=\nabla^\perp\psi$. Based on this fact, we define the corresponding discrete velocity field as follows:

$$\mathcal{P}_H(\boldsymbol{u})=\nabla_h^\perp\psi=(-D_y\psi,D_x\psi)^T.$$

As a result, this definition ensures $\nabla_h\cdot\mathcal{P}_H(\boldsymbol{u})=0$ at a point-wise level. Furthermore, an $O(h^2)$ truncation error is available between the continuous velocity vector $\boldsymbol{u}$ and its Helmholtz interpolation, $\mathcal{P}_H(\boldsymbol{u})$.

Therefore, we introduce $\boldsymbol{U}_{2,PH}=\mathcal{P}_H(\boldsymbol{U}_2)$. Using finite difference spatial approximation on the MAC mesh grid, we obtain the following truncation error estimate:

$$\frac{\hat{\boldsymbol{U}}_{2,PH}^{m+1}-\boldsymbol{U}_{2,PH}^m}{\tau}+b_h(\tilde{\boldsymbol{U}}_{2,PH}^{m+\frac{1}{2}},\hat{\boldsymbol{U}}_{2,PH}^{m+\frac{1}{2}})+\nabla P_2^m-\Delta\hat{\boldsymbol{U}}_{2,PH}^{m+\frac{1}{2}}$$
$$=-\mathcal{A}_h\tilde{N}_2^{m+\frac{1}{2}}\nabla M_{n,2,h}^{m+\frac{1}{2}}-\mathcal{A}_h\tilde{C}_2^{m+\frac{1}{2}}\nabla M_{c,2,h}^{m+\frac{1}{2}}+h^2G_h^{m+\frac{1}{2}}+O(\tau^4+h^4),\tag{6.21a}$$
$$\frac{N_2^{m+1}-N_2^m}{\tau}+\nabla\cdot(\mathcal{A}_h\tilde{N}_2^{m+\frac{1}{2}}\hat{\boldsymbol{U}}_{2,PH}^{m+\frac{1}{2}})=\nabla\cdot(\mathcal{A}_h\tilde{N}_2^{m+\frac{1}{2}}\nabla M_{n,2,h}^{m+\frac{1}{2}})+h^2H_{n,h}^{m+\frac{1}{2}}+O(\tau4+h^4),\tag{6.21b}$$
$$M_{n,2,h}^{m+\frac{1}{2}}=F_{N_2^m}(N_2^{m+1})+\tau(\ln N_2^{m+1}-\ln N_2^m)+N_2^{m+\frac{1}{2}}-C_2^{m+\frac{1}{2}}-\tilde{N}_2^{m+\frac{1}{2}},\tag{6.21c}$$
$$\frac{C_2^{m+1}-C_2^m}{\tau}+\nabla\cdot(\mathcal{A}_h\tilde{C}_2^{m+\frac{1}{2}}\hat{\boldsymbol{U}}_{2,PH}^{m+\frac{1}{2}})=-M_{c,2,h}^{m+\frac{1}{2}}+h^2H_{c,h}^{m+\frac{1}{2}}+O(\tau^4+h^4),\tag{6.21d}$$
$$M_{c,2,h}^{m+\frac{1}{2}}=-\Delta C_2^{m+\frac{1}{2},*}+\alpha C_2^{m+\frac{1}{2}}-N_2^{m+\frac{1}{2}}+C_2^{m+\frac{1}{2}}-\tilde{C}_2^{m+\frac{1}{2}},\tag{6.21e}$$
$$\frac{\boldsymbol{U}_{2,PH}^{m+1}-\hat{\boldsymbol{U}}_{2,PH}^{m+1}}{\tau}+\frac{1}{2}\nabla(P_2^{m+1}-P_2^m)=0,\tag{6.21f}$$
$$\nabla\cdot\boldsymbol{U}_{2,PH}^{m+1}=0,\tag{6.21g}$$

where $\|G_h\|_2$, $\|H_{n,h}\|_2$, and $\|H_{c,h}\|_2$ are bounded by a constant B, which depends only on the regularity of the exact solution. Subsequently, the spatial correction functions $U_{h,1}$, $N_{h,1}$, $C_{h,1}$, and $P_{h,1}$ are determined by the following linear PDE system:

$$\partial_t\boldsymbol{U}_{h,1}+(\boldsymbol{U}_{h,1}\cdot\nabla)\boldsymbol{U}_2+(\boldsymbol{U}_2\cdot\nabla)\boldsymbol{U}_{h,1}+\nabla P_{h,1}-\Delta\boldsymbol{U}_{h,1}=-N_{h,1}\nabla M_{n,2}-N_2\nabla M_{n,h,1}-C_{h,1}\nabla M_{c,2}-C_2\nabla M_{c,h,1}-\boldsymbol{G}_h,$$
$$\partial N_{h,1}+\nabla\cdot(N_{h,1}\boldsymbol{U}_2+N_2\boldsymbol{U}_{h,1})=\nabla\cdot(N_{h,1}\nabla M_{n,2}+N_2\nabla M_{n,h,1})-H_{n,h},$$
$$M_{n,2}=\ln N_2-C_2,$$
$$M_{n,h,1}=\frac{1}{N_2}N_{h,1}-C_{h,1},$$
$$\partial_t C_{h,1}+\nabla\cdot(C_{h,1}\boldsymbol{U}_2+C_2\boldsymbol{U}_{h,1})=-M_{c,h,1},$$
$$M_{c,h,1}=-\Delta C_{h,1}+\alpha C_{h,1}-N_{h,1},$$
$$\nabla\cdot\boldsymbol{U}_{h,1}=0.$$

In the same way, homogeneous Neumann boundary conditions are applied to $N_{h,1}$ and $C_{h,1}$, along with no-penetration and free-slip conditions for $\boldsymbol{U}_{h,1}$. We then define $\boldsymbol{U}_{h,1,PH}=\mathcal{P}_H(\boldsymbol{U}_{h,1})$, and set $\hat{\boldsymbol{U}}_{h,1,PH}^{m+1}=\boldsymbol{U}_{h,1,PH}^{m+1}+\frac{1}{2}\tau\nabla_h(P_{h,1}^{m+1}-P_{h,1}^m)$. Applying both temporal and spatial approximations to the PDE system leads to the following result

$$\frac{\hat{\boldsymbol{U}}_{h,1,PH}^{m+1}-\boldsymbol{U}_{h,1,PH}^m}{\tau}+b_h(\tilde{\boldsymbol{U}}_{h,1,PH}^{m+\frac{1}{2}},\hat{\boldsymbol{U}}_{2,PH}^{m+\frac{1}{2}})+b_h(\tilde{\boldsymbol{U}}_{2,PH}^{m+\frac{1}{2}},\hat{\boldsymbol{U}}_{h,1,PH}^{m+\frac{1}{2}})+\nabla P_{h,1}^m-\Delta\boldsymbol{U}_{h,1,PH}^{m+\frac{1}{2}}$$
$$=-\mathcal{A}_h\tilde{N}_{h,1}^{m+\frac{1}{2}}\nabla M_{n,2,h}^{m+\frac{1}{2}}-\mathcal{A}_h\tilde{N}_2^{m+\frac{1}{2}}\nabla M_{n,h,1}^{m+\frac{1}{2}}-\mathcal{A}_h\tilde{C}_{h,1}^{m+\frac{1}{2}}\nabla M_{c,2,h}^{m+\frac{1}{2}}-\mathcal{A}_h\tilde{C}_2^{m+\frac{1}{2}}\nabla M_{c,h,1}^{m+\frac{1}{2}}-\boldsymbol{G}_h^{m+\frac{1}{2}}+O(\tau^2+h^2),\tag{6.23a}$$

$$\frac{N_{h,1}^{m+1}-N_{h,1}^{m}}{\tau}+\nabla\cdot(\mathcal{A}_h\tilde{N}_{h,1}^{m+\frac{1}{2}}\hat{\boldsymbol{U}}_{2,PH}^{m+\frac{1}{2}}+\mathcal{A}_h\tilde{N}_{2}^{m+\frac{1}{2}}\hat{\boldsymbol{U}}_{h,1,PH}^{m+\frac{1}{2}})$$
$$=\nabla\cdot(\mathcal{A}_h\tilde{N}_{h,1}^{m+\frac{1}{2}}\nabla M_{n,2}^{m+\frac{1}{2}}+\mathcal{A}_h\tilde{N}_{2}^{m+\frac{1}{2}}\nabla M_{n,h,1}^{m+\frac{1}{2}})-H_{n,h}^{m+\frac{1}{2}}+O(\tau^2+h^2),\tag{6.23b}$$

$$M_{n,2,h}^{m+\frac{1}{2}}=F_{N_2^m}(N_2^{m+1})+\tau(\ln N_2^{m+1}-\ln N_2^{m})+N_2^{m+\frac{1}{2}}-C_2^{m+\frac{1}{2}}-\tilde{N}_2^{m+\frac{1}{2}},\tag{6.23c}$$

$$M_{n,h,1}^{m+\frac{1}{2}}=\frac{1}{N_2^{m+\frac{1}{2}}}N_{h,1}^{m+\frac{1}{2}}-C_{h,1}^{m+\frac{1}{2}},\tag{6.23d}$$

$$\frac{C_{h,1}^{m+1}-C_{h,1}^{m}}{\tau}+\nabla\cdot(\mathcal{A}_h\tilde{C}_{h,1}^{m+\frac{1}{2}}\hat{\boldsymbol{U}}_{2,PH}^{m+\frac{1}{2}}+\mathcal{A}_h\tilde{C}_{1}^{m+\frac{1}{2}}\hat{\boldsymbol{U}}_{h,1,PH}^{m+\frac{1}{2}})=-M_{c,h,1}^{m+\frac{1}{2}}-H_{c,h}^{m+\frac{1}{2}}+O(\tau^2+h^2),\tag{6.23e}$$

$$M_{c,h,1}^{m+\frac{1}{2}}=-\Delta C_{h,1}^{m+\frac{1}{2},*}+\alpha C_{h,1}^{m+\frac{1}{2}}-N_{h,1}^{m+\frac{1}{2}}+C_{h,1}^{m+\frac{1}{2}}-\tilde{C}_{h,1}^{m+\frac{1}{2}},\tag{6.23f}$$

$$\frac{\boldsymbol{U}_{h,1}^{m+1}-\hat{\boldsymbol{U}}_{h,1}^{m+1}}{\tau}+\frac{1}{2}\nabla(P_{h,1}^{m+1}-P_{h,1}^{m})=0,\tag{6.23g}$$

$$\nabla\cdot\boldsymbol{U}_{h,1,PH}^{m+1}=0.\tag{6.23h}$$

Finally, a combination of (6.21) with (6.23) results in an $O(h^4+\tau^4)$ local truncation error for $\check{\boldsymbol{U}}$, $\check{N}$, $\check{C}$, and $\check{P}$:

$$\frac{\hat{\check{\boldsymbol{U}}}^{m+1}-\check{\boldsymbol{U}}^{m}}{\tau}+b_h(\tilde{\boldsymbol{U}}^{m+\frac{1}{2}},\hat{\check{\boldsymbol{U}}}^{m+\frac{1}{2}})+\nabla_h\check{P}^{m}-\Delta_h\hat{\check{\boldsymbol{U}}}^{m+\frac{1}{2}}=-\mathcal{A}_h\tilde{\check{N}}^{m+\frac{1}{2}}\nabla_h\check{M}_n^{m+\frac{1}{2}}-\mathcal{A}_h\tilde{\check{C}}^{m+\frac{1}{2}}\nabla_h\check{M}_c^{m+\frac{1}{2}}+\zeta_{\boldsymbol{u}}^{m},\tag{6.24a}$$

$$\frac{\check{N}^{m+1}-\check{N}^{m}}{\tau}+\nabla_h\cdot(\mathcal{A}_h\tilde{N}^{m+\frac{1}{2}}\hat{\check{\boldsymbol{U}}}^{m+\frac{1}{2}})=\nabla_h\cdot(\mathcal{A}_h\tilde{N}^{m+\frac{1}{2}}\nabla_h\check{M}_n^{m+\frac{1}{2}})+\zeta_n^{m},\tag{6.24b}$$

$$\check{M}_n^{m+\frac{1}{2}}=F_{\check{N}^m}(\check{N}^{m+1})+\tau(\ln\check{N}^{m+1}-\ln\check{N}^{m})+\check{N}^{m+\frac{1}{2}}-\check{C}^{m+\frac{1}{2}}-\tilde{\check{N}}^{m+\frac{1}{2}},\tag{6.24c}$$

$$\frac{\check{C}^{m+1}-\check{C}^{m}}{\tau}+\nabla_h\cdot(\mathcal{A}_h\tilde{C}^{m+\frac{1}{2}}\hat{\check{\boldsymbol{U}}}^{m+\frac{1}{2}})=-\check{M}_c^{m+\frac{1}{2}}+\zeta_c^{m},\tag{6.24d}$$

$$\check{M}_c^{m+\frac{1}{2}}=-\Delta_h\check{C}^{m+\frac{1}{2},*}+\alpha\check{C}^{m+\frac{1}{2}}-\check{N}^{m+\frac{1}{2}}+\check{C}^{m+\frac{1}{2}}-\tilde{\check{C}}^{m+\frac{1}{2}},\tag{6.24e}$$

$$\frac{\check{\boldsymbol{U}}^{m+1}-\hat{\check{\boldsymbol{U}}}^{m+1}}{\tau}+\frac{1}{2}\nabla_h(\check{P}^{m+1}-\check{P}^{m})=0,\tag{6.24f}$$

$$\nabla\cdot\check{\boldsymbol{U}}^{m+1}=0,\tag{6.24g}$$

with $\|\zeta_{\boldsymbol{u}}^{m}\|_2$, $\|\zeta_n^{m}\|_2$, $\|\zeta_c^{m}\|_2\le B(\tau^4+h^4)$.

Additional explanations are provided to highlight the details of this higher-order consistency analysis.

1. For the cell density variables, the following mass conservation identities are valid:

$$n^0\equiv\check{N}^0,\quad\overline{n^k}=\overline{n^0},\quad\overline{\zeta_n^k}=0,\quad\overline{\check{N}^k}=\frac{1}{|\Omega|}\int_\Omega\check{N}(\cdot,t_k)\mathrm{d}\boldsymbol{x}=\frac{1}{|\Omega|}\int_\Omega\check{N}^0\mathrm{d}\boldsymbol{x}=\overline{n^0},\quad\forall k\ge0.\tag{6.25}$$

2. A corresponding phase separation estimate for the constructed $\check{N}$ becomes available, by ensuring τ and h are sufficiently small:

$$\check{N}\ge\frac{5\delta}{8},\ \text{for}\ \delta>0,\ \text{at a point-wise level.}\tag{6.26}$$

3. A discrete $W_h^{1,\infty}$ bound is established for the profile $(\check{\boldsymbol{U}},\check{N},\check{C})$ and its discrete temporal derivative:

$$\begin{aligned}&\|\check{N}^k\|_\infty\le B^*,\quad\|\check{C}^k\|_\infty\le B^*,\quad\|\check{\boldsymbol{U}}^k\|_\infty\le B^*,\quad\|\hat{\check{\boldsymbol{U}}}^{k+\frac{1}{2}}\|_\infty\le B^*,\quad\|\nabla_h\check{N}^k\|_\infty\le B^*,\quad\|\nabla_h\check{C}^k\|_\infty\le B^*,\\&\|\nabla_h\check{\boldsymbol{U}}^k\|_\infty\le B^*,\quad\|\check{N}^{k+1}-\check{N}^k\|_\infty\le B^*\tau,\quad\|\check{C}^{k+1}-\check{C}^k\|_\infty\le B^*\tau,\quad\forall k\ge0.\end{aligned}\tag{6.27}$$

Moreover, since $\check{M}_n^{m+\frac{1}{2}}$ and $\check{M}_c^{m+\frac{1}{2}}$ are determined only by the exact solution (N,C) and some correction functions, a discrete $W_h^{1,\infty}$ bound is naturally assumed:

$$\|\nabla_h\check{M}_n^{m+1/2}\|_\infty\le B^*,\quad\|\nabla_h\check{M}_c^{m+1/2}\|_\infty\le B^*.\tag{6.28}$$

Remark 6.1. Based on the phase separation estimate (6.26) for the constructed functions $\check{N}$ and their temporal regularity, it is evident that the explicit extrapolation formula for the mobility function in (6.24b) must ensure a pointwise positive mobility concentration at the time instant $t^{m+1/2}$. Consequently, the positive regularization formula in (3.2) can be omitted from the consistency analysis.

Remark 6.2. Periodic boundary conditions could also be used in the process of obtaining estimate (6.24) through asymptotic expansion analysis of high-order errors, and similar results could be derived.

6.2. A rough error estimate

The following error functions are defined:

$$
\begin{aligned}
&e_{\boldsymbol{u}}^{m} = \breve{\boldsymbol{U}}^{m} - \boldsymbol{u}^{m}, && e_{\boldsymbol{u}}^{m+\frac{1}{2}} = \breve{\boldsymbol{U}}^{m+\frac{1}{2}} - \boldsymbol{u}^{m+\frac{1}{2}}, && \tilde{e}_{\boldsymbol{u}}^{m+\frac{1}{2}} = \tilde{\boldsymbol{U}}^{m+\frac{1}{2}} - \tilde{\boldsymbol{u}}^{m+\frac{1}{2}}, && \hat{e}_{\boldsymbol{u}}^{m+1} = \hat{\boldsymbol{U}}^{m+1} - \hat{\boldsymbol{u}}^{m+1},\\
&\hat{e}_{\boldsymbol{u}}^{m+\frac{1}{2}} = \frac{1}{2}(e_{\boldsymbol{u}}^{m} + \hat{e}_{\boldsymbol{u}}^{m+1}), && e_{p}^{m} = \breve{P}^{m} - p^{m}, && e_{p}^{m+\frac{1}{2}} = \breve{P}^{m+\frac{1}{2}} - p^{m+\frac{1}{2}}, && e_{\mu_n}^{m+\frac{1}{2}} = \breve{M}_{n}^{m+\frac{1}{2}} - \mu_{n}^{m+\frac{1}{2}},\\
&e_{n}^{m} = \breve{N}^{m} - n^{m}, && e_{n}^{m+\frac{1}{2}} = \frac{1}{2}(e_{n}^{m+1} + e_{n}^{m}), && \tilde{e}_{n}^{m+\frac{1}{2}} = \frac{3}{2}e_{n}^{m} - \frac{1}{2}e_{n}^{m-1}, && e_{\mu_c}^{m+\frac{1}{2}} = \breve{M}_{c}^{m+\frac{1}{2}} - \mu_{c}^{m+\frac{1}{2}},\\
&e_{c}^{m} = \breve{C}^{m} - c^{m}, && e_{c}^{m+\frac{1}{2}} = \frac{1}{2}(e_{c}^{m+1} + e_{c}^{m}), && \tilde{e}_{c}^{m+\frac{1}{2}} = \frac{3}{2}e_{c}^{m} - \frac{1}{2}e_{c}^{m-1}, && e_{c}^{m+\frac{1}{2},*} = \frac{3}{4}e_{c}^{m+1} + \frac{1}{4}e_{c}^{m-1}.
\end{aligned}
$$

Due to the mass conservation identity (6.25), it is evident that the error functions e_n^k are always average-free: $\overline{e_n^k} = 0$ for any $k \geq 0$. As a result, their $\|\cdot\|_{-1,h}$ norms are well-defined.

Lemma 6.2. *A trilinear form is introduced as $\mathcal{B}(\boldsymbol{u},\boldsymbol{w},\boldsymbol{w}) = \langle b_h(\boldsymbol{u},\boldsymbol{w}),\boldsymbol{w}\rangle_1$. The following estimates are valid:*

$$
\mathcal{B}(\boldsymbol{u},\boldsymbol{w},\boldsymbol{w}) = 0, \quad |\mathcal{B}(\boldsymbol{u},\boldsymbol{w},\boldsymbol{w})| \leq \frac{1}{2}\|\boldsymbol{u}\|_2(\|\nabla_h \boldsymbol{w}\|_\infty \cdot \|\boldsymbol{w}\|_2 + \|\nabla_h \boldsymbol{w}\|_2 \cdot \|\boldsymbol{w}\|_\infty). \tag{6.29}
$$

Subtracting the numerical system (3.2) from the consistency estimate (6.24) leads to the following error evolution equations:

$$
\begin{aligned}
&\frac{\hat{e}_{\boldsymbol{u}}^{m+1} - e_{\boldsymbol{u}}^{m}}{\tau} + b_h(\tilde{e}_{\boldsymbol{u}}^{m+\frac{1}{2}}, \hat{\boldsymbol{U}}^{m+\frac{1}{2}}) + b_h(\tilde{\boldsymbol{u}}^{m+\frac{1}{2}}, \hat{e}_{\boldsymbol{u}}^{m+\frac{1}{2}}) + \nabla_h e_p^m - \Delta_h \hat{e}_{\boldsymbol{u}}^{m+\frac{1}{2}} + \mathcal{A}_h \tilde{e}_n^{m+\frac{1}{2}} \nabla_h \breve{M}_n^{m+\frac{1}{2}} + \mathcal{A}_h \tilde{n}^{m+\frac{1}{1}} \nabla_h e_{\mu_n}^{m+\frac{1}{2}}\\
&\qquad + \mathcal{A}_h \tilde{e}_c^{m+\frac{1}{2}} \nabla_h \breve{M}_c^{m+\frac{1}{2}} + \mathcal{A}_h \tilde{c}^{m+\frac{1}{1}} \nabla_h e_{\mu_c}^{m+\frac{1}{2}} = \zeta_{\boldsymbol{u}}^{m}, && \text{(6.30a)}\\
&\frac{e_n^{m+1} - e_n^m}{\tau} + \nabla_h \left(\mathcal{A}_h \tilde{e}_n^{m+\frac{1}{2}} \hat{\boldsymbol{U}}^{m+\frac{1}{2}} + \mathcal{A}_h \tilde{n}^{m+\frac{1}{2}} \hat{e}_{\boldsymbol{u}}^{m+\frac{1}{2}} \right) = \nabla_h \cdot \left(\mathcal{A}_h \tilde{e}_n^{m+\frac{1}{2}} \nabla_h \breve{M}_n^{m+\frac{1}{2}} + \mathcal{A}_h \tilde{n}^{m+\frac{1}{2}} \nabla_h e_{\mu_n}^{m+\frac{1}{2}} \right) + \zeta_n^m, && \text{(6.30b)}\\
&e_{\mu_n}^{m+\frac{1}{2}} = F_{\breve{N}^m}(\breve{N}^{m+1}) - F_{n^m}(n^{m+1}) + \tau \left(\ln \breve{N}^{m+1} - \ln n^{m+1} - \ln \breve{N}^m + \ln n^m \right) + e_n^{m+\frac{1}{2}} - e_c^{m+\frac{1}{2}} - \tilde{e}_n^{m+\frac{1}{2}}, && \text{(6.30c)}\\
&\frac{e_c^{m+1} - e_c^m}{\tau} + \nabla_h \left(\mathcal{A}_h \tilde{e}_c^{m+\frac{1}{2}} \hat{\boldsymbol{U}}^{m+\frac{1}{2}} + \mathcal{A}_h \tilde{c}^{m+\frac{1}{2}} \hat{e}_{\boldsymbol{u}}^{m+\frac{1}{2}} \right) = -e_{\mu_c}^{m+\frac{1}{2}} + \zeta_c^m, && \text{(6.30d)}\\
&e_{\mu_c}^{m+\frac{1}{2}} = -\Delta_h e_c^{m+\frac{1}{2},*} + \alpha e_c^{m+\frac{1}{2}} - e_n^{m+\frac{1}{2}} + e_c^{m+\frac{1}{2}} - \tilde{e}_c^{m+\frac{1}{2}}, && \text{(6.30e)}\\
&\frac{e_{\boldsymbol{u}}^{m+1} - \hat{e}_{\boldsymbol{u}}^{m+1}}{\tau} + \frac{1}{2}\nabla_h(e_p^{m+1} - e_p^m) = 0, && \text{(6.30f)}\\
&\nabla_h \cdot e_{\boldsymbol{u}}^{m+1} = 0. && \text{(6.30g)}
\end{aligned}
$$

To proceed with the convergence analysis, we make the following a-priori assumption about the numerical error functions at previous time steps:

$$
\|e_{\boldsymbol{u}}^k\|_2, \|e_n^k\|_2, \|e_c^k\|_2 \leq \tau^{\frac{15}{4}} + h^{\frac{15}{4}}, \quad k = m, m-1, \quad \|\nabla_h e_p^m\|_2 \leq \tau^{\frac{11}{4}} + h^{\frac{11}{4}}. \tag{6.31}
$$

in the next time step based on the error estimate, as will be shown later. Naturally, this assumption leads to a $W_h^{1,\infty}$ bound for the numerical error at previous time steps, which follows from the inverse inequality, the linear refinement condition $\lambda_1 h \leq \tau \leq \lambda_2 h$, and the discrete Poincaré inequality (as stated in Proposition 3.2):

$$
\begin{aligned}
&\|e_n^k\|_\infty \leq \frac{B\|e_n^k\|_2}{h} \leq B(\tau^{\frac{11}{4}} + h^{\frac{11}{4}}) \leq \tau^{\frac{5}{4}} + h^{\frac{5}{4}} \leq \frac{\delta}{8}, \quad \|e_c^k\|_\infty \leq \frac{B\|e_c^k\|_2}{h} \leq B(\tau^{\frac{11}{4}} + h^{\frac{11}{4}}) \leq \tau^{\frac{5}{4}} + h^{\frac{5}{4}} \leq \frac{\delta}{8},\\
&\|\nabla_h e_n^k\|_\infty \leq \frac{B\|e_n^k\|_\infty}{h} \leq B(\tau^{\frac{7}{4}} + h^{\frac{7}{4}}) \leq \tau + h \leq 1, \quad \|\nabla_h e_c^k\|_\infty \leq \frac{B\|e_c^k\|_\infty}{h} \leq B(\tau^{\frac{7}{4}} + h^{\frac{7}{4}}) \leq \tau + h \leq 1,
\end{aligned} \tag{6.32}
$$

for $k = m, m-1$, provided that τ and h are sufficiently small. Therefore, using the regularity assumption in (6.27), an ℓ^∞ bound for the numerical solution can be derived for the previous time steps:

$$
\|n^k\|_\infty \leq \|\breve{N}^k\|_\infty + \|e_n^k\|_\infty \leq \tilde{C}_1 := B^* + 1. \tag{6.33}
$$

Furthermore, a combination of the ℓ^∞ estimate (6.32) for the numerical error with the separation estimate (6.26) provides a similar separation bound for the numerical solution at previous time steps:

$$n^k \geq \breve{N}^k - \|e_n^k\|_\infty \geq \frac{\delta}{2}. \tag{6.34}$$

Therefore, at the intermediate time instant $t^{m+1/2}$, the following estimates can be obtained:

$$\begin{aligned}
&\text{since } \breve{N}^{m+1} - 2\breve{N}^m + \breve{N}^{m-1} = O(\tau^2), \quad \frac{3}{2}\breve{N}^m - \frac{1}{2}\breve{N}^{m-1} = \frac{1}{2}(\breve{N}^{m+1} + \breve{N}^m) + O(\tau^2),\\
&\quad \frac{1}{2}(\breve{N}^{m+1} + \breve{N}^m) = \breve{N}(t^{m+1/2}) + O(\tau^2), \quad \breve{N}(t^{m+1/2}) \geq \frac{5\delta}{8}, \quad \text{(by (6.26))},\\
&\text{so that } \frac{3}{2}\breve{N}^m - \frac{1}{2}\breve{N}^{m-1} \geq \frac{5\delta}{8} - O(\tau^2), \|\frac{3}{2}e_n^m - \frac{1}{2}e_n^{m-1}\|_\infty \leq C(\tau^{\frac{11}{4}} + h^{\frac{11}{4}}), \quad \text{(by (6.32))},\\
&\quad \tilde{n}^{m+1/2} = \frac{3}{2}n^m - \frac{1}{2}n^{m-1} = \frac{3}{2}\breve{N}^m - \frac{1}{2}\breve{N}^{m-1} - \frac{3}{2}e_n^m - \frac{1}{2}e_n^{m-1} \geq \frac{5\delta}{8} - O(\tau^2) - O(\tau^{\frac{11}{4}} + h^{\frac{11}{4}}) \geq \frac{\delta}{2}.
\end{aligned} \tag{6.35}$$

Consequently, the phase separation bound for the average mobility function, $\tilde{n}^{m+\frac{1}{2}}$, has also been established, and this bound will be helpful in the subsequent analysis.

Taking a discrete inner product with (6.30) by $2\hat{e}_{\boldsymbol{u}}^{m+1/2} = \hat{e}_{\boldsymbol{u}}^{m+1} + e_{\boldsymbol{u}}^m$ leads to

$$\begin{aligned}
&\frac{1}{\tau}(\|\hat{e}_{\boldsymbol{u}}^{m+1}\|_2^2 - \|e_{\boldsymbol{u}}^m\|_2^2) + 2\mathcal{B}(\tilde{e}_{\boldsymbol{u}}^{m+1/2}, \hat{\boldsymbol{U}}^{m+1/2}, \hat{e}_{\boldsymbol{u}}^{m+1/2}) + 2\mathcal{B}(\tilde{\boldsymbol{u}}^{m+1/2}, \hat{e}_{\boldsymbol{u}}^{m+1/2}, \hat{e}_{\boldsymbol{u}}^{m+1/2}) + 2\|\nabla_h \hat{e}_{\boldsymbol{u}}^{m+1/2}\|_2^2\\
&\quad = -\langle \nabla_h e_p^m, \hat{e}_{\boldsymbol{u}}^{m+1} + e_{\boldsymbol{u}}^m\rangle_1 - 2\langle \mathcal{A}_h \tilde{e}_n^{m+1/2} \nabla_h \breve{M}_n^{m+1/2}, \hat{e}_{\boldsymbol{u}}^{m+1/2}\rangle_1 - 2\langle \mathcal{A}_h \tilde{n}^{m+1/2} \nabla_h e_{\mu_n}^{m+1/2}, \hat{e}_{\boldsymbol{u}}^{m+1/2}\rangle_1\\
&\qquad - 2\langle \mathcal{A}_h \tilde{e}_c^{m+1/2} \nabla_h \breve{M}_c^{m+1/2}, \hat{e}_c^{m+1/2}\rangle_1 - 2\langle \mathcal{A}_h \tilde{c}^{m+1/2} \nabla_h e_{\mu_c}^{m+1/2}, \hat{e}_{\boldsymbol{u}}^{m+1/2}\rangle_1 + 2\langle \zeta_{\boldsymbol{u}}^m, \hat{e}_{\boldsymbol{u}}^{m+1/2}\rangle_1.
\end{aligned} \tag{6.36}$$

By applying the nonlinear identity (6.29) in Lemma 6.2, we immediately obtain

$$\mathcal{B}(\tilde{\boldsymbol{u}}^{m+1/2}, \hat{e}_{\boldsymbol{u}}^{m+1/2}, \hat{e}_{\boldsymbol{u}}^{m+1/2}) = 0. \tag{6.37}$$

The second term on the left-hand side of (6.36) can be bounded with the help of inequality (6.29):

$$\begin{aligned}
2|\mathcal{B}(\tilde{e}_{\boldsymbol{u}}^{m+1/2}, \hat{\boldsymbol{U}}^{m+1/2}, \hat{e}_{\boldsymbol{u}}^{m+1/2})| &\leq \|\tilde{e}_{\boldsymbol{u}}^{m+1/2}\|_2 (\nabla_h \hat{\boldsymbol{U}}^{m+1/2}\|_\infty \cdot \|\hat{e}_{\boldsymbol{u}}^{m+1/2}\|_2 + \|\hat{\boldsymbol{U}}^{m+1/2}\|_\infty \cdot \|\nabla_h \hat{e}_{\boldsymbol{u}}^{m+1/2}\|_2)\\
&\leq B^* \|\tilde{e}_{\boldsymbol{u}}^{m+1/2}\|_2 (\|\hat{e}_{\boldsymbol{u}}^{m+1/2}\|_2 + \|\nabla_h \hat{e}_{\boldsymbol{u}}^{m+1/2}\|_2) \leq B^*(C_0+1)\|\tilde{e}_{\boldsymbol{u}}^{m+1/2}\|_2 \cdot \|\nabla_h \hat{e}_{\boldsymbol{u}}^{m+1/2}\|_2\\
&\leq \frac{(B^*(C_0+1))^2}{2}\|\tilde{e}_{\boldsymbol{u}}^{m+1/2}\|_2^2 + \frac{1}{2}\|\nabla_h \hat{e}_{\boldsymbol{u}}^{m+1/2}\|_2^2 \leq \tilde{C}_2\left(3\|e_{\boldsymbol{u}}^m\|_2^2 + \|e_{\boldsymbol{u}}^{m-1}\|_2^2\right) + \frac{1}{2}\|\nabla_h \hat{e}_{\boldsymbol{u}}^{m+1/2}\|_2^2,
\end{aligned} \tag{6.38}$$

in which $\tilde{C}_2 = \frac{(B^*(C_0+1))^2}{2}$, and the $W_h^{1,\infty}$ assumption in (6.27) (for the constructed solution $\breve{\boldsymbol{U}}$) was used in the derivation. In fact, the discrete Pincaré inequality, $\|\hat{e}_{\boldsymbol{u}}^{m+1/2}\|_2 \leq C_0 \|\nabla_h \hat{e}_{\boldsymbol{u}}^{m+1/2}\|_2$, which follows from Proposition 3.2, was employed in the second step due to the no-penetration boundary condition for $\hat{e}_{\boldsymbol{u}}^{m+1/2}$.

For the numerical error inner product involving the pressure gradient, we see that

$$\langle \nabla_h e_p^m, e_{\boldsymbol{u}}^k\rangle_1 = -\langle e_p^m, \nabla \cdot e_{\boldsymbol{u}}^{m+1}\rangle_1 = 0, \quad \text{since } \nabla_h \cdot e_{\boldsymbol{u}}^m = 0,\ k = m, m+1, \tag{6.39}$$

based on the summation by parts formula (3.1b). For the other pressure gradient inner product term, an application of (6.30) gives

$$\begin{aligned}
\langle \nabla_h e_p^m, \hat{e}_{\boldsymbol{u}}^{m+1}\rangle_1 &= \langle \nabla_h e_p^m, e_{\boldsymbol{u}}^{m+1}\rangle_1 + \frac{\tau}{2}\langle \nabla_h e_p^m, \nabla_h (e_p^{m+1} - e_p^m)\rangle_1 = \frac{\tau}{2}\langle \nabla_h e_p^m, \nabla_h (e_p^{m+1} - e_p^m)\rangle_1\\
&= \frac{\tau}{4}\left(\|\nabla_h e_p^{m+1}\|_2^2 - \|\nabla_h e_p^m\|_2^2 - \|\nabla_h (e_p^{m+1} - e_p^m)\|_2^2\right),
\end{aligned} \tag{6.40}$$

where the second step relies on the identity $\langle \nabla_h e_p^m, e_{\boldsymbol{u}}^{m+1}\rangle_1 = 0$. For the second term on the right-hand side of (6.36), the discrete Hölder inequality can be applied

$$\begin{aligned}
-2\langle \mathcal{A}_h \tilde{e}_n^{m+1/2} \nabla_h \breve{M}_n^{m+1/2}, \hat{e}_{\boldsymbol{u}}^{m+1/2}\rangle_1 &\leq 2\|\tilde{e}_n^{m+1/2}\|_2 \cdot \|\nabla_h \breve{M}_n^{m+1/2}\|_\infty \cdot \|\hat{e}_{\boldsymbol{u}}^{m+1/2}\|_2 \leq 2B^* \|\tilde{e}_n^{m+1/2}\|_2 \|\hat{e}_{\boldsymbol{u}}^{m+1/2}\|_2\\
&\leq 2C_0 B^* \|\tilde{e}_n^{m+1/2}\|_2 \cdot \|\nabla_h \hat{e}_{\boldsymbol{u}}^{m+1/2}\|_2 \leq 8C_0^2(B^*)\|\tilde{e}_n^{m+1/2}\|_2^2 + \frac{1}{8}\|\nabla_h \hat{e}_{\boldsymbol{u}}^{m+1/2}\|_2^2\\
&\leq \tilde{C}_3(3\|e_n^m\|_2^2 + \|e_n^{m-1}\|_2^2) + \frac{1}{8}\|\nabla_h \hat{e}_{\boldsymbol{u}}^{m+1/2}\|_2^2,
\end{aligned} \tag{6.41a}$$

$$\begin{aligned}
-2\langle \mathcal{A}_h \tilde{e}_c^{m+1/2} \nabla_h \breve{M}_c^{m+1/2}, \hat{e}_{\boldsymbol{u}}^{m+1/2}\rangle_1 &\leq 2\|\tilde{e}_c^{m+1/2}\|_2 \cdot \|\nabla_h \breve{M}_c^{m+1/2}\|_\infty \cdot \|\hat{e}_{\boldsymbol{u}}^{m+1/2}\|_2 \leq 2B^* \|\tilde{e}_c^{m+1/2}\|_2 \cdot \|\hat{e}_{\boldsymbol{u}}^{m+1/2}\|_2\\
&\leq 2C_0 B^* \|\tilde{e}_c^{m+1/2}\|_2 \cdot \|\nabla_h \hat{e}_{\boldsymbol{u}}^{m+1/2}\|_2 \leq 8C_0^2(B^*)\|\tilde{e}_c^{m+1/2}\|_2^2 + \frac{1}{8}\|\nabla_h \hat{e}_{\boldsymbol{u}}^{m+1/2}\|_2^2\\
&\leq \tilde{C}_3(3\|e_c^m\|_2^2 + \|e_c^{m-1}\|_2^2) + \frac{1}{8}\|\nabla_h \hat{e}_{\boldsymbol{u}}^{m+1/2}\|_2^2,
\end{aligned} \tag{6.41b}$$

with $\tilde{C}_3 = 8C_0^2(B^*)^2$. Again, the $W_h^{1,\infty}$ assumption (6.28) and the discrete Poincaré inequality, $\|\hat{e}_{\boldsymbol{u}}^{m+1/2}\|_2 \leq C_0 \|\nabla_h e_{\boldsymbol{u}}^{m+1/2}\|_2$, have been applied in the derivation. A bound for the local truncation error term follows directly:

$$2\langle \zeta_{\boldsymbol{u}}^{m}, \hat{e}_{\boldsymbol{u}}^{m+1/2}\rangle_1 \le 2\|\zeta_{\boldsymbol{u}}^{m}\|_2 \cdot \|\hat{e}_{\boldsymbol{u}}^{m+1/2}\|_2 \le 2C_0\|\zeta_{\boldsymbol{u}}^{m}\|_2 \cdot \|\nabla_h \hat{e}_{\boldsymbol{u}}^{m+1/2}\|_2 \le 4C_0^2\|\zeta_{\boldsymbol{u}}^{m}\|_2^2 + \frac{1}{4}\|\nabla_h \hat{e}_{\boldsymbol{u}}^{m+1/2}\|_2^2. \tag{6.42}$$

Consequently, substituting (6.38)-(6.42) into (6.36) yields

$$\begin{aligned}
&\frac{1}{\tau}(\|\hat{e}_{\boldsymbol{u}}^{m+1}\|_2^2 - \|e_{\boldsymbol{u}}^{m}\|_2^2) + \|\nabla_h \hat{e}_{\boldsymbol{u}}^{m+1/2}\|_2^2 + \frac{\tau}{4}(\|\nabla_h e_p^{m+1}\|_2^2 - \|\nabla_h e_p^{m}\|_2^2) \\
&\quad \le -2\langle \mathcal{A}_h \tilde{n}^{m+1/2}\nabla_h e_{\mu_n}^{m+1/2}, \hat{e}_{\boldsymbol{u}}^{m+1/2}\rangle_1 - 2\langle \mathcal{A}_h \tilde{c}^{m+1/2}\nabla_h e_{\mu_c}^{m+1/2}, \hat{e}_{\boldsymbol{u}}^{m+1/2}\rangle_1 + \frac{\tau}{4}\|\nabla_h(e_p^{m+1} - e_p^{m})\|_2^2 \\
&\quad + \tilde{C}_2(3\|e_{\boldsymbol{u}}^{m}\|_2^2 + \|e_{\boldsymbol{u}}^{m-1}\|_2^2) + \tilde{C}_3(3\|e_n^{m}\|_2^2 + \|e_n^{m-1}\|_2^2 + 3\|e_c^{m}\|_2^2 + \|e_c^{m-1}\|_2^2) + 4C_0^2\|\zeta_{\boldsymbol{u}}^{m}\|_2^2.
\end{aligned} \tag{6.43}$$

Meanwhile, taking a discrete inner product with (6.30) by $2e_{\boldsymbol{u}}^{m+1}$ results in

$$\|e_{\boldsymbol{u}}^{m+1}\|_2^2 - \|\hat{e}_{\boldsymbol{u}}^{m+1}\|_2^2 + \|e_{\boldsymbol{u}}^{m+1} - \hat{e}_{\boldsymbol{u}}^{m+1}\|_2^2 = 0, \quad \text{so that} \quad \|e_{\boldsymbol{u}}^{m+1}\|_2^2 - \|\hat{e}_{\boldsymbol{u}}^{m+1}\|_2^2 + \frac{\tau^2}{4}\|\nabla_h(e_p^{m+1} - e_p^{m})\|_2^2 = 0, \tag{6.44}$$

where the discrete divergence-free condition for $e_{\boldsymbol{u}}^{m+1}$ has been utilized. By combining (6.43) and (6.44), we get

$$\begin{aligned}
&\frac{1}{\tau}(\|e_{\boldsymbol{u}}^{m+1}\|_2^2 - \|e_{\boldsymbol{u}}^{m}\|_2^2) + \|\nabla_h \hat{e}_{\boldsymbol{u}}^{m+1/2}\|_2^2 + \frac{\tau}{4}(\|\nabla_h e_p^{m+1}\|_2^2 - \|\nabla_h e_p^{m}\|_2^2) \\
&\quad \le -2\langle \mathcal{A}_h \tilde{n}^{m+1/2}\nabla_h e_{\mu_n}^{m+1/2}, \hat{e}_{\boldsymbol{u}}^{m+1/2}\rangle_1 - 2\langle \mathcal{A}_h \tilde{c}^{m+1/2}\nabla_h e_{\mu_c}^{m+1/2}, \hat{e}_{\boldsymbol{u}}^{m+1/2}\rangle_1 + \tilde{C}_2(3\|e_{\boldsymbol{u}}^{m}\|_2^2 + \|e_{\boldsymbol{u}}^{m-1}\|_2^2) \\
&\quad + \tilde{C}_3(3\|e_n^{m}\|_2^2 + \|e_n^{m-1}\|_2^2 + 3\|e_c^{m}\|_2^2 + \|e_c^{m-1}\|_2^2) + 4C_0^2\|\zeta_{\boldsymbol{u}}^{m}\|_2^2.
\end{aligned} \tag{6.45}$$

Next, we derive a rough error estimate for the KS error evolution equation. Taking a discrete inner product with (6.30b) and (6.30d) by $e_{\mu_n}^{m+1/2}$ and $e_{\mu_c}^{m+1/2}$, respectively, and a summation yields

$$\begin{aligned}
&\frac{1}{\tau}\langle e_n^{m+1}, e_{\mu_n}^{m+1/2}\rangle_C + \frac{1}{\tau}\langle e_c^{m+1}, e_{\mu_c}^{m+1/2}\rangle_C - \langle \mathcal{A}_h \tilde{n}^{m+1/2}\nabla_h e_{\mu_n}^{m+1/2}, \hat{e}_{\boldsymbol{u}}^{m+1/2}\rangle_1 \\
&\quad + \langle \mathcal{A}_h \tilde{n}^{m+1/2}\nabla_h e_{\mu_n}^{m+1/2}, \nabla_h e_{\mu_n}^{m+1/2}\rangle_1 - \langle \mathcal{A}_h \tilde{c}^{m+1/2}\nabla_h e_{\mu_c}^{m+1/2}, \hat{e}_{\boldsymbol{u}}^{m+1/2}\rangle_1 + \langle e_{\mu_c}^{m+1/2}, e_{\mu_c}^{m+1/2}\rangle_1 \\
&= \langle \mathcal{A}_h \tilde{e}_n^{m+1/2}\nabla_h e_{\mu_n}^{m+1/2}, \hat{\check{\boldsymbol{U}}}^{m+1/2}\rangle_1 - \langle \mathcal{A}_h \tilde{e}_n^{m+1/2}\nabla_h \check{M}_n^{m+1/2}, \nabla_h e_{\mu_n}^{m+1/2}\rangle_1 - \langle \nabla_h(\mathcal{A}_h \tilde{e}_c^{m+1/2}\hat{\check{\boldsymbol{U}}}^{m+1/2}), e_{\mu_c}^{m+1/2}\rangle_1 \\
&\quad + \langle \zeta_n^{m}, e_{\mu_n}^{m+1/2}\rangle_C + \frac{1}{\tau}\langle e_n^{m}, e_{\mu_n}^{m+1/2}\rangle_C + \langle \zeta_c^{m}, e_{\mu_c}^{m+1/2}\rangle_C + \frac{1}{\tau}\langle e_c^{m}, e_{\mu_c}^{m+1/2}\rangle_C,
\end{aligned} \tag{6.46}$$

with an application of summation by parts formula (3.1e). The right-hand side terms can then be bounded using the ℓ^∞ bounds from (6.27) and (6.28):

$$\begin{aligned}
\langle \mathcal{A}_h \tilde{e}_n^{m+1/2}\nabla_h e_{\mu_n}^{m+1/2}, \hat{\check{\boldsymbol{U}}}^{m+1/2}\rangle_1 &\le \|\tilde{e}_n^{m+1/2}\|_2 \cdot \|\nabla_h e_{\mu_n}^{m+1/2}\|_2 \cdot \|\hat{\check{\boldsymbol{U}}}^{m+1/2}\|_\infty \le B^*\|\tilde{e}_n^{m+1/2}\|_2\|\nabla_h e_{\mu_n}^{m+1/2}\|_2 \\
&\le 4(B^*)^2\delta^{-1}(3\|e_n^{m}\|_2^2 + \|e_n^{m-1}\|_2^2) + \frac{\delta}{16}\|\nabla_h e_{\mu_n}^{m+1/2}\|_2^2,
\end{aligned} \tag{6.47a}$$

$$\begin{aligned}
-\langle \nabla_h(\mathcal{A}_h \tilde{e}_c^{m+1/2}\hat{\check{\boldsymbol{U}}}^{m+1/2}), e_{\mu_c}^{m+1/2}\rangle_1 &= -\langle e_{\mu_c}^{m+1/2}, \tilde{e}_c^{m+1/2}\nabla_h \hat{\check{\boldsymbol{U}}}^{m+1/2} + \hat{\check{\boldsymbol{U}}}^{m+1/2}\nabla_h \tilde{e}_c^{m+1/2}\rangle_1 \\
&\le \|e_{\mu_c}^{m+1/2}\|_2 \cdot \|\tilde{e}_c^{m+1/2}\|_2 \cdot \|\nabla_h \hat{\check{\boldsymbol{U}}}^{m+1/2}\|_\infty + \|e_{\mu_c}^{m+1/2}\|_2 \cdot \|\nabla_h \tilde{e}_c^{m+1/2}\|_2 \cdot \|\hat{\check{\boldsymbol{U}}}^{m+1/2}\|_\infty \\
&\le \frac{1}{8}\|e_{\mu_c}^{m+1/2}\|_2^2 + 4(B^*)^2(\|\tilde{e}_c^{m+1/2}\|_2^2 + \|\nabla_h \tilde{e}_c^{m+1/2}\|_2^2)
\end{aligned} \tag{6.47b}$$

$$\begin{aligned}
-\langle \mathcal{A}_h \tilde{e}_n^{m+1/2}\nabla_h \check{M}_n^{m+1/2}, \nabla_h e_{\mu_n}^{m+1/2}\rangle_1 &\le \|\tilde{e}_n^{m+1/2}\|_2 \cdot \|\nabla_h e_{\mu_n}^{m+1/2}\|_2 \cdot \|\nabla_h \check{M}_n^{m+1/2}\|_\infty \\
&\le B^*\|\tilde{e}_n^{m+1/2}\|_2 \cdot \|\nabla_h e_{\mu_n}^{m+1/2}\|_2 \le 4(B^*)^2\delta^{-1}(3\|e_n^{m}\|_2^2 + \|e_n^{m-1}\|_2^2) + \frac{\delta}{16}\|\nabla_h e_{\mu_n}^{m+1/2}\|_2^2,
\end{aligned} \tag{6.47c}$$

$$\langle \zeta_n^{m}, e_{\mu_n}^{m+1/2}\rangle_C \le \|\zeta_n^{m}\|_{-1,h} \cdot \|\nabla_h e_{\mu_n}^{m+1/2}\|_2 \le 4\delta^{-1}\|\zeta_n^{m}\|_{-1,h}^2 + \frac{\delta}{16}\|\nabla e_{\mu_n}^{m+1/2}\|_2^2, \tag{6.47d}$$

$$\langle \zeta_c^{m}, e_{\mu_c}^{m+1/2}\rangle_C \le 4\|\zeta_c^{m}\|_2^2 + \frac{1}{16}\|e_{\mu_c}^{m+1/2}\|_2^2, \tag{6.47e}$$

$$\langle e_n^{m}, e_{\mu_n}^{m+1/2}\rangle_C \le \|e_n^{m}\|_{-1,h} \cdot \|\nabla_h e_{\mu_n}^{m+1/2}\|_2 \le \frac{4}{\delta}\|e_n^{m}\|_{-1,h}^2 + \frac{\delta}{16}\|\nabla_h e_{\mu_n}^{m+1/2}\|_2^2, \tag{6.47f}$$

$$\langle e_c^{m}, e_{\mu_c}^{m+1/2}\rangle_C \le 4\|e_c^{m}\|_2^2 + \frac{1}{16}\|e_{\mu_c}^{m+1/2}\|_2^2. \tag{6.47g}$$

With the help of the phase separation bound (6.35) for the average mobility functions, the following estimate could be established:

$$\langle \mathcal{A}_h \tilde{n}^{m+1/2}\nabla_h e_{\mu_n}^{m+1/2}, \nabla_h e_{\mu_n}^{m+1/2}\rangle_1 \ge \frac{\delta}{2}\|\nabla_h e_{\mu_n}^{m+1/2}\|_2^2. \tag{6.48}$$

For the first two terms on the left-hand side of (6.46), we refer to a preliminary rough estimate previously derived in [28].

Lemma 6.3. *[28] The constructed approximate solution $\check{N}$ is assumed to satisfy the regularity condition (6.27) and the phase separation assumption (6.26). In addition, the a-priori assumption (6.31) is applied to the numerical solution at the previous time steps. Additionally, we introduce the following sets:*

$$\Lambda_n = \left\{ (i,j) : n_{i,j}^{m+1} \geq 2B^* + 1 \right\}, \tag{6.49}$$

and let $K_n^* = |\Lambda_n|$ *represent the number of grid points within* Λ_n*. Then we have a rough bound control of the following nonlinear inner products:*

$$\langle e_n^{m+1}, F_{\check{N}^m}(\check{N}^{m+1}) - F_{n^m}(n^{m+1})\rangle_C + \tau\langle e_n^{m+1}, \ln \check{N}^{m+1} - \ln n^{m+1} - (\ln \check{N}^m - \ln n^m)\rangle_C \geq \frac{1}{2}B^* K_n^* h^2 - \tilde{C}_4 \|e_n^m\|_2^2, \tag{6.50}$$

in which $\tilde{C}_4$ *is a constant that depends only on* δ *and* B^**, independent of* τ *and* h*.*

As a direct consequence of Lemma 6.3, we see that

$$\begin{aligned}
&\langle e_n^{m+1}, e_{\mu_n}^{m+1/2}\rangle_C + \langle e_c^{m+1}, e_{\mu_c}^{m+1/2}\rangle_C = \langle e_n^{m+1}, F_{\check{N}^m}(\check{N}^{m+1}) - F_{n^m}(n^{m+1}) + \langle e_n^{m+1/2} - e_c^{m+1/2} - \tilde{e}_n^{m+1/2}, e_n^{m+1}\rangle_C \\
&\qquad + \tau\langle e_n^{m+1}, \ln \check{N}^{m+1} - \ln n^{m+1}\rangle_C - \tau\langle e_n^{m+1}, \ln \check{N}^m - \ln n^m\rangle_C \\
&\qquad + \langle e_c^{m+1}, -\Delta_h e_c^{m+1/2,*} + \alpha e_c^{m+1/2} - e_n^{m+1/2} + e_c^{m+1/2} - \tilde{e}_c^{m+1/2}\rangle_C \\
&\geq \frac{1}{2}B^* K_n^* h^2 - \tilde{C}_4\|e_n^m\|_2^2 + \langle e_n^{m+1/2} - e_c^{m+1/2} - \tilde{e}_n^{m+1/2}, e_n^{m+1}\rangle_C \\
&\qquad + \langle e_c^{m+1}, -\Delta_h e_c^{m+1/2,*} + \alpha e_c^{m+1/2} - e_n^{m+1/2} + e_c^{m+1/2} - \tilde{e}_c^{m+1/2}\rangle_C \\
&\geq \frac{1}{2}B^* K_n^* h^2 + \frac{5\beta_0}{16}\|e_n^{m+1}\|_2^2 + \frac{\alpha}{8}\|e_c^{m+1}\|_2^2 + \frac{1}{2}\|\nabla_h e_c^{m+1}\|_2^2 - \frac{1}{16}\|\nabla_h e_c^{m-1}\|_2^2 \\
&\qquad - (\frac{4}{\beta_0} + \frac{2}{\alpha} + \tilde{C}_4)\|e_n^m\|_2^2 - (\frac{1}{\beta_0} + 2\alpha + \frac{8}{\alpha})\|e_c^m\|_2^2 - \frac{1}{\beta_0}\|e_n^{m-1}\|_2^2 - \frac{2}{\alpha}\|e_c^{m-1}\|_2^2,
\end{aligned} \tag{6.51}$$

with $\beta_0 \leq \frac{\alpha}{2+\alpha}$. Subsequently, a substitution of (6.47)-(6.51) into (6.46) yields

$$\begin{aligned}
&\frac{1}{\tau}\left(\frac{1}{2}B^* K_n^* h^2 + \frac{5\beta_0}{16}\|e_n^{m+1}\|_2^2 + \frac{\alpha}{8}\|e_c^{m+1}\|_2^2 + \frac{1}{2}\|\nabla_h e_c^{m+1}\|_2^2\right) + \frac{\delta}{4}\|\nabla_h e_{\mu_n}^{m+1/2}\|_2^2 + \frac{1}{4}\|e_{\mu_c}^{m+1/2}\|_2^2 \\
&\qquad - \langle \mathcal{A}_h \tilde{n}^{m+1/2}\nabla_h e_{\mu_n}^{m+1/2}, \hat{e}_{\boldsymbol{u}}^{m+1/2}\rangle_1 - \langle \mathcal{A}_h \tilde{c}^{m+1/2}\nabla_h e_{\mu_c}^{m+1/2}, \hat{e}_{\boldsymbol{u}}^{m+1/2}\rangle_1 \\
&\leq 4(B^*)^2(\|\tilde{e}_c^{m+1/2}\|_2^2 + \|\nabla_h \tilde{e}_c^{m+1/2}\|_2^2) + \frac{1}{16\tau}\|\nabla_h e_c^{m-1}\|_2^2 + 4\delta^{-1}\|\zeta_n^m\|_{-1,h}^2 + 4\|\zeta_c^m\|_2^2 + \frac{4}{\tau\delta}\|e_n^m\|_{-1,h}^2 \\
&\qquad + (24(B^*)^2\delta^{-1} + 4\beta_0^{-1}\tau^{-1} + 2\alpha^{-1}\tau^{-1} + \tilde{C}_4\tau^{-1})\|e_n^m\|_2^2 + (8(B^*)^2\delta^{-1} + \beta_0^{-1}\tau^{-1})\|e_n^{m-1}\|_2^2 \\
&\qquad + (4\tau^{-1} + \beta_0^{-1}\tau^{-1} + 2\alpha\tau^{-1} + 8\alpha^{-1}\tau^{-1})\|e_c^m\|_2^2 + \frac{2}{\alpha\tau}\|e_c^{m-1}\|_2^2.
\end{aligned} \tag{6.52}$$

Moreover, a combination of (6.45) and (6.52) leads to

$$\begin{aligned}
&\frac{1}{2}\|e_{\boldsymbol{u}}^{m+1}\|_2^2 + \frac{\tau^2}{8}\|\nabla_h e_p^{m+1}\|_2^2 + \frac{\tau\delta}{4}\|\nabla_h e_{\mu_n}^{m+1/2}\|_2^2 + \frac{\tau}{4}\|e_{\mu_c}^{m+1/2}\|_2^2 + \frac{5\beta_0}{16}\|e_n^{m+1}\|_2^2 + \frac{\alpha}{8}\|e_c^{m+1}\|_2^2 + \frac{1}{2}\|\nabla_h e_c^{m+1}\|_2^2 + \frac{1}{2}B^* K_n^* h^2 \\
&\leq \frac{1}{2}\|e_{\boldsymbol{u}}^m\|_2^2 + \frac{\tau^2}{8}\|\nabla_h e_p^m\|_2^2 + \frac{\tilde{C}_3\tau}{2}(3\|e_n^m\|_2^2 + \|e_n^{m-1}\|_2^2 + 3\|e_c^m\|_2^2 + \|e_c^{m-1}\|_2^2) + \frac{\tilde{C}_2\tau}{2}(3\|e_{\boldsymbol{u}}^m\|_2^2 + \|e_{\boldsymbol{u}}^{m-1}\|_2^2) \\
&\qquad + 4(B^*)^2\tau(\|\tilde{e}_c^{m+1/2}\|_2^2 + \|\nabla_h \tilde{e}_c^{m+1/2}\|_2^2) + \frac{1}{16}\|\nabla_h e_c^{m-1}\|_2^2 + 4\delta^{-1}\tau\|\zeta_n^m\|_{-1,h}^2 + 4\tau\|\zeta_c^m\|_2^2 + \frac{4}{\delta}\|e_n^m\|_{-1,h}^2 \\
&\qquad + (24(B^*)^2\delta^{-1}\tau + 4\beta_0^{-1} + 2\alpha^{-1} + \tilde{C}_4)\|e_n^m\|_2^2 + (8(B^*)^2\delta^{-1}\tau + \beta_0^{-1})\|e_n^{m-1}\|_2^2 + 2C_0^2\tau\|\zeta_{\boldsymbol{u}}^m\|_2^2 \\
&\qquad + (4 + \beta_0^{-1} + 2\alpha + 8\alpha^{-1})\|e_c^m\|_2^2 + \frac{2}{\alpha}\|e_c^{m-1}\|_2^2.
\end{aligned} \tag{6.53}$$

At the same time, the following estimates for the right-hand side of (6.53) can be derived using the a-priori assumption (6.31):

$$4\delta^{-1}\|e_n^m\|_{-1,h}^2 \leq 4C_0\delta^{-1}\|e_n^m\|_2^2 \leq B(\tau^{\frac{15}{2}} + h^{\frac{15}{2}}), \tag{6.54a}$$

$$4\delta^{-1}\tau\|\zeta_n^m\|_{-1,h}^2, 2C_0^2\tau\|\zeta_{\boldsymbol{u}}^m\|_2^2 \leq B(\tau^9 + \tau h^8), \tag{6.54b}$$

$$\frac{\tilde{C}_3\tau}{2}(3\|e_n^m\|_2^2 + \|e_n^{m-1}\|_2^2 + 3\|e_c^m\|_2^2 + \|e_c^{m-1}\|_2^2) \leq B(\tau^{\frac{17}{2}} + h^{\frac{17}{2}}), \tag{6.54c}$$

$$\frac{1 + 3\tilde{C}_2\tau}{2}\|e_{\boldsymbol{u}}^m\|_2^2 + \frac{\tilde{C}_2\tau}{2}\|e_{\boldsymbol{u}}^{m-1}\|_2^2 \leq B(\tau^{\frac{15}{2}} + h^{\frac{15}{2}}), \tag{6.54d}$$

$$4(B^*)^2\tau(\|\tilde{e}_c^{m+1/2} + \|\nabla_h \tilde{e}_c^{m+1/2}\|_2^2) \leq B(\tau^{\frac{13}{2}} + h^{\frac{13}{2}}) \tag{6.54e}$$

$$\frac{\tau^2}{8}\|\nabla_h e_p^m\|_2^2 \leq B(\tau^{\frac{15}{2}} + h^{\frac{15}{2}}), \tag{6.54f}$$

$$\|\nabla_h e_c^{m-1}\|_2^2 \leq B(\tau^{\frac{11}{2}} + h^{\frac{11}{2}}), \tag{6.54g}$$

$$4\delta^{-1}\tau\|\zeta_n^m\|_{-1,h}^2,\ 4\tau\|\zeta_c^m\|_2^2,\ 2C_0^2\tau\|\zeta_{\boldsymbol{u}}^m\|_2^2 \leq B(\tau^9 + h^8). \tag{6.54h}$$

In fact, these results rely on repeated application of the discrete Poincaré inequality, $\|f\|_{-1,h} \le C_0\|f\|_2$, along with the linear refinement condition $\lambda_1 h \le \tau \le \lambda_2 h$. Moreover, its combination with (6.54) and (6.45)-(6.48) yields

$$\frac{1}{2}\|e_{\boldsymbol{u}}^{m+1}\|_2^2 + \tilde{C}_5(\|e_n^{m+1}\|_2^2 + \|e_c^{m+1}\|_2^2) \le B(\tau^{\frac{11}{2}} + h^{\frac{11}{2}}).$$

As a result, the following rough error estimate can be established:

$$\|e_{\boldsymbol{u}}^{m+1}\|_2 + \|e_n^{m+1}\|_2 + \|e_c^{m+1}\|_2 \le \hat{C}(\tau^{\frac{11}{4}} + h^{\frac{11}{4}}),$$

under the linear refinement requirement $\lambda_1 h \le \tau \le \lambda_2 h$, where $\hat{C}$ depends only on the physical parameters and the computational domain.

As an immediate implication of this rough error estimate, an application of the 2-D inverse inequality gives

$$\|e_n^{m+1}\|_\infty \le \frac{B\|e_n^{m+1}\|_2}{h} \le B(\tau^{\frac{7}{4}} + h^{\frac{7}{4}}) \le \frac{\delta}{8}, \tag{6.55}$$

under the same linear refinement requirement, provided that τ and h are sufficiently small. With the help of the separation estimate (6.26) for the constructed approximate solution $\check{N}$, a similar property becomes available for the numerical solution at time step t^{m+1}:

$$\frac{\delta}{2} \le n^{m+1} \le B^* + \frac{\delta}{2} \le \tilde{C}_1. \tag{6.56}$$

This $\|\cdot\|_\infty$ bound is essential for the forthcoming refined error analysis. In addition, we are able to derive the following estimate for the discrete temporal derivative of the numerical solution:

$$\begin{aligned} &\|e_n^{m+1} - e_n^m\|_\infty \le \|e_n^{m+1}\|_\infty + \|e_n^m\|_\infty \le B(\tau^{\frac{7}{4}} + h^{\frac{7}{4}}) \le \tau, \quad \text{(by (6.32), (6.55))}, \quad \|\check{N}^{m+1} - \check{N}^m\|_\infty \le B^*\tau, \quad \text{(by (6.27))}, \\ &\|n^{m+1} - n^m\|_\infty \le \|\check{N}^{m+1} - \check{N}^m\|_\infty + \|e_n^{m+1} - e_n^m\|_\infty \le (B^* + 1)\tau. \end{aligned} \tag{6.57}$$

6.3. A refined error estimate

We review the preliminary results that have been established in existing an work [28].

Lemma 6.4. *[28] Given the a-priori $\|\cdot\|_\infty$ estimate (6.33), (6.34) for the numerical solution at the previous time steps, along with the rough $\|\cdot\|_\infty$ estimates (6.56), (6.57) for the one at the next time step, we obtain*

$$\begin{aligned} &\langle e_n^{m+1} - e_n^m, F_{\check{N}^m}(\check{N}^{m+1}) - F_{n^m}(n^{m+1})\rangle_C \ge \frac{1}{2}\left(\langle \frac{1}{\check{N}^{m+1}}, (e_n^{m+1})^2\rangle_C - \langle \frac{1}{\check{N}^m}, (e_n^m)^2\rangle_C\right) - \tilde{C}_6\tau(\|e_n^{m+1}\|_2^2 + \|e_n^m\|_2^2), \\ &\langle e_n^{m+1} - e_n^m, \ln \hat{N}^{m+1} - \ln n^{m+1} - (\ln \hat{N}^m - \ln n^m)\rangle_C \ge -\tilde{C}_7\tau(\|e_n^{m+1}\|_2^2 + \|e_n^m\|_2^2), \end{aligned} \tag{6.58}$$

in which the constants $\tilde{C}_6$ and $\tilde{C}_7$ only depend on δ, and C^*.

Now we proceed into the refined error estimate. A combination of the inner product equation (6.46) with the estimates (6.47) and (6.48) yields

$$\begin{aligned} &\langle e_n^{m+1} - e_n^m, e_{\mu_n}^{m+1/2}\rangle_C + \langle e_c^{m+1} - e_c^m, e_{\mu_c}^{m+1/2}\rangle_C + \frac{5\tau\delta}{16}\|\nabla_h e_{\mu_n}^{m+1/2}\|_2^2 + \frac{\tau}{2}\|e_{\mu_c}^{m+1/2}\|_2^2 \\ &\quad - \tau\langle \mathcal{A}_h\tilde{n}^{m+1/2}\nabla_h e_{\mu_n}^{m+1/2}, \hat{e}_{\boldsymbol{u}}^{m+1/2}\rangle_1 - \tau\langle \mathcal{A}_h\tilde{c}^{m+1/2}\nabla_h e_{\mu_c}^{m+1/2}, \hat{e}_{\boldsymbol{u}}^{m+1/2}\rangle_1 \\ &\le 8(B^*)^2\delta^{-1}\tau(3\|e_n^m\|_2^2 + \|e_n^{m-1}\|_2^2) + 4(B^*)^2\tau(\|\tilde{e}_c^{m+1/2}\|_2^2 + \|\nabla_h\tilde{e}_c^{m+1/2}\|_2^2) + 4\delta^{-1}\tau\|\xi_n^m\|_{-1,h}^2 + 4\tau\|\xi_c^m\|_2^2. \end{aligned} \tag{6.59}$$

Meanwhile, the temporal stencil inner product requires a more detailed analysis. An explicit expansion of $e_{\mu_n}^{m+1/2}$ and $e_{\mu_c}^{m+1/2}$ shows that

$$\begin{aligned} &\langle e_n^{m+1} - e_n^m, e_{\mu_n}^{m+1/2}\rangle_C + \langle e_c^{m+1} - e_c^m, e_{\mu_c}^{m+1/2}\rangle_C = \langle e_n^{m+1} - e_n^m, F_{\check{N}^m}(\check{N}^{m+1}) - F_{n^m}(n^{m+1})\rangle_C \\ &\quad + \langle e_n^{m+1} - e_n^m, e_n^{m+1/2} - e_c^{m+1/2} - \tilde{e}_n^{m+1/2}\rangle_C + \tau\langle e_n^{m+1} - e_n^m, \ln\check{N}^{m+1} - \ln n^{m+1} - (\ln\check{N}^m - \ln n^m)\rangle_C \\ &\quad + \langle e_c^{m+1} - e_c^m, -\Delta_h e_c^{m+1/2,*} + \alpha e_c^{m+1/2} - e_n^{m+1/2} + e_c^{m+1/2} - \tilde{e}_c^{m+1/2}\rangle_C \\ &\ge \mathcal{F}^{m+1} - \mathcal{F}^m - (\tilde{C}_6\tau + \tilde{C}_7\tau + \frac{1}{2})(\|e_n^{m+1}\|_2^2 + \|e_n^m\|_2^2 + \|e_c^{m+1}\|_2^2 + \|e_c^m\|_2^2), \\ &\mathcal{F}^{m+1} = \frac{1}{2}\left\langle \frac{1}{\check{N}^{m+1}}, (e_n^{m+1})^2\right\rangle_C + \frac{1}{4}(\|e_n^{m+1} - e_n^m\|_2^2 + \|e_c^{m+1} - e_c^m\|_2^2) + \frac{1}{2}\|\nabla_h e_c^{m+1}\|_2^2 + \frac{1}{8}\|\nabla_h(e_c^{m+1} - e_c^m)\|_2^2 + \frac{\alpha}{2}\|e_c^{m+1}\|_2^2. \end{aligned} \tag{6.60}$$

In turn, a substitution of (6.60) into (6.59) results in

$$\begin{aligned}
&\mathcal{F}^{m+1}-\mathcal{F}^{m}-\tau\langle\mathcal{A}_h\tilde{n}^{m+1/2}\nabla_h e_{\mu_n}^{m+1/2},\hat{e}_{\boldsymbol{u}}^{m+1/2}\rangle_1-\tau\langle\mathcal{A}_h\tilde{c}^{m+1/2}\nabla_h e_{\mu_c}^{m+1/2},\hat{e}_{\boldsymbol{u}}^{m+1/2}\rangle_1+\frac{5\tau\delta}{16}\|\nabla_h e_{\mu_n}^{m+1/2}\|_2^2+\frac{\tau}{2}\|e_{\mu_c}^{m+1/2}\|_2^2\\
&\quad\le(\tilde{C}_6\tau+\tilde{C}_7\tau+\frac{1}{2})(\|e_n^{m+1}\|_2^2+\|e_n^m\|_2^2+\|e_c^{m+1}\|_2^2+\|e_c^m\|_2^2)+8(B^*)^2\delta^{-1}\tau(3\|e_n^m\|_2^2+\|e_n^{m-1}\|_2^2)\\
&\qquad+4(B^*)^2\tau(\|\tilde{e}_c^{m+1/2}\|_2^2+\|\nabla_h\tilde{e}_c^{m+1/2}\|_2^2)+4\delta^{-1}\tau\|\zeta_n^m\|_{-1,h}^2+4\tau\|\zeta_c^m\|_2^2\\
&\quad\le\tilde{C}_8\tau(\mathcal{F}^{m+1}+\mathcal{F}^m+\mathcal{F}^{m-1})+4\delta^{-1}\tau\|\zeta_n^m\|_{-1,h}^2+4\tau\|\zeta_c^m\|_2^2,
\end{aligned}\tag{6.61}$$

with $\tilde{C}_8=2(\tilde{C}_6+\tilde{C}_7+\frac{1}{2}+8(B^*)^2\delta^{-1})B^*$, and the following bound has been applied in the last step:

$$\left\langle\frac{1}{\check{N}^k},(e_n^k)^2\right\rangle_C\ge\frac{1}{B^*}\|e_n^k\|_2^2,\quad\text{so that}\quad\mathcal{F}^k\ge\frac{1}{2B^*}\|e_n^k\|_2^2+\frac{\alpha}{2}\|e_c^k\|_2^2+\frac{1}{2}\|\nabla_h e_c^k\|_2^2.$$

In addition, a combination of (6.61) and (6.45) leads to

$$\begin{aligned}
&\frac{1}{2}(\|e_{\boldsymbol{u}}^{m+1}\|_2^2-\|e_{\boldsymbol{u}}^m\|_2^2)+\frac{\tau}{2}\|\nabla_h\hat{e}_{\boldsymbol{u}}^{m+1/2}\|_2^2+\frac{\tau^2}{8}(\|\nabla_h e_p^{m+1}\|_2^2-\|\nabla_h e_p^m\|_2^2)+\mathcal{F}^{m+1}-\mathcal{F}^m+\frac{5\tau\delta}{16}\|\nabla_h e_{\mu_n}^{m+1/2}\|_2^2+\frac{\tau}{2}\|e_{\mu_c}^{m+1/2}\|_2^2\\
&\quad\le\tilde{C}_8\tau(\mathcal{F}^{m+1}+\mathcal{F}^m+\mathcal{F}^{m-1})++4\delta^{-1}\tau\|\zeta_n^m\|_{-1,h}^2+4\tau\|\zeta_c^m\|_2^2+4C_0^2\tau\|\zeta_{\boldsymbol{u}}^m\|_2^2\\
&\qquad+\tilde{C}_2\tau(3\|e_{\boldsymbol{u}}^m\|_2^2+\|e_{\boldsymbol{u}}^{m-1}\|_2^2)+\tilde{C}_3\tau(3\|e_n^m\|_2^2+\|e_n^{m-1}\|_2^2+3\|e_c^m\|_2^2+\|e_c^{m-1}\|_2^2).
\end{aligned}$$

With an introduction of a unified error functional, $\mathcal{G}^k=\mathcal{F}^k+\frac{1}{2}\|e_{\boldsymbol{u}}^k\|_2^2+\frac{\tau^2}{8}\|\nabla_h e_p^k\|_2^2$, we see that

$$\mathcal{G}^{m+1}-\mathcal{G}^m\le\tilde{C}_9\tau(\mathcal{G}^{m+1}+\mathcal{G}^m+\mathcal{G}^{m-1})+4C_0^2\tau\|\zeta_{\boldsymbol{u}}^m\|_2^2+4\delta^{-1}\tau\|\zeta_n^m\|_{-1,h}^2+4\tau\|\zeta_c^m\|_2^2,$$

with $\tilde{C}_9=\max(\tilde{C}_8+6\tilde{C}_3B^*,6\tilde{C}_2)$. Therefore, with sufficiently small τ and h, an application of discrete Gronwall inequality results in the desired higher order convergence estimate

$$\mathcal{G}^{m+1}\le B(\tau^8+h^8),\quad\text{so that}\quad\|e_{\boldsymbol{u}}^{m+1}\|_2+\|e_n^{m+1}\|_2+\|e_c^{m+1}\|_2+\tau\|\nabla_h e_p^{m+1}\|_2\le B(\tau^4+h^4),\tag{6.62}$$

in which the higher order truncation error accuracy, $\|\zeta_{\boldsymbol{u}}^m\|_2,\|\zeta_n^m\|_2,\|\zeta_c^m\|_2\le B(\tau^4+h^4)$, has been applied in the analysis. This completes the refined error estimate.

Recovery of the a-priori assumption (6.31)

With the higher order convergence estimate (6.62) at hand, the a-priori assumption (6.31) is recovered at the next time step t^{m+1}:

$$\|e_{\boldsymbol{u}}^{m+1}\|_2,\|e_n^{m+1}\|_2,\|e_c^{m+1}\|_2\le B(\tau^4+h^4)\le\tau^{\frac{15}{4}}+h^{\frac{15}{4}},\quad\|\nabla_h e_p^{m+1}\|_2\le B(\tau^3+h^3)\le\tau^{\frac{11}{4}}+h^{\frac{11}{4}},$$

provided that τ and h are sufficiently small and the linear refinement condition holds. This enables the use of induction, completing the higher-order convergence analysis.

Furthermore, the error estimate (6.6) for the solution variables is derived by combining (6.62) with the constructed expansion (6.7) of the approximate solution $(\check{N},\check{C})$, together with the projection estimate (6.3). A similar procedure yields the error bound (6.6) for the pressure variable.

This concludes the proof of Theorem 6.1.

Remark 6.3. An extension of the present convex-splitting scheme to the third (or higher) order accuracy turns out to be highly nontrivial. Naturally, it is very important for gradient flow-fluid coupled system to keep the total energy dissipation at numerical level. On the other hand, it becomes difficult to define the numerically corrected energy using multi-step numerical solutions for the higher order schemes. For the KSNS system studied in this manuscript, we are trying to construct a BDF3 scheme with corrected numerical energy, which will be our future work.

7. Numerical experiments

This section presents a few numerical experiments to validate the theoretical analysis, including tests for the convergence rate, energy stability, mass conservation, and density positivity. The computational domain is set as $\Omega=[0,2\pi]\times[0,2\pi]$, with $\alpha=1$, and a first-order scheme is used to obtain the numerical solution at the initial time step.

Example 1. The initial data is chosen as

$$\begin{aligned}
&n_0(x,y)=0.5+0.2\sin(x)\cos(y),\quad c_0(x,y)=0.8\exp\left(-\frac{(x-\pi)^2+(y-\pi)^2}{2.25^2}\right),\\
&u_0(x,y)=-0.25\sin^2(x)\sin(2y),\quad v_0(x,y)=0.25\sin(2x)\sin^2(y),\quad p_0(x,y)=\cos(0.5x)\cos(0.5y).
\end{aligned}\tag{7.1}$$

The computation is based on a sequence of uniform mesh resolutions, where the time step size is set to $\tau=0.005h$. As the exact solution cannot be explicitly represented, we evaluate the convergence rate by measuring the Cauchy error, similar to the method in

Table 1
The ℓ^2 error and convergence rate for n and c at $T = 0.1$, with $\tau = 0.005h$ and the initial condition (7.1).

h	$\|e_n\|_2$	Order	$\|e_c\|_2$	Order
2^{-3}	2.1438E-02	-	1.9485E-02	-
2^{-4}	5.8785E-03	1.8666	5.6975E-03	1.7740
2^{-5}	1.4742E-03	1.9955	1.4381E-03	1.9862
2^{-6}	3.6903E-04	1.9981	3.5787E-04	2.0067

Table 2
The ℓ^2 error and convergence rate for u, v and p at $T = 0.1$, with $\tau = 0.005h$ and the initial condition (7.1).

h	$\|e_u\|_2$	Order	$\|e_v\|_2$	Order	$\|e_p\|_2$	Order
2^{-3}	4.8148E-02	-	4.8149E-02	-	1.8048E-02	-
2^{-4}	1.2964E-02	1.8930	1.2964E-02	1.8930	4.6242E-03	1.9646
2^{-5}	3.2664E-03	1.9887	3.2664E-03	1.9887	1.3076E-03	1.8223
2^{-6}	8.1868E-04	1.9963	8.1868E-04	1.9963	3.4283E-04	1.9313

Table 3
The ℓ^∞ error and convergence rate for n and c at $T = 0.1$, with $\tau = 0.005h$ and the initial condition (7.1).

h	$\|e_n\|_\infty$	Order	$\|e_c\|_\infty$	Order
2^{-3}	6.1816E-03	-	9.2931E-03	-
2^{-4}	1.9060E-03	1.6974	2.8172E-03	1.7219
2^{-5}	5.0416E-04	1.9186	7.1463E-04	1.9790
2^{-6}	1.2823E-04	1.9752	1.7779E-04	2.0071

Table 4
The ℓ^∞ error and convergence rate for u, v and p at $T = 0.1$, with $\tau = 0.005h$ and the initial condition (7.1).

h	$\|e_u\|_\infty$	Order	$\|e_v\|_\infty$	Order	$\|e_p\|_\infty$	Order
2^{-3}	7.9622E-03	-	7.9621E-03	-	7.5462E-03	-
2^{-4}	3.1473E-03	1.3391	3.1463E-03	1.3395	2.3278E-03	1.6968
2^{-5}	8.7145E-04	1.8526	8.7104E-04	1.8529	7.1734E-04	1.6982
2^{-6}	2.2328E-04	1.9645	2.2326E-04	1.9640	1.8326E-04	1.9688

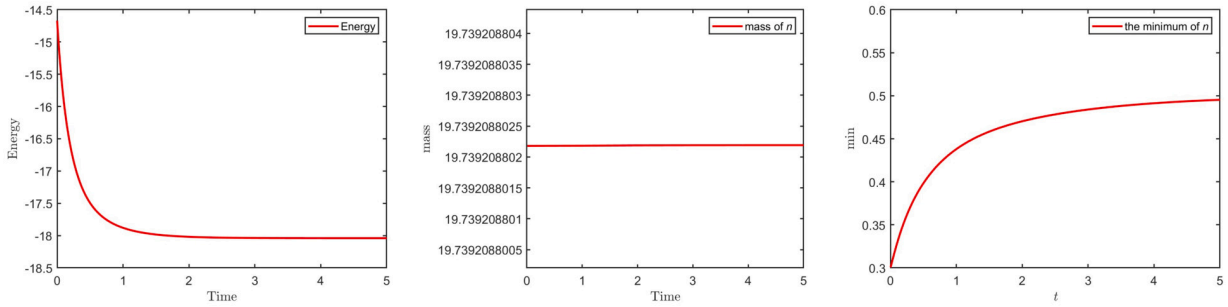

Fig. 1. Time evolution of the total energy (left), the mass of n (middle), and the minimum value of n (right) at $T = 5$ with initial data (7.1).

[40]. Specifically, the error between grid spacings h and $h/2$ is computed as $\|e_\zeta\| = \|\zeta_h - \zeta_{h/2}\|$. The ℓ^2 error (see Tables 1 and 2) and ℓ^∞ error (see Tables 3 and 4) for all physical variables at $T = 0.1$ are reported, while the results have indicated almost perfect second-order accuracy in both time and space, consistent with the theoretical analysis.

The simulation results further confirm the numerical scheme's ability to preserve key physical properties. Total mass conservation of the cell density variable is validated on the middle of Fig. 1, while the left side implies a monotone dissipation of the discrete total energy E_h, supporting the theoretical findings. The positivity-preserving property is examined by tracking the minimum cell density value (right of Fig. 1), demonstrating that the numerical solutions remain positive throughout, even if a few very small values have appeared. These results have validated that the proposed scheme successfully maintains mass conservation, total energy dissipation, and positivity at the discrete level.

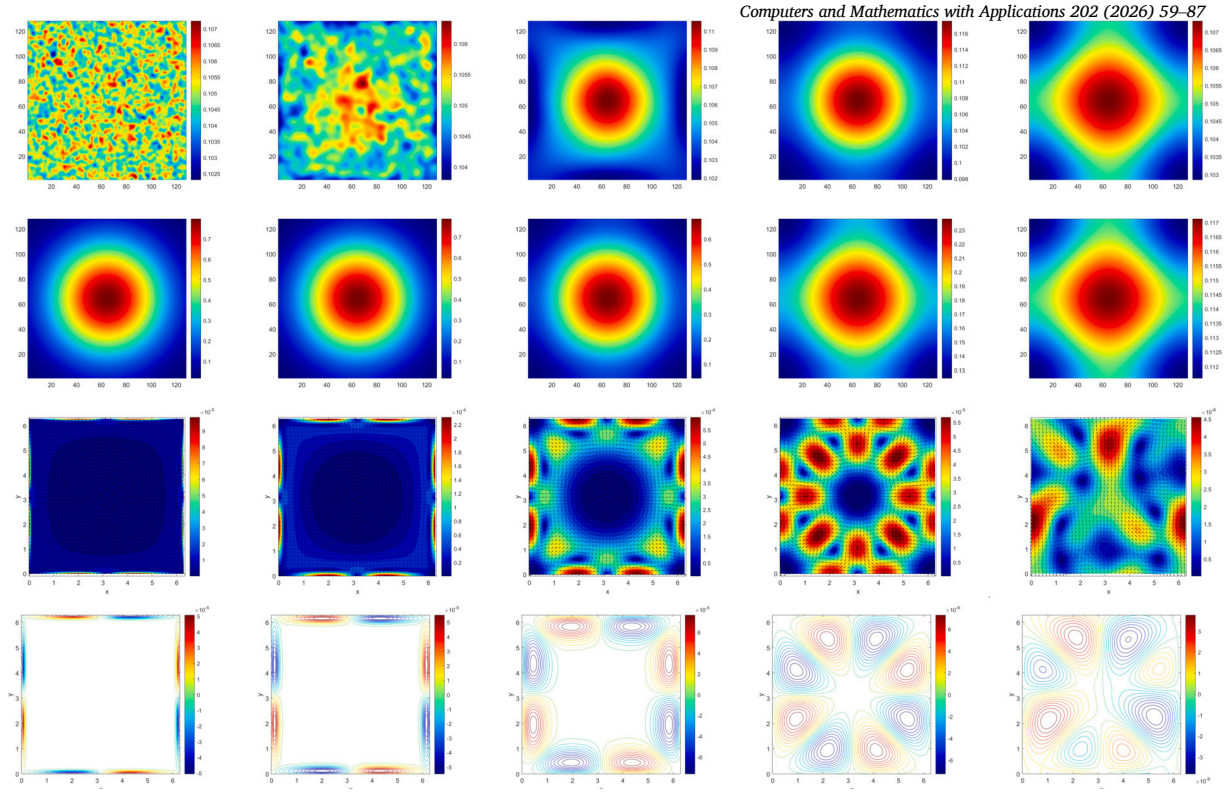

Fig. 2. Snapshots of the KSNS system with initial data (7.2) at $T = 0.002, 0.01, 0.1, 1, 3$. From top to bottom are the cell density n, chemo-attractant c, fluid velocity $\boldsymbol{u}$, and vorticity contours.

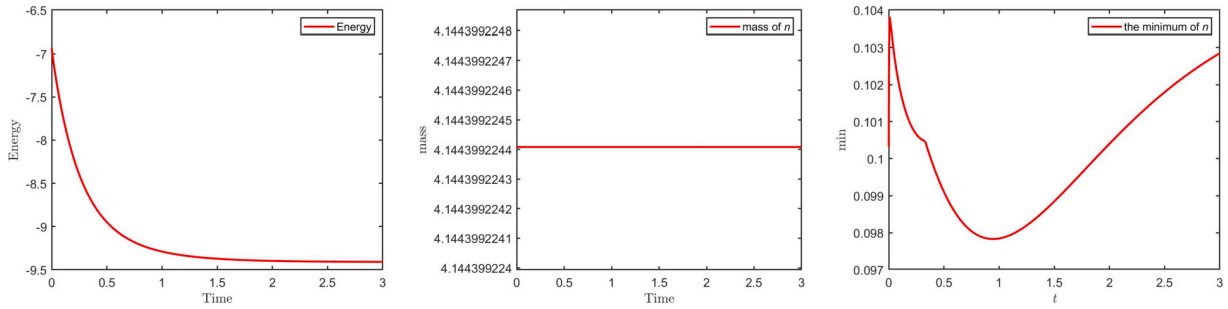

Fig. 3. Time evolution of the total energy (left), the mass of n (middle), and the minimum value of n (right) at $T = 3$ with initial data (7.2).

Example 2. The initial data is chosen as

$$n_0(x,y) = 0.1 + 0.01\text{rand}(x,y), \quad c_0(x,y) = 0.8\exp\left(-\frac{(x-\pi)^2+(y-\pi)^2}{2.25^2}\right), \quad u_0(x,y) = v_0(x,y) = p_0(x,y) = 0, \tag{7.2}$$

with $M_n \approx 4.15 < 8\pi$. The computation is performed on a uniform 128×128 mesh, and the time step size is taken as $\tau = 10^{-3}$. Snapshots of the cell density n, chemo-attractant c, fluid velocity u and vorticity contours are shown in Fig. 2. Fig. 3 displays evolutions of total energy E_{tot}, mass of n, and minimum value of n in the KSNS system. It is observed that the total energy is dissipative, the mass of n is preserved, and the value of n remains non-negative.

Example 3. To rigorously test the structure-preserving properties of the proposed numerical scheme, we consider the following initial conditions

$$n_0(x,y) = 0.01 + 0.005\,\mathbf{r}(x,y), \quad c_0(x,y) = 0.8\exp\Big(-\frac{(x-\pi)^2+(y-\pi)^2}{2.25^2}\Big), \quad u_0(x,y) = v_0(x,y) = p_0(x,y) = 0, \tag{7.3}$$

where $M_n \approx 0.39 < 8\pi$ and $\mathbf{r}(x,y)$ denotes a spatially dependent random perturbation uniformly distributed in $[-1,1]$. The computation is performed on a uniform 128×128 mesh, and the time step size is taken as $\tau = 0.01$. Fig. 4 indicates that for the KSNS

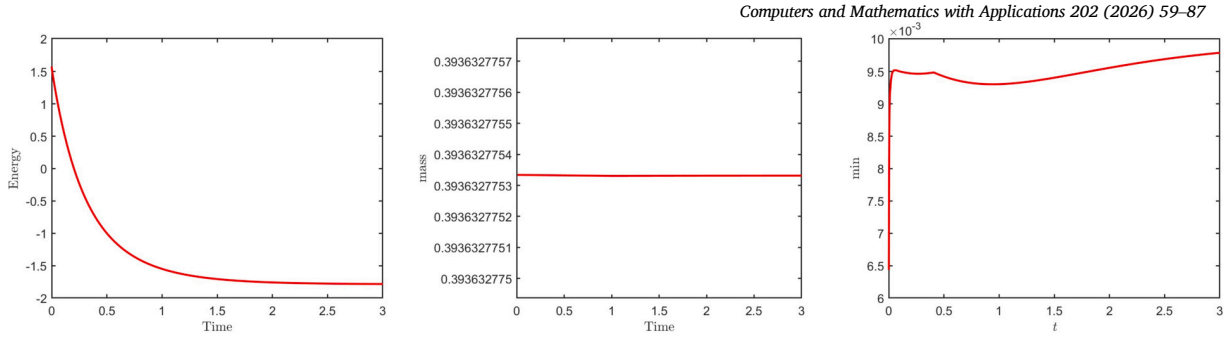

Fig. 4. Time evolution of the total energy (left), the mass of n (middle), and the minimum value of n (right) at $T = 3$ with initial data (7.3).

system, the total energy is dissipative, the mass of n is preserved, and the value of n remains positive. This demonstrates the physical consistency and numerical stability of the scheme even for an initial value n_0 close to zero.

Example 4. In this example, we consider the blow-up phenomenon with a larger $M_n \approx 251.32 > 8\pi$ with the following initial cell density setting

$$n_0(x,y) = 80\exp(-((x-\pi)^2+(y-\pi)^2)), \quad c_0(x,y) = 5\exp(-((x-\pi)^2+(y-\pi)^2)), \quad u_0(x,y) = v_0(x,y) = p_0(x,y) = 0. \tag{7.4}$$

The computation is performed on a uniform 128×128 mesh, and the time step size is taken as $\tau = 10^{-3}$. Fig. 5 presents snapshots of the cell density n, chemo-attractant c, fluid velocity u, and vorticity contours, demonstrating that the cell density n progressively concentrates toward the center as time evolves.

8. Conclusions

A second-order accurate numerical scheme (in both time and space) for the KSNS system has been proposed and analyzed. The KS equation couples the non-constant mobility H^{-1} gradient flow with the L^2 gradient flow, and the Energetic Variational Approach (EnVarA) leads to a total energy dissipation. The MAC finite difference approximation is used as the spatial discretization, while a modified Crank-Nicolson approximation is applied to the singular logarithmic term. Its inner product with the discrete temporal derivative precisely captures the nonlinear energy difference, ensuring energy stability for the logarithmic part. The mobility function is computed via a second-order extrapolation formula, preserving the elliptic nature of the temporal derivative and ensuring unique solvability. Additionally, nonlinear artificial regularization terms are introduced to facilitate positivity-preserving analysis, leveraging the singularity of the logarithmic function. The convective terms in both the KS evolutionary equation and the fluid momentum equation are updated semi-implicitly with second-order temporal accuracy. Theoretical analyses have established unique solvability, positivity preservation, and total energy stability. In addition, an optimal rate convergence analysis is provided, in which the higher order asymptotic expansion for the numerical solution, and the rough and refined error estimate techniques have to be included to accomplish such an analysis. In the authors' knowledge, this is the first work to combine these three theoretical properties for any second order accurate scheme for the KSNS system.

Acknowledgements

The research of C. Wang was partially supported by the National Science Foundation (Grant No. 2012269 and 2309548). The research of Y. Qin was partially supported by the National Natural Science Foundation of China (Grant No. 12201369). The research of Z. Zhang was partially supported by the National Natural Science Foundation of China (Grant No. 11871105 and 12231003).

Appendix A

A.1. Model derivation based on Energetic Variational Approach

In the appendix, we present the detailed modeling precess based on energetic variational approach. Following the analysis in [30,35], the temporal derivative of total energy functional (2.3) turns out to be

$$\frac{\mathrm{d}E_{total}}{\mathrm{d}t} = \frac{\mathrm{d}}{\mathrm{d}t}\int_\Omega \left\{ n(\ln n - 1) - nc + \frac{1}{2}(|\nabla c|^2 + \alpha c^2) \right\} \mathrm{d}\boldsymbol{x} + \frac{\mathrm{d}}{\mathrm{d}t}\int_\Omega \frac{\rho}{2}|\boldsymbol{u}|^2 \mathrm{d}\boldsymbol{x} =: \frac{\mathrm{d}E_1}{\mathrm{d}t} + \frac{\mathrm{d}E_2}{\mathrm{d}t}.$$

In terms of the free energy E_1, the temporal derivative could be derived with the help of the boundary condition (2.2):

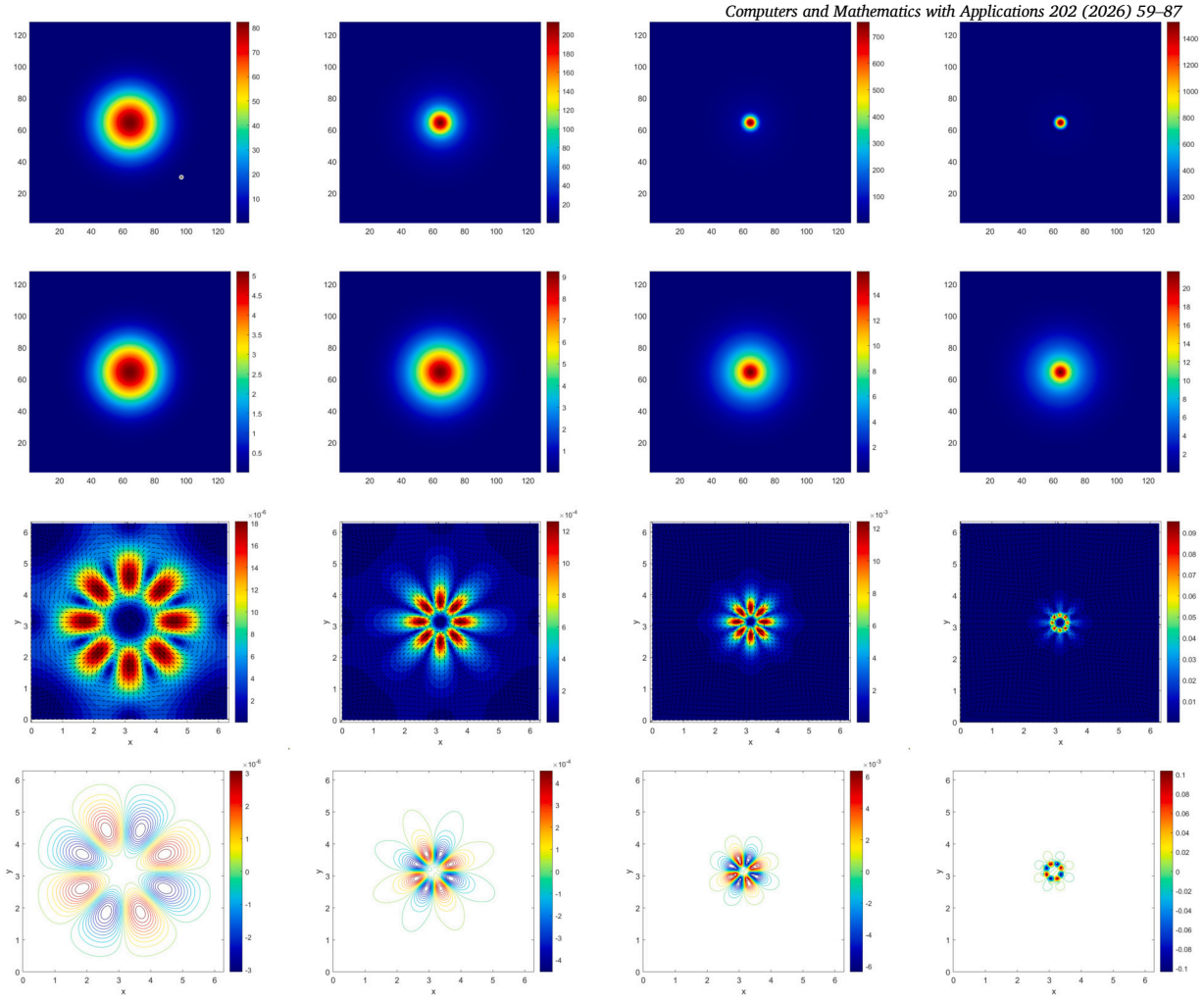

Fig. 5. Snapshots of the KSNS system with initial data (7.4) at $T = 0.002, 0.05, 0.08, 0.092$. From top to bottom are the cell density n, chemo-attractant c, fluid velocity $\boldsymbol{u}$, and vorticity contours.

$$\begin{aligned}\frac{\mathrm{d}E_1}{\mathrm{d}t} &= \int_\Omega \left\{ n_t \ln n - n_t c - n c_t + \nabla c \cdot \nabla c_t + \alpha c c_t \right\} \mathrm{d}\boldsymbol{x} = \int_\Omega \left\{ n_t (\ln n - c) + c_t (-n - \Delta c + \alpha c) \right\} \mathrm{d}\boldsymbol{x} \\ &= \int_\Omega \left\{ (\frac{\mathrm{D}n}{\mathrm{D}t} - \boldsymbol{u} \cdot \nabla n)\mu_n + (\frac{\mathrm{D}c}{\mathrm{D}t} - \boldsymbol{u} \cdot \nabla c)\mu_c \right\} \mathrm{d}\boldsymbol{x} = \int_\Omega (-\nabla \cdot \boldsymbol{j}_n)\mu_n \mathrm{d}\boldsymbol{x} + \int_\Omega j_c \mu_c \mathrm{d}\mathbf{x} - \int_\Omega (\boldsymbol{u} \cdot \nabla n)\mu_n \mathrm{d}\boldsymbol{x} - \int_\Omega (\boldsymbol{u} \cdot \nabla c)\mu_c \mathrm{d}\boldsymbol{x}.\end{aligned}$$

Similarly, the corresponding temporal derivative of the kinetic energy E_2 becomes

$$\begin{aligned}\frac{\mathrm{d}E_2}{\mathrm{d}t} &= \frac{1}{2}\int_\Omega (\rho_t |\boldsymbol{u}|^2 + 2\rho \boldsymbol{u} \cdot \boldsymbol{u}_t)\mathrm{d}\boldsymbol{x} = \frac{1}{2}\int_\Omega (\rho_t |\boldsymbol{u}|^2 + 2\rho \boldsymbol{u} \cdot (\boldsymbol{u}_t + \boldsymbol{u} \cdot \nabla \boldsymbol{u} - \boldsymbol{u} \cdot \nabla \boldsymbol{u}))\mathrm{d}\boldsymbol{x} \\ &= \int_\Omega \rho \boldsymbol{u} \cdot (\boldsymbol{u}_t + \boldsymbol{u} \cdot \nabla \boldsymbol{u})\mathrm{d}\boldsymbol{x} + \frac{1}{2}\int_\Omega (\rho_t |\boldsymbol{u}|^2 - 2\rho \boldsymbol{u} \cdot (\boldsymbol{u} \cdot \nabla \boldsymbol{u}))\mathrm{d}\boldsymbol{x} = \int_\Omega \boldsymbol{u} \cdot (\nabla \cdot \boldsymbol{\sigma}_\eta + \boldsymbol{F})\mathrm{d}\boldsymbol{x} + \frac{1}{2}\int_\Omega (\rho_t |\boldsymbol{u}|^2 - \rho \boldsymbol{u} \cdot \nabla |\boldsymbol{u}|^2)\mathrm{d}\boldsymbol{x} \\ &= \int_\Omega (-\nabla \boldsymbol{u} : \boldsymbol{\sigma}_\eta + \boldsymbol{u} \cdot \boldsymbol{F})\mathrm{d}\boldsymbol{x} + \frac{1}{2}\int_\Omega (\rho_t |\boldsymbol{u}|^2 + \nabla \cdot (\rho \boldsymbol{u})|\boldsymbol{u}|^2)\mathrm{d}\boldsymbol{x} = \int_\Omega (-\nabla \boldsymbol{u} : \boldsymbol{\sigma}_\eta + \boldsymbol{u} \cdot \boldsymbol{F})\mathrm{d}\boldsymbol{x} - \int_\Omega p \nabla \cdot \boldsymbol{u} \mathrm{d}\boldsymbol{x},\end{aligned}$$

where we have used the mass conservation equation

$$\rho_t + \nabla \cdot (\rho \boldsymbol{u}) = 0.$$

In turn, a combination of these two parts yields

$$\frac{\mathrm{d}E_{total}}{\mathrm{d}t} = \int_{\Omega} (-\nabla \boldsymbol{u} : \boldsymbol{\sigma}_{\eta} + \boldsymbol{u} \cdot \boldsymbol{F}) \mathrm{d}\boldsymbol{x} - \int p\mathbf{I} : \nabla \boldsymbol{u} \mathrm{d}\boldsymbol{x} + \int_{\Omega} (-\nabla \cdot \boldsymbol{j}_n)\mu_n \mathrm{d}\boldsymbol{x} + \int_{\Omega} j_c \mu_c \mathrm{d}\mathbf{x} - \int_{\Omega} (\boldsymbol{u} \cdot \nabla n)\mu_n \mathrm{d}\boldsymbol{x} - \int_{\Omega} (\boldsymbol{u} \cdot \nabla c)\mu_c \mathrm{d}\boldsymbol{x}. \tag{A.1}$$

Comparing the right side of (A.1) with the dissipation functional Q and making use of the boundary conditions (2.2), we obtain

$$\boldsymbol{j}_n = -n\nabla\mu_n, \quad j_c = -\mu_c, \quad \boldsymbol{\sigma}_{\eta} = 2\eta \boldsymbol{D}_{\eta} - p\mathbf{I}, \quad \boldsymbol{F} = -n\nabla\mu_n - c\nabla\mu_c.$$

Subsequently, the following PDE system is formulated:

$$\begin{aligned}
&\frac{\mathrm{D}n}{\mathrm{D}t} = \nabla \cdot (n\nabla\mu_n), \quad \mu_n = \ln n - c, \\
&\frac{\mathrm{D}c}{\mathrm{D}t} = -\mu_c, \quad \mu_c = -\Delta c + \alpha c - n, \\
&\rho\frac{\mathrm{D}\boldsymbol{u}}{\mathrm{D}t} = \nabla \cdot \boldsymbol{\sigma}_{\eta} + \boldsymbol{F}, \quad \nabla \cdot \boldsymbol{u} = 0, \quad \boldsymbol{\sigma}_{\eta} = 2\eta \boldsymbol{D}_{\eta} - p\mathrm{I}, \quad \boldsymbol{F} = -n\nabla\mu_n - c\nabla\mu_c,
\end{aligned}$$

with the following simplified boundary condition:

$$\nabla n \cdot \boldsymbol{n}|_{\partial\Omega} = 0, \quad \nabla c \cdot \boldsymbol{n}|_{\partial\Omega} = 0, \quad \boldsymbol{u}|_{\partial\Omega} = 0, \quad \boldsymbol{F} \cdot \boldsymbol{n}|_{\partial\Omega} = 0.$$

Data availability

No data was used for the research described in the article.

References

[1] J. Adler, Chemotaxis in bacteria, Science 153 (3737) (1966) 708–716.
[2] G. Arumugam, J. Tyagi, Keller–Segel chemotaxis models: a review, Acta Appl. Math. 171 (1) (2021) 1–82.
[3] G. Chamoun, M. Saad, R. Talhouk, Numerical analysis of a chemotaxis-swimming bacteria model on a general triangular mesh, Appl. Numer. Math. 127 (1) (2018) 324–348.
[4] W. Chen, J. Jing, Q. Liu, C. Wang, X. Wang, A second order accurate, positivity-preserving numerical scheme of the Cahn–Hilliard–Navier–Stokes system with Flory-Huggins potential, Commun. Comput. Phys. 35 (3) (2024) 633–661.
[5] W. Chen, J. Jing, C. Wang, X. Wang, A positivity preserving, energy stable finite difference scheme for the Flory–Huggins–Cahn–Hilliard–Navier–Stokes system, J. Sci. Comput. 92 (2) (2022) 1–24.
[6] W. Chen, J. Jing, C. Wang, X. Wang, S.M. Wise, A modified Crank-Nicolson numerical scheme for the Flory–Huggins Cahn–Hilliard model, Commun. Comput. Phys. 31 (1) (2022) 60–93.
[7] W. Chen, Y. Liu, C. Wang, S.M. Wise, Convergence analysis of a fully discrete finite difference scheme for the Cahn–Hilliard–Hele–Shaw equation, Math. Comput. 85 (301) (2016) 2231–2257.
[8] W. Chen, C. Wang, X. Wang, S.M. Wise, Positivity-preserving, energy stable numerical schemes for the Cahn–Hilliard equation with logarithmic potential, J. Comput. Phys. X 3 (2019) 100031.
[9] A. Chertock, Y. Epshteyn, H. Hu, A. Kurganov, High-order positivity-preserving hybrid finite-volume-finite-difference methods for chemotaxis systems, Adv. Comput. Math. 44 (1) (2018) 327–350.
[10] A. Chertock, A. Kurganov, A second-order positivity preserving central-upwind scheme for chemotaxis and haptotaxis models, Numer. Math. 111 (2) (2008) 169–205.
[11] A.E. Diegel, C. Wang, X. Wang, S.M. Wise, Convergence analysis and error estimates for a second order accurate finite element method for the Cahn–Hilliard–Navier–Stokes system, Numer. Math. 137 (3) (2017) 495–534.
[12] Y. Dolak, C. Schmeiser, The Keller–Segel model with logistic sensitivity function and small diffusivity, SIAM J. Appl. Math. 66 (1) (2005) 286–308.
[13] C. Duan, W. Chen, C. Liu, C. Wang, X. Yue, A second order accurate, energy stable numerical scheme for the one-dimensional porous medium equation by an energetic variational approach, Commun. Math. Sci. 20 (4) (2022) 987–1024.
[14] W. E, J. Liu, Projection method III: spatial discretization on the staggered grid, Math. Comput. 71 (237) (2002) 27–47.
[15] D. Feng, L. Bin, Global weak solutions in a three-dimensional Keller–Segel–Navier–Stokes system with indirect signal production, J. Differ. Equ. 333 (2022) 436–488.
[16] F. Filbet, A finite volume scheme for the Patlak–Keller–Segel chemotaxis model, Numer. Math. 104 (4) (2006) 457–488.
[17] J. Guo, C. Wang, S.M. Wise, X. Yue, An H^2 convergence of a second-order convex-splitting, finite difference scheme for the three-dimensional Cahn–Hilliard equation, Commun. Math. Sci. 14 (2) (2016) 489–515.
[18] Y. Guo, C. Wang, S.M. Wise, Z. Zhang, Convergence analysis of a positivity-preserving numerical scheme for the Cahn–Hilliard–Stokes system with Flory-Huggins energy potential, Math. Comput. 93 (349) (2024) 2185–2214.
[19] F.H. Harlow, J.E. Welch, Numerical calculation of time-dependent viscous incompressible flow of fluid with free surface, Phys. Fluids 8 (12) (1965) 2182–2189.
[20] T. Hillen, K.J. Painter, Global existence for a parabolic chemotaxis model with prevention of overcrowding, Adv. Appl. Math. 26 (4) (2001) 280–301.
[21] T. Hillen, K.J. Painter, A user's guide to PDE models for chemotaxis, J. Math. Biol. 58 (1) (2009) 183–217.
[22] D. Horstmann, From 1970 until present: the Keller–Segel model in chemotaxis and its consequences I, Jahresber. Dtsch. Math.-Ver. 105 (3) (2003) 103–165.
[23] X. Huang, X. Feng, X. Xiao, K. Wang, Fully decoupled, linear and positivity-preserving scheme for the chemotaxis–Stokes equations, Comput. Methods Appl. Mech. Eng. 383 (2021) 113909.
[24] X. Huang, J. Shen, Bound/positivity preserving SAV schemes for the Patlak–Keller–Segel–Navier–Stokes system, J. Comput. Phys. 480 (2023) 112034.
[25] E.F. Keller, L.A. Segel, Model for chemotaxis, J. Theor. Biol. 30 (2) (1971) 225–234.
[26] H. Kozono, M. Miura, Y. Sugiyama, Existence and uniqueness theorem on mild solutions to the Keller–Segel system coupled with the Navier–Stokes fluid, J. Funct. Anal. 270 (5) (2016) 1663–1683.
[27] X. Li, Z. Qiao, C. Wang, Stabilization parameter analysis of a second-order linear numerical scheme for the nonlocal Cahn–Hilliard equation, IMA J. Numer. Anal. 43 (2) (2023) 1089–1114.
[28] C. Liu, C. Wang, S.M. Wise, X. Yue, S. Zhou, A second order accurate, positivity preserving numerical method for the Poisson–Nernst–Planck system and its convergence analysis, J. Sci. Comput. 97 (1) (2023) 23.

[29] Y. Qian, C. Wang, S. Zhou, A positive and energy stable numerical scheme for the Poisson–Nernst–Planck–Cahn–Hilliard equations with steric interactions, J. Comput. Phys. 426 (2021) 109908.
[30] Y. Qin, H. Huang, Y. Zhu, C. Liu, S. Xu, A phase field model for mass transport with semi-permeable interfaces, J. Comput. Phys. 464 (2022) 111334.
[31] Y. Qin, C. Wang, A second-order accurate, positivity-preserving numerical scheme for the Poisson–Nernst–Planck–Navier–Stokes system, IMA J. Numer. Anal. (2025) draf027.
[32] Y. Qin, C. Wang, Z. Zhang, A positivity-preserving and convergent numerical scheme for the binary fluid-surfactant system, Int. J. Numer. Anal. Model. 18 (3) (2021) 399–425.
[33] J. Shen, C. Wang, X. Wang, S.M. Wise, Second-order convex splitting schemes for gradient flows with Ehrlich–Schwoebel type energy: application to thin film epitaxy, SIAM J. Numer. Anal. 50 (1) (2012) 105–125.
[34] J. Shen, J. Xu, Unconditionally bound preserving and energy dissipative schemes for a class of Keller–Segel equations, SIAM J. Numer. Anal. 58 (3) (2020) 1674–1695.
[35] L. Shen, Z. Xu, P. Lin, H. Huang, S. Xu, An energy stable C^0 finite element scheme for a phase-field model of vesicle motion and deformation, SIAM J. Sci. Comput. 44 (1) (2022) B122–B145.
[36] R. Temam, Navier–Stokes Equations: Theory and Numerical Analysis, American Mathematical Society, Providence, Rhode Island, 2001.
[37] J.L. Velázquez, Point dynamics in a singular limit of the Keller–Segel model 1: motion of the concentration regions, SIAM J. Appl. Math. 64 (4) (2004) 1198–1223.
[38] C. Wang, J. Liu, Convergence of gauge method for incompressible flow, Math. Comput. 69 (232) (2000) 1385–1407.
[39] M. Winkler, Finite-time blow-up in the higher-dimensional parabolic-parabolic Keller–Segel system, J. Math. Pures Appl. 100 (5) (2013) 748–767.
[40] S.M. Wise, J. Kim, J.S. Lowengrub, Solving the regularized, strongly anisotropic Cahn–Hilliard equation by an adaptive nonlinear multigrid method, J. Comput. Phys. 226 (1) (2007) 414–446.
[41] P. Zeng, G. Zhou, The positivity-preserving finite volume coupled with finite element method for the Keller–Segel–Navier–Stokes model, Commun. Comput. Phys. 35 (4) (2024) 1073–1119.